DEPARTMENT OF PHYSICS, LIBPhys-UNL

NOVA SCHOOL OF SCIENCE & TECHNOLOGY

DEVELOPMENT OF RAMAN SPECTROSCOPY INSTRUMENTATION FOR DENTAL RESEARCH

IULIAN OTEL

Master's Degree in Biomedical Engineering

DOCTORATE IN I4H – Innovation for Health, BIOMEDICAL ENGINEERING

NOVA University Lisbon

March 2023

NOVA SCHOOL OF
SCIENCE & TECHNOLOGY

DEVELOPMENT OF RAMAN SPECTROSCOPY INSTRUMENTATION FOR DENTAL RESEARCH

Doctoral dissertation for the obtention of PhD degree in Biomedical Engineering

IULIAN OTEL

NOVA SCHOOL OF SCIENCE & TECHNOLOGY

DEPARTMENT OF PHYSICS

DEVELOPMENT OF RAMAN SPECTROSCOPY INSTRUMENTATION FOR DENTAL RESEARCH

Doctoral dissertation for the obtention of PhD degree in Biomedical Engineering

IULIAN OTEL

Master's Degree in Biomedical Engineering

Adviser: **Alda Sofia Pessanha de Sousa Moreno**
Assistant Researcher, FCT - NOVA University Lisbon

Co-advisers: **Valentina Vassilenko**
Assistant Professor, FCT - NOVA University Lisbon

João Miguel Lourenço Silveira
Assistant Professor, FMDUL, University of Lisbon

Examination Committee:

Chair: José Paulo Moreira dos Santos,
Full Professor, FCT-NOVA

Rapporteurs: Sofia de Mello Lima T. Santos Arrantes e Oliveira,
Associate Professor, FMDUL, University of Lisbon
Maria do Rosário Correia,
Assistant Professor, University of Aveiro

Adviser: Alda Sofia Pessanha de Sousa Moreno,
Assistant Researcher, FCT-NOVA

Members: José Paulo Moreira dos Santos,
Full Professor, FCT-NOVA
Paulo António Ferreira Ribeiro,
Associate Professor, FCT-NOVA

DOCTORATE IN I4H – Innovation for Health, Biomedical Engineering

NOVA University Lisbon
March, 2023

Development of Raman spectroscopy instrumentation for dental research

To my Parents

Few of the studies presented in this doctoral dissertation resulted in two scientific papers and one conference paper (printed in conference proceedings), that were published, as follows:

I. Otel, K. Dias, R. Pereira, M. Fonseca, A. P. Jesus, A. Mata, V. Vassilenko, J. M. Silveira, S. Pessanha, Investigation of the protective suitability of a dental fluorinated varnish by means of X Ray fluorescence and Raman spectroscopy, Journal of Trace Elements in Medicine and Biology, 71, 2022. https://doi.org/10.1016/j.jtemb.2022.126938.

I. Otel, J. M. Silveira, V. Vassilenko, A. Mata, M. L. Carvalho, J. P. Santos, S. Pessanha, Application of Unsupervised Multivariate Analysis Methods to Raman Spectroscopic Assessment of Human Dental Enamel. Computers, 11, 5, 2022. https://doi.org/10.3390/computers11010005.

I. Otel, J. M. Silveira, V. Vassilenko, A. Mata, S. Pessanha, Application of Machine Learning Methods to Raman Spectroscopy Technique in Dentistry, DoCEIS 2021, IFIP AICT 626, pp. 339–348, 2021. https://doi.org/10.1007/978-3-030-78288-7_33.

ACKNOWLEDGMENTS

I would like to express my sincere gratitude and respect to my parents. I will always be grateful to them for their support and trustworthy advice.

I would like to thank my supervisors, for their supervision, guidance, systematic remarks, and comments.

I would also like to recognize the joint effort of other professors from several doctoral courses for teaching and illuminating my academic path when needed. Also, a special mention for their helpful advice, criticism, overall corrections, and all shown support from the start of my 1st year of PhD program, and throughout my entire doctoral research project.

Special thanks are owed to the Foundation of Science and Technology for funding and making possible this doctoral research; and to the Department of Physics of NOVA School of Science and Technology - UNL, for providing the Raman and EDXRF facilities.

"It takes something more than intelligence to act intelligently."

(Fyodor Dostoyevsky)

ABSTRACT

Raman spectroscopy is, in general, a non-invasive and non-destructive analytical technique used for the identification and analysis of chemical composition, and characterization of molecular structures, providing detailed information on structural arrangement, crystal orientations, crystallinity, phase, and polymorphism, as well as for the assessment of molecular interactions and the effects of bonding, chemical surrounding environment, and stress on samples. This method is becoming progressively important in biomedical research especially for its high biochemical specificity, low water sensitivity, simplicity in analyzing the spectral parameters, capability to work in the near-infrared region and *in-vivo* remote potential by means of fiber-optics. Raman technique has been confirmed to be a very appropriate technique to characterize both organic and inorganic superficial components of dental tissues, enabling the acquisition of accurate and precise spectral information on present minerals through the observation of the characteristic energies of their vibrational modes. The sensitivity of this spectroscopic technique for changes in the symmetric stretching band of phosphate ions in the hydroxyapatite matrix could be used as a powerful tool and complementary method for early diagnostics of incipient caries and assessment of dental mineral content, even before signs of tooth demineralization are detected with conventional methods – visual-tactile examination combined with radiography. The present doctoral thesis aims to promote the application of Raman technique as a promising tool for dental examination, tooth decay and caries diagnostics, with emphasis on 1) the relevance and appropriateness of Raman spectroscopy in dentistry; 2) improvement of the accuracy for the spectral data processing and interpretation; 3) development of instrumentation for *ex-vivo* and *in-vivo* analysis, based on the design and assembly of a remote fiber-optic Raman probe with potential applications for the *ex-vivo* and *in-vivo* assessment of the human enamel and early caries diagnosis, presenting additionally a comparison study between Raman benchtop measurements and remote fiber-optic probe-based measurements. The accomplishment of the mentioned objectives should confirm the functioning principle of the Raman probe concept, improve the remote application, and help to implement the Raman technique in modern dentistry area, for a better counselling and assistance of the patients in preventing demineralization, the appearance of white spot lesion (WSL) and caries progression.

Keywords: *Raman spectroscopy, remote fiber-optic probe, enamel, probe-based, precise measurements, accurate spectral information, dental sample analysis.*

RESUMO

A espectroscopia Raman é, em geral, uma técnica analítica não-invasiva e não-destrutiva, utilizada para a identificação e análise química, e a caracterização de estruturas moleculares, fornecendo informações detalhadas sobre o arranjo estrutural, orientações cristalinas, fase e polimorfismo, bem como para a avaliação das interações moleculares e os efeitos da ligação, ambiente químico circundante e tensão nas amostras. Este método é cada vez mais importante na investigação biomédica, especialmente devido a sua alta especificidade bioquímica, baixa sensibilidade à água, simplicidade na análise dos parâmetros espectrais, capacidade de trabalhar na região do infravermelho (NIR), potencial remoto e aplicação *in-vivo* por meio de fibra ótica. A técnica Raman é considerada muito apropriada para caracterizar componentes superficiais orgânicos e inorgânicos de tecidos dentais, permitindo a aquisição de informações espectrais exatas e precisas sobre os minerais presentes através da observação das energias características de seus modos vibracionais. A sensibilidade desta técnica espectroscópica para alterações na banda de alongamento simétrico dos iões de fosfato na matriz de hidroxiapatita pode ser usada como uma ferramenta poderosa e como um método adjuvante alternativo para diagnóstico precoce da cárie incipiente, início de lesão dentária ou perda de minerais, mesmo antes dos sinais de desmineralização serem detetados por métodos convencionais – a examinação visual-tátil em combinação com o exame radiológico. A presente tese visa promover a aplicação da técnica Raman como uma ferramenta promissora, bem como um método complementar, para o diagnóstico dentário, precisamente na deteção precoce da cárie incipiente e avaliação do estado de mineralização, demonstrando a 1) relevância e adequação da técnica por espectroscopia Raman na área dentária; 2) melhoria da precisão do processamento e interpretação dos dados espectrais; 3) desenvolvimento de instrumentação para análise efetuada *ex-* ou *in-vivo*, baseada no desenho e montagem de uma sonda remota Raman acoplada a fibras óticas, apresentando adicionalmente, um estudo comparativo entre as medições com o microscópio Raman e as medições remotas através da sonda. A concretização dos objetivos referidos deverá confirmar o princípio de funcionamento do conceito de sonda Raman, melhorar a aplicação remota e ajudar a implementar a técnica Raman na área da medicina dentária moderna, para um melhor aconselhamento e assistência dos pacientes na prevenção de desmineralização, aparecimento de lesão branca (WSL) e progressão da cárie.

Palavras-chave: *Espectroscopia Raman, especificidade bioquímica, sonda remota, fibra ótica, esmalte, informação espectroscópica, análise ex-vivo.*

CONTENTS

LIST OF FIGURES

LIST OF TABLES

GLOSSARY

Anisotropy Term used to specify that physical properties are different when measured along different directions, as opposed to isotropy, meaning that optical effects are dependent on the orientation in space.

Anisotropic samples Directionally oriented samples, such as crystal lattices, polymers.

Anti-Stokes scattering Raman scattering where the scattered light has a shorter wavelength (higher energy) than the incident beam.

Back-scattering geometry Optical configuration where the incoming radiation that is measured is back-scattered in the direction of the incident laser radiation, at an angle of 180°.

Confocal measurements Approach where a confocal pinhole is positioned in the light path, so that only information of a specific depth (axial resolution) is obtained.

Depolarization ratio Parameter that provides information on the symmetry of a crystalline structure of a molecule, and the vibrational mode represented by a Raman band associated to a group (such as phosphate). It helps to identify vibrational modes, the structure and identity of samples. It is defined as a ratio of vertically to horizontally polarized scattered light at 90° and 0°, respectively, to the polarization direction of the polarized incident light.

Fluorescence Emission of radiation caused by electronic transitions.

Isotropic samples Randomly oriented samples, such as liquids, microcrystalline powders.

Polarizability Quantity expressing how easily electrons in a molecule can be moved to induce a dipole.

Polarized Raman spectroscopy Technique that provides information about molecular orientation and symmetry of the bond vibrations, in addition to the general chemical identification.

Quantum efficiency (QE) Quantity used to express the sensitivity of a detector. Expresses how many photons correspond with a detected electron or electron–hole pair.

Raman spectroscopy Technique used to determine the chemical composition, molecular structure, as well as crystal structure and orientation, stress and strain, degree of crystallinity and amorphousness.

Rayleigh scattering Elastic scattering where the scattered light has the same wavelength as the incident beam.

Stokes scattering Raman scattering where the scattered light has a longer wavelength (lower energy) than the incident beam.

ACRONYMS

µCT	Microcomputed tomography
µ-Raman	Micro-Raman
2D	Two-dimensional
3D	Three-dimensional
BP	Band-pass
C	Control (with reference number, such as C1, C2…Cn)
CCD	Charge coupled devices
EDXRF	Energy Dispersive X-Ray Fluorescence
DEJ	Dentin-enamel junction
DIFOTI	Digital imaging fiber-optic transillumination
FAp	Fluorapatite
FOTI	Fiber-optic transillumination
FSB	Fiber spectral background
FP	Fingerprint (spectral region)
FTIR	Fourier transform infrared
FWHM	Full-width-at-half-maximum
HAp	Hydroxyapatite
HW	High wavenumber
HWP	Rotating half-wave plate
IBM SPSS	IBM statistics analytical software
ICDAS	International Caries Detection and Assessment System
IR	Infrared
LASER	Light Amplification by Stimulated Emission of Radiation
LDA	Linear discriminant analysis
LF	Laser fluorescence-based method
LIBPhys	Laboratory for Instrumentation, Biomed. Engineering and Radiation Physics
LP	Long-pass (filter); also Linearly polarized or Linear polarizer
MVA	Multivariate analysis
NA	Numerical aperture
NILT	Near-infrared laser transillumination
NIR	Near Infrared (wavelength)
OH	Hydroxyl Ion
OWD	Optimal working distance

PA	Polarizer analyzer
PC	Principal Component
PCA	Principal Component Analysis
PhD	Doctor in Philosophy
PIGE	Particle Induced Gamma Emission
QE	Quantum efficiency
QLF	Quantitative laser/light-induced fluorescence
R	Red (wavelength)
ROI	Region of interest
RS	Raman spectroscopy
RSI	Raman spectroscopy imaging
S	Sample (enamel sample)
SP	Short pass
SNR	Signal-to-noise ratio
T	Treatment
UV	Ultraviolet
VIS	Visible
WHO	World Health Organization
XRF	X-Ray Fluorescence
WSL	White spot lesion

SYMBOLS

$\mathbf{A_{959}}$	Polarization anisotropy
$\tilde{\alpha}$	Proportionality factor between the external field and induced dipole moment
C	Carbon
$\mathbf{CCl_4}$	Carbon tetrachloride
Ca-P-O	Apatite
$\mathbf{Ca/Ca^{2+}}$	Calcium/Calcium Ion
$\mathbf{Ca_5(PO_4)_3F}$	Fluorapatite
$\mathbf{(Ca_{10}(PO_4)_6(OH)_2)}$	Hydroxyapatite
E	Electric field
F	Fluorine
μ	Micro; also, Molecular dipole
ω_0	Oscillation frequency
ρ_{959}	Depolarization ratio
$\mathbf{I_{959}(\perp)}$	Integrated peak intensity of the ~959 cm^{-1} band with the analyzer oriented perpendicular (⊥) to the polarization direction
$\mathbf{I_{959}(\|\|)}$	Integrated peak intensities of the ~959 cm^{-1} band detected with the analyzer oriented parallel (‖) to the polarization direction
$\mathbf{OH^-}$	Hydroxyl Ion
P	Phosphorus
p	Dipole moment
$\mathbf{PO_4^{3-}}$	Phosphate Ion (group)
$\mathbf{T_3 – H_2O}$	Chloramine
v	Phosphate vibrational band (symmetric or asymmetric, according to case)

1

MOTIVATION, SIGNIFICANCE AND AIMS

The major goals of modern medicine are the prevention, early detection, and treatment of diseases. Raman spectroscopy is a highly promising optical technique, label-free (no need for previous preparation or labelling), non-destructive, non-intrusive and non-invasive, that enables the obtention and delivery in real-time of reliable, and precise distinctive characteristic information of molecular vibrations, and has been successfully applied in several different fields, such as biology, pharmacy, medicine, biomedical, analytical chemistry, material science, and clinical analytics. This technique is increasingly and widely used, considered as a powerful tool, which provides an exceptionally unique and specific chemical fingerprint for the detection of functional groups and the identification of specific compounds or a certain measured sample. Small chemical and/or structural differences between similar samples or even more complex compounds can be precisely detected, identified, and assessed qualitatively by noticeable spectral band changes of the acquired spectrum - band positions/shifts, and quantitatively by analyzing spectral parameters, such as band width and band intensity variations, and polarization dependent band alterations and derived ratios.

Raman spectroscopy has been proven to be suitable for the characterization of dental tissues, from **caries detection** to the evaluation of overall demineralization (mineral loss) caused by **acidic external agents**. The sensitivity of this spectroscopic technique for alterations in the symmetric stretching band of phosphate ions in the hydroxyapatite matrix could be used as a powerful tool for early diagnostics, even before signs of demineralization are detected with conventional methods, such as visual-tactile examination combined with radiography. There is not, however, to the best of our knowledge, any device that allows *in-vivo* evaluation of dental tissues making use of this method. Raman spectroscopy can be used as a complementary or alternative method to provide additional, however valuable, and detailed biochemical information for the early detection of incipient caries, initial stage of white spot lesion (WSL) and other hypo-mineralization related dental diseases.

Therefore, the present doctoral thesis is based on three main structural parts, describing three key aspects, with regards to the 1) relevance and appropriateness of Raman spectroscopy in dentistry; 2) improvement of accuracy of the spectral data processing and interpretation of the acquired

spectral information, based on results obtained experimentally; 3) instrumentation for *ex-vivo* and *in-vivo* analysis, by means of a remote fiber-optic Raman probe, with potential applications for the assessment of the human enamel overall mineralization (of outer/superficial layers) and early caries diagnosis. Additionally, it is described a comparison study between remote fiber-coupled probe-based measurements and benchtop acquisitions.

The main objectives of my PhD work consisted in the design, development, testing and implementation of novel instrumentation – Raman fiber-optic probe, connected to a commercial Raman microscope (Horiba XploRA), to remote *ex-vivo* analysis of human teeth. The accomplishment of the mentioned objectives should confirm the functioning principle of the probe concept, improve the remote application, and help to implement *in-vivo* the Raman technique in modern dentistry as a non-invasive and pain-free diagnostic tool and/or assessment method.

The developed Raman fiber-optic probe, coupled to the Raman confocal microscope, must be perfectly capable of transmitting, directing, and focusing the monochromatic excitation laser to the examined dental sample, along with collecting the Raman scattered light and afterwards directing it to the spectrometer, in order to provide precise Raman spectral information for both *ex-* and *in-vivo* measurements, with high quality signal, good spectral resolution (app. 4-6 cm^{-1}) and high signal-to-noise ratio - SNR, parameters that are often required for sample assessment and for diagnostic in a clinical setting. The work described in this thesis concerns a remote Raman probe build only with single-fiber configurations, operating in a backscattering geometry (reflection mode), with an angle of approximately 180° between the excitation laser and Raman signal collection, in opposite directions, with distinct optical waveguides delivering simultaneously the excitation light to the sample (output signal) and collecting the Raman scattered photons (input Raman signal).

The main challenges in obtaining precise results, which are provided by high-quality spectra: with sharp and well-defined peaks, low noise and good SNR, rely on the following: (1) tissue fluorescence being several orders of magnitude greater than the Raman signal; (2) the Raman signal from tissue being, intrinsically and inherently, extremely weak and require higher excitation power and increased collection times to obtain spectra with acceptable SNRs; (3) contamination signal from the delivery and collection fiber optics – noise and spectral background caused by the Raman scattering and fluorescence signals that are originated within the silica core of the excitation and collection fibers; (4) probe lens focus difficulty - employing probes equipped with a focal objective lens requires the user to maintain permanently and constantly the probe steady at a fixed focal distance or working optimal distance, in normal direction to the examined sample surface for an efficient delivery of the laser signal and to maximize the collection of the Raman scattered signal.

2

INTRODUCTION

2.1 - Human dental enamel

Tooth enamel (Figure 2.1) is the most highly mineralized and hardest tissue in the human body that covers and protects the anatomic crown of the tooth. The enamel is structurally heterogeneous, with a biochemical composition that varies noticeably from the outer surface to the inner layers and from one region of the tooth to another, as well as from one subject to another. It resists chewing forces and protects the internal layers, dentin, and pulp. Mineralization is an essential property that positively correlates with the mechanical behavior of dental tissues. Dental enamel contains 95-96 % weight mineral in the crystalline form of hydroxyapatite (HAp), up to 1-2 % of organic material, mostly represented by proteins – (remaining of) amelogenin, ameloblastin, tuftelin and enamelin, and approximately 3-4% water by weight [1-5].

a) 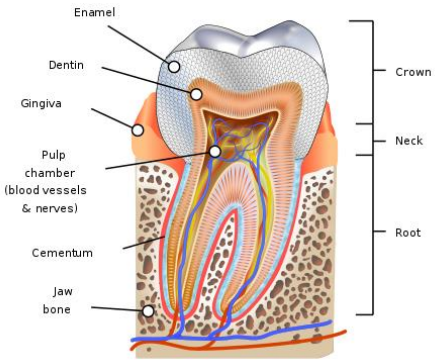

b) 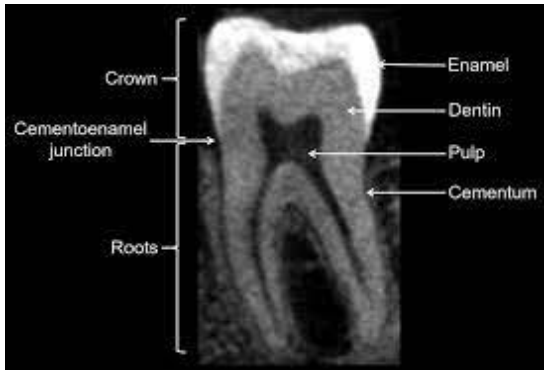

Figure 2.1 – a) Schematic 3D representation of human tooth anatomy with detailed description of tooth components, layers, and dental regions. Illustration of tooth cross section [6]; **b)** Cross-sectional anatomic view of the tooth obtained by means of computed tomography (CT) technique [adapted from 7].

The main mineral component of human dental enamel is hydroxyapatite (HAp), which is characterized by a more complex varying microstructure. Its physical-chemical and physiological properties, such as strength, brittleness, permeability, efficiency of exchange and diffusion processes show a strong dependence on enamel thickness, structural arrangement, rod orientation, morphology, mineralization level and chemical composition [8].

The chemical formula of hydroxyapatite is $Ca_{10}(PO_4)_6(OH)_2$. In biological tissues, the major form of HA is the carbonated HA, in which PO_4^{3-} or OH^- can be substituted by CO_3^{2-} (type B or type A respectively). The remaining ions can be also substituted in trace quantities in apatite crystal structure. The PO_4^{3-} and OH^- groups can be replaced in the apatite lattice by AsO_4^{3-}, SO_4^{2-}, CO_3^{2-}, SiO_4^{4-} Cl^- and F^- anions respectively. In turn, the cations such as K^+, Na^+, NH^{4+}, Mn^{2+}, Ni^{2+}, Cu^{2+}, Mg^{2+}, Fe^{2+}, or Zn^{2+} can occupy the Ca^{2+} position. The incorporation of trace elements into the apatite crystal structure modifies their solubility, and consequently, it affects the physicochemical and mechanical properties of enamel [4].

Regarding the structural arrangement, the human dental enamel is organized into rod like structures, known as enamel prisms, that can be discovered from the junction between enamel and dentin (the dentin-enamel junction - DEJ) until the outer enamel surface layer, which is the most exposed. From a structural point of view, the enamel prisms are usually interlocked with each other and organized in a keyhole configuration, with inter-crystalline spaces. Such structural arrangement with tiny spaces allows diffusion process of ions as it occurs in the process of caries development. Between the enamel prisms, there are small, tiny portions of organic matrix, which determines the permeability of the enamel structure. In sound enamel, the rods tend to orient themselves in perpendicular direction to the tooth surface, except the cervical margin of permanent teeth, where they are oriented outward in a slightly apical direction. The enamel prisms can vary from 4 to 6 µm in width. Each enamel prism is formed by numerous smaller crystals of hydroxyapatite $Ca_5(PO_4)_3OH$ [4, 9].

Nevertheless, most mineral crystals of the enamel prisms have a certain proportion of substitutions for calcium, phosphate, and hydroxyl groups. Fluoride can easily replace hydroxyl groups leading to the more stable crystal structure of fluorapatite ($Ca_5(PO_4)_3F$ - FAp). A less stable apatite can also be formed, when carbonate replaces the hydroxyl group or when phosphate and magnesium replace the calcium [10].

According to Marin et al. [11], enamel layers are constantly prone to natural demineralization and remineralization processes that can be caused by many different factors, such as food and beverages intake, presence of microbes, excessive brushing, dry mouth, and bruxism. It is already established that only a proper salivation and a good dental hygiene can compensate for the dissolution by reintroducing calcium and phosphate ions, in a slightly alkaline environment. Furthermore, the mechanisms and dynamics of the demineralization/remineralization processes are said to be complex and difficult to predict clinically, but when a certain threshold is reached, demineralization might become irreversible [11].

In [12], it was stated that the imbalance between the de/remineralization periods in enamel is the main cause of dental caries formation and progression. As the demineralization process proceeds, a lesion known as "white spot" is continuously developing, signaling changes in enamel chemical composition. By improving the diagnostic ability of initial caries lesions, will be consequently improved the potential of treatment as well, without any surgical intervention. Thus, the development of new diagnostic technologies with high sensitivity and high specificity is considered extremely necessary. As a result, based on the light scattering and fluorescence properties of dental tissues, Raman spectroscopic technique is a promising method that has the potential to detect dental caries much earlier than previously done [12].

According to Bulatov et al. [13], the mineral loss is mainly caused by the presence of acidogenic bacteria in the dental plaque, also known as cariogenic bacteria, which lead to a high production of low pH acids, mainly lactic acid, but also acetic and propionic acids, as by-products resulted from the carbohydrate metabolism. Lactic acid dissociates more readily and in a higher extent than the other acids, releasing hydrogen ions that rapidly decrease the overall pH of the dental plaque. As the pH declines, the present acid diffuses into the underlying enamel or dentin layers and dissolves the dental mineral content, causing calcium and phosphate ions to diffuse out of the surface, resulting in a constant and continuous demineralization. The demineralization process can be stopped only by tooth cleaning and compensated by remineralization, in order to re-establish the previous mineral balance [13].

2.2 - Dental caries

Dental caries is a common infectious bacterial oral disease that affects the teeth [14] and represents the leading prevalent chronic disease in the world [15]. Dental caries is considered a disease of multifactorial etiology, mediated by biofilms which depend directly on diet. Social, behavioral, and environmental factors influence dramatically the caries risk. It is a disease with a very high prevalence, representing a worldwide public health problem, while the taken decisions and resulting measures for its control are indeed a global challenge [15].

Dental caries is mainly caused by the presence of carbohydrates and acids produced by the present bacteria in the oral environment. *Streptococcus mutans* and *lactobacilli* are strong acid producers and, consequently, create a highly erosive environment which destroys gradually the enamel and dentine layers of the tooth. Dental caries, in long term, result in major tooth losses.

According to the World Health Organization report worldwide, between 60 and 90% of school teenagers and up to 100% of adults have dental caries [15, 16].

Caries represents a serious health problem, which can vary from the subsurface enamel layer demineralization to extensive deeper dentinal layer involvement at a clinical level [16]. According to the International Caries Detection and Assessment System (ICDAS), which is a clinical scoring system developed for clinical research, clinical practice and other epidemiological matters, the detection codes for the assessment of caries activity vary within the following range: 0 – Sound; 1 – 1st visual change in enamel; 2 – distinct visual change in enamel; 3 – localized enamel breakdown (fissure); 4 – underlying dark shadow from dentin; 5 – distinct cavity with visible dentin; and 6 – extensive distinct cavity with visible dentin [14].

2.3 - Current methods used for the clinical diagnosis of dental carious lesions

Correct and precise diagnosis of the carious lesion is of extreme importance in daily dental practice, which is increasingly focused on performing evidence-based non-invasive and painless modalities, or minimally invasive intervention treatments, aiming to reduce the dental tissues removal whenever possible, to promote and maintain the overall dental health [14, 15].

There are numerous methods employed for the diagnosis of carious lesions. Still, none of them has reached the maximal sensitivity and/or specificity (> 99%), so further research is still required to find a method that meets all the needs of dental care professionals. Despite all research studies dedicated for the development of improved methods for the early detection of dental carious lesions, in clinical practice the caries detection is still mostly limited to conventional visual and visual-tactile tools such as sharp explorers and dental radiographs [15, 17]. For instance, bitewing radiographs are still considered the gold standard for the diagnosis of interproximal caries [14, 15]. Dental radiographs are also useful in detecting larger, advanced dental caries, but limited image resolution and poor radiographic contrast of early carious lesions confer to radiographs reduced sensitivity for detecting early-stage dental caries [17-19].

Digital radiography method, combined with visual examination is the most common, widely used, and routine diagnostic technique for caries detection. Dental practitioners use frequently radiographs for the identification of mature and/or advanced caries. High demineralization in enamel and dentine layers, caused by the caries, results in a significant decrease in the attenuation of the X-ray beam through the dental hard tissue. An identified lesion appears in the visualized image as radiolucency. For the radiolucency to be clearly visible and

distinguishable, first must occur a major loss in the mineral content of the tooth (app. 40% to 60%). This technique was found to be more sensitive in detecting carious lesions and cavities that are deeply advanced into dentin, however not too efficient in detecting non-cavitated fissure caries. Evidence suggested higher specificity (59% - 90%) than sensitivity (14% – 38%) for detection of non-cavitated fissure caries, which means that a false-negative diagnosis is highly probably to occur [4, 14-16, 20].

The use and frequency of radiography must be always justified in routine examination since the exposure to ionizing radiation can be harmful to patients. The introduction of digital radiography replaced physical films and the images stored digitally, with the detection performance for dental caries reported to be approximately the same as analogue radiography. The main strengths of digital radiography include a lesser radiation exposure for the patient (reduced dose of received radiation), the obtainment of instant and reliable images, possibility of image enhancement, lack of necessity for a dark room, no hazards of film development, and data sharing capacity for easy and simple transfer/transmission of information. At the same time, numerous factors can impact the accuracy of radiography, such as exposure time, image processing, viewing conditions, training, and experience of the examiner. Another two major limitations are the high cost and durability of the used chip [16, 20].

Diagnosis adjunct methods based on light scattering property such as fiber-optic transillumination (FOTI) and digital imaging fiber-optic transillumination (DIFOTI), are additionally used by stomatologists for the obtention of relevant diagnostic information, complementary to the data obtained by conventional diagnostic methods. The FOTI method makes use of high-intensity white light in the visible range spectra (400–700 nm) to illuminate the tooth and to emphasize the contrast between the healthy and diseased enamel tissues. DIFOTI was developed to reduce the perceived inadequacies and to solve the deficiencies of FOTI, by combining FOTI with a digital CCD camera. DIFOTI has elevated traditional transillumination to more sophisticated diagnostic levels. The carious enamel scatters and absorbs more light compared to the sound enamel and, consequently, shows to be darker than the sound enamel, which is transparent. On the other hand, dentin layers show brown to grey colored spots or larger regions underneath the enamel. These distinct colors highlight the contrast between the examined tissues, revealing a clear differentiation between enamel and dentin lesions. The main advantages of this technique rely on the detection of initial areas of demineralization, pits and fissures, cracks, tooth fractures, and wear. Its use does not imply any ionizing harmful radiation, using instead safe white light. It provides images of all dental coronal sides, including interproximal,

occlusal, smooth surfaces. It can easily determine the depth of the examined lesion with great accuracy, being the only dental diagnostic imaging instrument approved by the Food and Drug Administration for detection of incipient and recurrent caries. Real-time visualization with a magnification of up to ×16 is possible. On the other hand, it is an expensive method (especially DIFOTI), which implies high cost of acquisition and maintenance; it is not quantitative, with diagnostic decisions based mostly on subjective outcomes determined and discerned visually. Therefore, this technique can result in low reliability scores due to subjective interpretation of the image by the operator. Furthermore, variability of the ambient light can interfere with the light beam used by this method, which implies having the dental operating lights switched during the use of such devices [16, 20].

Near-infrared laser transillumination (NILT) method employs NIR light for the detection of enamel lesions and can discriminate between the extent of the lesion limited to the enamel from the ones that have reached the dentin-enamel junction (DEJ). This technology works on a similar mechanism to FOTI technique, having the visible white light is replaced by NIR light (range between 750–1500 nm), which appears to have a more efficient and deeper penetration depth in the enamel. The enamel layers are highly transparent in the NIR range due to less scattering and absorption. The main strengths of NILT are that is a non-invasive and painless method, not confounded by stains, which can be used to map the horizontal extension of a caries lesion. Furthermore, the performance of NILT is comparable to a LF system DIAGNOdent® pen and QLF methods and therefore it is established as a valid and reliable technique for the detection of incipient occlusal caries on the permanent teeth [16, 20].

Quantitative laser/light-induced fluorescence (QLF) technique involves the principle of fluorescence. This method allows the early detection of carious lesions, mainly the progression or regression of white spots of smooth surface lesions. QLF is based on the excitation of the tooth with ultraviolet/purple light at a wavelength of 370 nm, which results in the emission of yellow-green fluorescence caused by fluorophores that are located within the DEJ, providing this way a fluorescent image of the examined tooth surface in a spectrum of yellow-green visible light that quantifies mineral loss and provides the size of the lesion – area, depth, and volume, which are relevant parameters. It is considered an appropriate method for quantitative assessment of early enamel lesions in areas that are visually unreachable. Demineralized areas between the outer enamel layers and DEJ appear dark on a green fluorescence background. This process is caused by the increased scattered light by the porous demineralized area resulting in less light reaching the DEJ, hence decreasing the fluorescence photons that reach the surface from the

DEJ. Therefore, this substantial difference in fluorescence between the sound and demineralized enamel can be precisely quantified and used to monitor the identified lesion progression over time [16, 20].

The key strengths of QLF are the following: very early caries detection and quantification; *in-vivo* and *in-vitro* quantitative assessment of carious lesions, plaque, calculus, and staining; besides the quantification of mineral loss and lesion dimensions, helps to assess the severity; it has high sensitivity, precision, and repeatability; the acquired images can be safely stored and transmitted for transfer purposes. Its main limitations are the difficulty of detecting effectively incipient lesions; it can only distinguish enamel demineralization but cannot differentiate between decay, hyperplasia, or unusual anatomic features; it is unable to detect or monitor interproximal lesions, being limited to measurements of enamel lesions at few hundred micrometres depth. It is an expensive device, and although this technique has confirmed the ability of monitoring early enamel lesions on the smooth surface, there is a tremendous lack of studies on its specific utility for non-cavitated caries detection [16, 20].

Laser fluorescence-based method (LF) is another modality frequently used for the detection and quantification of dental caries. The DIAGNOdent® is a commercially available LF device that contains a sensor for the detection of dental superficial tissue changes, measured in backscattered fluorescence, to detect and identify the carious lesions. This technique uses a monochromatic red laser beam (655 nm wavelength) that is emitted onto and incident upon the tooth surface and the backscattered red fluorescence from the tooth is detected. This modern technique responds to fluorescence radiated from proto-porphyrin, meso-porphyrin, and other metabolites of cariogenic bacteria present in the porosities of caries lesions. The exhibited fluorescence is directly proportional to the severity degree and extension of detected caries. That is, numeric values varying between 0 (minimum fluorescence level) and 99 (maximum fluorescence level) show the degree of fluorescence, with higher fluorescence corresponding to very severe lesion. The major advantages of this method are mainly the high sensitivity and specificity, precision, and reliability. It provides reproducible results that enable checking, stabilization, and documentation. Small lesions that are usually missed out or unobserved by conventional methods can be detected by it at the earliest stages, with over 90% accuracy to diagnose pit-and-fissure caries, proximal caries, calculus, and periodontitis. It provides a simply early detection of slight pathological changes that are unseen or undiagnosed by conventional methods. Simply, user-friendly, non-invasive, pain-free, safe, easy, and quick to use, without any radiation exposure. It can yield accurate, real-time, and good-time results, exposed through

elevated scale readings on the display. In addition, it is readily transportable with flexible unit which is battery operated [16, 20].

However, it is not a flawless technique, with a relatively high cost, and with several disadvantages. Among them, the obtention of false results with plaque and debris. It may not be useful for a precise detection of proximal caries and recurrent caries, while the displayed readings do not relate to the amount of dentinal decay. Moreover, it was also observed, in real practice, that DIAGNOdent® works unsurpassed in detecting advanced carious lesions but it's not too indicated for the detection of early carious lesions. It was reported that DIAGNOdent® results did not correlate well [Pearson correlation coefficient (0.21)] with the depth of incipient occlusal caries. Furthermore, since the fundamental basis of DIAGNOdent® is registering the presence of porphyrin fluorescence and not the overall mineral content of the enamel structure, high false-positive readings and poor correlation coefficients with the mineral content are probable. This fluorescent phenomenon can also be confounded by stain, plaque, and calculus that are commonly present in carious pits and fissures. It has also been reported that the quality of obtained evidence for the detection of non-cavitated fissure caries was poor, with the recommendation that this recent tool should be used with attention, due to high probability of false-positive diagnosis [16, 20].

DIAGNOdent® pen is a more recent advancement made in the DIAGNOdent technology, which is considered by many as a perfect option to detect enamel superficial fissures and smooth surface caries accurately. It is a cordless mobile device, which can be easily transported and used anywhere. It is also handy, user-friendly, simple, precise, fast and use to always there when needed, providing complete caries detection, with a high intra-examiner reliability [20].

Another method used for the caries diagnosis is based on the ultrasound principle. The ultrasonic caries detector is considered as a reliable tool that provides fast and accurate results for the detection of dental caries, being more effective in detecting proximal caries that cannot be seen on radiographs. It is mainly limited by the fact that is not a quantitative method [20].

Usually, conventional tools are qualitative, often showing a poor validity with low sensitivity and moderate specificity, a fact that turns a quantitative diagnosis method more valuable than a qualitative one. Therefore, there is still a tremendous need for quantitative detection techniques and advanced diagnosis methods, with more sophisticated data analysis. This implies that caries diagnosis, as normally performed in daily clinical practice, can be a very subjective and inexact procedure that might result in both over- and under-diagnosis. Advanced diagnostic

methods, such as DIFOTI, QLF and LF, can detect and quantify the severity degree of the carious lesions at an earlier stage and, in many cases, appear to be a lot more reliable than the conventional or traditional methods [20]. For these reasons, they are increasingly used as complementary or alternative diagnostic methods to the conventional methods, based on visual-tactile examinations combined with digital radiography, to increase the precision and accuracy of recognition and identification of incipient caries and superficial lesions that are difficult to observe in occlusal and interproximal regions, also to confirm and help quantify their severity.

There are many options for caries diagnosis and several techniques for dental mineralization assessment, each of them functioning better for certain types of lesions. However, an ideal diagnostic tool should detect dental caries and incipient lesions in the earliest stage possible, provide valid potential caries risk and severity degree assessment for different age groups, and above all, make possible to determine exactly the caries activity and monitor the carious lesions behavior and progress over time. Based on the described diagnostic methods, the main analytical requirements of a highly efficient method for caries diagnosis would be: accuracy, precision, high sensitivity and specificity, objectivity, validity, reproducibility, and consistency; as well as instrumental requisites such as measurement repeatability, non-invasiveness, pain-free, simple and easy to apply, user-friendly, rapidity and real-time outcome, useful for all surfaces and orientation angles of teeth surfaces, cost-efficient, able to identify carious lesions even in inaccessible or hard-to-reach regions of the examined tooth, detect caries adjacent to restorations, resistant to environment changes (humidity, pressure and temperature), robustness of the equipment and durability (batteries, filters, laser and other components) [14-16, 20].

3

RAMAN SPECTROSCOPY

3.1 - Background

Raman technique, a form of vibrational spectroscopy [21] and a highly versatile technique, is presently considered a promising and viable optical method for different biomedical applications on both organic and inorganic materials, mainly due to its uniqueness and precise results, reliability, non-destructive and non-invasive modality to analyze and provide detailed information about chemical composition and structure, chemical bonding, phase and polymorphism, degree of crystallinity, intramolecular bonds and molecular interactions of molecules within a material or mixed compound, based on the use of light-excited vibrational energy states in molecules. It provides a structural fingerprint for the identification of a particular molecule, or several molecules contained by a certain material/compound, mixture of compounds – solid, powder or within solution, by a vital biological tissue or sample layer - enamel [2, 21, 22].

Raman spectroscopy is also well-known and widely used especially for its high biochemical specificity (applied for analysis from bulk mixtures down to micro or nano scale), low water sensitivity in the fingerprint region (water is a weak Raman scatterer, and it doesn't interfere in the spectral analysis of inorganic materials within the range of 200-2000 cm^{-1}, being Raman active only in the high-wavenumber region, at around 3600 cm^{-1}) and capability to work in the near-infrared (NIR) region with fiber-optics, as well as great flexibility during the spectra acquisition (of several types of contents, such as powders, solid samples of different sizes under different angles, liquid solutions) and sample analysis process. Additionally, is a highly sensitive and selective technique, meaning that it can distinguish with a very good precision slight molecular alterations and distinct molecules in different chemical species or compounds that are very similar. Moreover, it requires little to no sample preparation, with real-time and fast measurements that can be performed directly through transparent containers, such as multi-layered plastic bags, glasses, jars, cuvettes, or other types [1, 17, 22].

Nowadays, Raman technique is widely employed due to the simplicity to measure samples/tissues, dry or within solution, which is highly compatible with physiological condition. It yields objective spectral results, being highly sensitive to the phase or state of the sample, or to the morphology of the examined specimen or material, according to the case, and provides possibility to perform measurements *in-situ* and *in-vivo*.

Although is a sensitive technique, the measurements (spectral acquisitions) are not affected by different conditions or by the sample type or characteristics, which enables its applications to different samples, of different shape, size, and phase. It is considered by many an excellent and powerful tool for the local analysis by using the laser beam as a monochromatic light source (laser signal can be easily transmitted and Raman scattered photons can be efficiently collected by optical fibers over short or long distances for remote and *in-situ* analysis). This technique provides a fast detection and identification of different molecules (based on chemical composition and structural arrangement) and minerals (chemical composition, structure, morphology and crystal orientation), since Raman spectra can be acquired quickly (short duration time, varying from seconds within few minutes, depending on the examined area). It can be employed for real time monitoring (for different types of samples, in distinct research areas, in this case - dentistry). Raman spectra can be obtained and collected even from a very small volume sample (< 1 μm in diameter, if coupled to a microscope), usually used in the analysis of micron-level sample contaminants, presence of porphyrins due to bacterial activity, defects, or deposition of extremely thin superficial layers (such as dental films) and the examination of surface micro-structures and orientation. Moreover, automated chemical analysis can be rapidly performed by any researchers with different levels of training and expertise [1, 17, 22-29].

According to Zhang et al. [30], Raman technique can yield clear and obvious differences between dental caries and intact tooth tissues, at compositional and structural levels. Hence, the potential of Raman spectroscopy in the diagnosis and prognosis of dental caries is more than obvious. It is a precise tool that can be used for oral hard and soft tissues assessment, differentiation, and classification [30].

However, despite of the fact that is an increasingly popular and widespread technique, the main disadvantages are (1) the high (or even unaffordable) cost of the equipment and related optical components or accessories, which can be a real obstacle to the widespread employment of this technique for routine analysis; (2) It cannot be used for pure metals or alloys, as they are Raman inactive; (3) Raman effect is intrinsically very weak (an extremely small fraction of light of approximately 1 in 10^7 photons is scattered from the incident photons) - the detection needs a

sensitive detector and highly optimized instrumentation, and especially for biological specimens, the Raman signals are inherently weak without utilizing enhancement or amplification effects, requiring for a performant pre-processing, highly efficient filtering, greater laser power or increased acquisition time; (4) Fluorescence (intrinsic, for organic samples, or caused by contaminants/impurities; several compounds fluoresce when irradiated by the laser beam) affect the quality of the Raman spectrum; (5) Sample local heating - through the intense laser radiation can destroy (alter, denature or decompose), cause irreversible damage to the sample or cover the acquired Raman spectra; (6) Shallow penetration depth of the light beam [1, 17, 22-27, 29].

3.2 - Fundamentals and basic principles of Raman Spectroscopy

Electromagnetic radiation can interact directly with matter through absorption, transmittance, and/or scattering phenomena. An absorption process requires a corresponding incident photon's energy with the energy gap between two existing electronic energy levels [31]. Raman technique is based on the main physical principle that when light arrives to an examined sample, a small part of it – 1 in 10^6-10^7 photons, gets scattered in many different directions [21, 23]. When considering Raman scattering, we can explain it by two possible theoretical approaches: (1) the classical approach and (2) the quantum-mechanical interpretation. If considering the (1) classical-wave definition, all electromagnetic radiation has an electric field associated with it, and the electric field of the incident light beam can interact with the molecules in the sample through the polarizability of these molecules [21, 31].

The Raman effect is mainly based upon the interaction of incident light with the chemical bonds of molecules within a material, leading to an interaction between the electron cloud of that material and the external electric field of the monochromatic light, which can cause an induced dipole moment – **p**, based on molecules' polarizability. For a vibration to be Raman active, a change in polarizability of a molecular bond must occur. Polarizability defines a molecules' capacity to distort its original shape by the influence of an external electrical field, also inducing a distortion of its electron cloud and changing the species polarization involving virtual states. It is a quantitative term expressing how easily electrons in a molecule can be moved to induce a dipole [21].

Therefore, when a certain molecule is positioned in an electrical field - **E**, is induced, as consequence, an electrical dipole moment - **p**. The relation between the induced dipole moment - **p** and the electrical field – **E** can be expressed as a power series – equation (3.1).

$$\mathbf{p = \alpha \bullet E + (1/2) \bullet \beta \bullet E^2 + (1/6) \bullet \gamma \bullet E^3 \ldots} \quad \textbf{(3.1) [21]}$$

In this equation (3.1), **α, β** and **γ** are tensors, which are known for **polarizability**, **hyperpolarizability** and **2nd hyperpolarizability**, respectively. These tensors are typically in the range of ca. $\boldsymbol{\alpha} \sim 10^{-40}$ C • V^{-1} • m^2, $\boldsymbol{\beta} \sim 10^{-50}$ C• V^{-2} • m^3 and $\boldsymbol{\gamma} \sim 10^{-60}$ C • V^{-3} • m^4. Since all these tensors are each a factor of 10^{-10} less intense, the influence of 2nd and 3rd factors can in many cases be neglected, resulting in a reduced equation (3.2). Therefore, the induced dipole moment - **p** can be considered as directly proportional to the electrical field – **E** [21].

$$\mathbf{p = \alpha \bullet E + (1/2) \bullet \beta \bullet E^2 + (1/6) \bullet \gamma \bullet E^3 \ldots} \quad \textbf{(3.1)} \quad \rightarrow \quad \mathbf{p = \alpha \bullet E} \qquad \textbf{(3.2) [21]}$$

In Equation (3.2) the term **α** is a polarizability tensor, which is directly dependent on the shape and dimensions of the chemical bond of the examined molecule or compound. Since chemical bonds change during vibrations, it means that **α** is highly dependent on the vibrations of the molecule. Therefore, it can be affirmed that the polarizability tensor (α) is dependent on the normal coordinate **Q** of the examined molecule. Approximating, Q oscillates according to the harmonic oscillator and varies as a function of time, with 2 main components: the amplitude of the normal vibration - $\mathbf{Q}_{v0}$ and the phase angle - $\boldsymbol{\varphi}_v$. It is assumed that the polarizability tensor **α** undergoes a harmonic oscillation, with a frequency ν_v, that equals the vibrational frequency of the normal coordinate **Q** [21].

The induced dipole moment - **p** can be regarded as a function of the vibrational frequencies of the molecule ($\boldsymbol{\nu}_v$) and of the incident radiation ($\boldsymbol{\nu}_0$), resulting in (3.3), with the induced dipole moment - **p** split into 3 different components, each with a different frequency-dependence.

$$\mathbf{p = p\,(\nu_0) + p\,(\nu_0 + \nu_v) + p\,(\nu_0 - \nu_v)} \qquad \textbf{(3.3) [21]}$$

The 1st term in (3.3) - $\mathbf{p(\nu_0)}$ – is the dipole moment induced by the elastic scattering process of the incident electromagnetic radiation and has the same frequency (hence the same energy) as the incoming incident radiation. This type of scattering is known as Rayleigh scattering. The 2nd and 3rd terms in equation (3.3) are assigned to the inelastic scattering of light: Raman scattering, with the 2nd term corresponding to a higher energy level of the scattered radiation,

compared to the initial incoming beam - called anti-Stokes scattering, while the 3rd term represents a decrease of the frequency – known as Stokes scattering [21].

Therefore, the occurrence of the Raman effect requires a change in its polarizability with respect to the vibrational state, being directly related to the ability of electronic clouds surrounding the molecule to interact with the electrical field, being a proportionality factor between the external field and the induced dipole moment in equation (3.2), being physically related directly to the extent to which the driving field can interact with the molecule, interfere with the molecule's vibration, and disturb the electron density out of its equilibrium configuration (which corresponds to its initial configuration in the absence of an external field). Consequently, the size of molecular vibrations (vibrational frequency) is inversely proportional to molecule's (reduced) mass - μ and directly proportional to the molecule's bond strength, directly depending on k, which is the force constant of the bond [21, 23].

By definition, light is composed by particles (photons). From the (2) quantum mechanical interpretation, Raman scattering is a result of an energy transition of the scattering molecule to a virtual excited state (the transition between energy levels is not real, being considered virtual) and its return to a higher (or lower) vibrational state with the emission of an altered incident photon, scattered with a different direction and energy from the incident photons. Because energy can be transferred from the photon to the molecule or in the opposite way - from the molecule to the photon, the scattered photon can have less or more energy compared to the incident photon. When the scattered photon has lower energy than the incident photons, the process is referred to as Raman Stokes scattering. And conversely, when the scattered photon has a higher energy than the incident photons, the process is referred to as Raman anti-Stokes scattering [2].

Thus, from the 2) quantum mechanical point-of-view, Raman scattering process can be interpreted by assessing the energy transitions of the involved molecules to virtual levels of unstable states that do not correspond to real electronic excited states. Raman scattering occurs with alterations at vibrational levels. When these light photons are scattered from a molecule or crystal, most photons are elastically and inelastically dispersed. The larger part of the scattered photons has the same frequency as the incident photons. However, a small fraction of light (approximately 1 in 10^7 photons) is scattered at optical frequencies different from, and usually lower than, the frequency of the incident photons. If the energy of the incident photon is not sufficient to excite the molecule to a superior electronic state, this will absorb the energy of the

incoming photon and will turn excited to a superior virtual level of energy. By relaxing from this virtual state to an inferior electronic state, ends by emitting a photon with a different frequency. If the scattering is elastic, the process is called Rayleigh scattering. If, contrarily, it is inelastic, the process is known as Raman scattering: Stokes (lower frequency, higher wavelength) and anti-Stokes (higher frequency, lower wavelength) [21], shown in Figure 3.1.

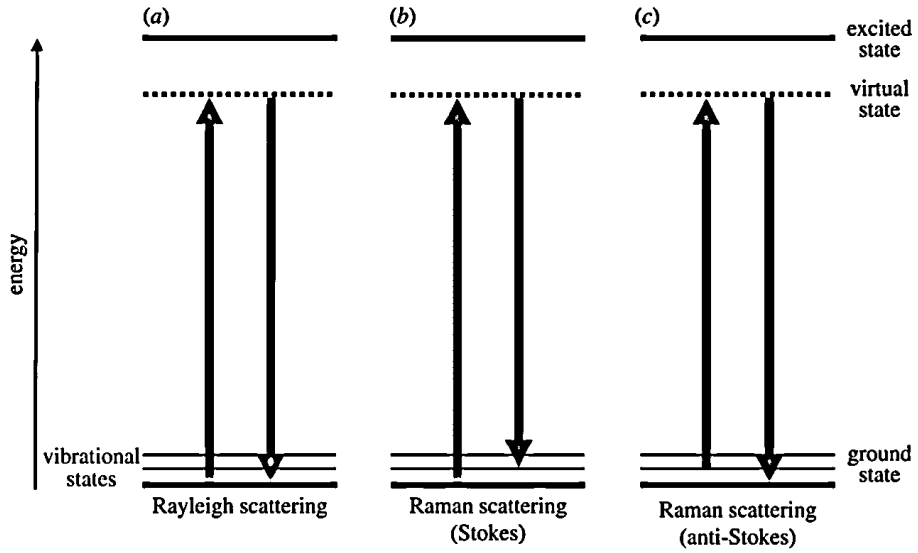

Figure 3.1 – Energy level diagram for Raman scattering: (a) Rayleigh, (b) Stokes, and (c) anti-Stokes scattering.

The intensity of the Raman scattered radiation - $\mathbf{I_R}$ can be described by the following:

$$\mathbf{I_R \propto I_0 \bullet \upsilon^4 \bullet} \ N \ (\partial \alpha / \partial Q)^2 \ \textbf{(3.4) [31]}$$

where $\mathbf{I_0}$ and $\boldsymbol{\upsilon}$ are the intensity and the frequency of the incident radiation beam, respectively; while N is the number of scattering molecules in a certain state; $\boldsymbol{\alpha}$ is the polarizability tensor; and, lastly, **Q** represents the amplitude of the vibrational coordinate. The incident laser beam intensity $\mathbf{I_0}$ can be measured in $W \bullet m^{-2}$, while the frequency $\boldsymbol{\upsilon}$ is expressed in Hz (s^{-1}), the polarizability tensor $\boldsymbol{\alpha}$ - in $C \bullet V^{-1} \bullet m^2$, and the amplitude Q - in m. The obtained Raman intensity $\mathbf{I_R}$ is usually expressed in arbitrary units or counts. The resulting Raman spectrum is a plot of Raman light intensity or inelastically scattered photon counts - $\mathbf{I_R}$ in function of the absolute frequency (Figure 3.2) or frequency differences (were Rayleigh = 0) of the measured scattered light, expressed in frequency units – wavenumbers (cm^{-1}). Once more, with the polarizability term included in this equation is proven that Raman scattering phenomenon can occur only with a change in polarizability due to the interaction with the incoming (incident) photon [31].

Raman spectroscopy technique implies the use of an intense, monochromatic beam of electromagnetic radiation (usually a laser) that is focused on the examined sample, and the intensity of the scattered Raman radiation is measured as a function of its wavelength. Usually, in a

Raman spectrum the spectral intensity is plotted as a function of the Raman wavenumber ω, expressed in cm^{-1}, which is related to the difference in frequency between the scattered light and the incident electromagnetic radiation. The band with lesser energy is known as Stokes band, the band with greater energy is referred to as the anti-Stokes band, while the central band is called the Rayleigh band [21, 31], as shown in Figure 3.1, and Figure 3.2 [32].

Summarizing, the Raman effect is identified as a main consequence of the change of frequency and related energy of an excitation monochromatic light beam, induced by vibrations of the molecule under examination.

Generally, the acquired spectra for sample investigation are mainly based on Stokes scattering, with the spectral bands varying in intensity (expressed in arbitrary units or counts of the detector), depending on the relative quantity or concentration of the analyzed compound or sample, and with variable band (frequency) position according to the chemical composition and vibrational modes of the analyzed molecules, band width and band (frequency) shifts (position increase or decrease), specific for each compound, according to its crystallinity degree, material phase, polymorphism or applied stress [21, 23, 31], as shown in Figure 3.2 [32].

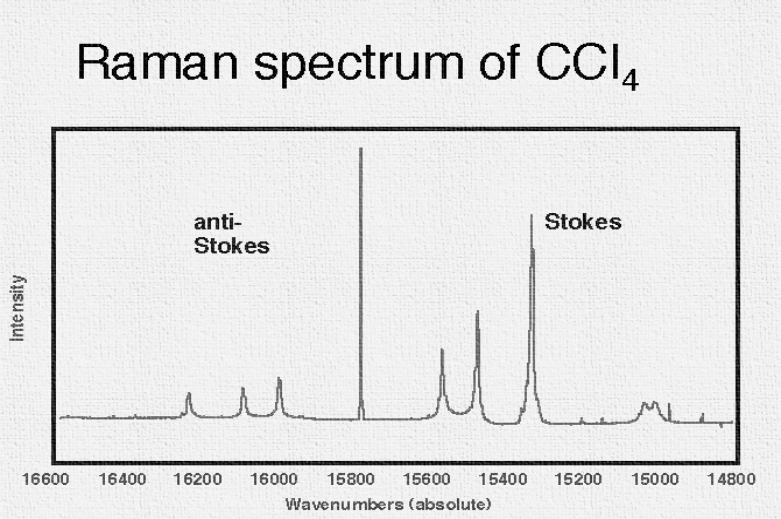

Figure 3.2 – Raman full spectrum of CCl_4 revealing 3 main types of scattering; Rayleigh (middle), Stokes (right), and anti-Stokes scattering (left) [32].

3.3 - Advantages and limitations

Until now, RS technique has been shown to be an advantageous and promising tool, with several unique strengths, however with major withdraws. According to Eberhardt et al. [33], this technique has the following advantages and disadvantages, represented in the Table 3.1:

Table 3.1 – Advantages and disadvantages of Raman technique for molecular diagnostics [33].

Advantages	Limitations and drawbacks
- Non-destructive, non-invasive (excitation wavelength and power dependent)	- Autofluorescence (sample dependent)
- No to minimal sample preparation	- In certain cases, low sensitivity
- Label free, no dyes and eventual toxic waste products	- Inherently weak Raman signal requires for long acquisition times
- High specificity	- Slow imaging by point-by-point scanning
- Simultaneous detection of different molecules or compounds	- Low scattering efficiency that results in increased measurement times
- Compatible with physiological measurements due to low-water interference	- Sophisticated multivariate data analysis algorithms often required
- Possibility of remote measurements and *in-vivo* applications through fiber-optic probes	- High-cost of the benchtop equipment and fiber-optic based technology
- Appropriate for chemical analysis, quantification, differentiation, classification, monitoring and virtual false-color mapping of biological samples	- Sample heating (may denature, decompose, or cause severe irreversible damages *in-vivo*), depending on the used power and acquisition time
- Real-time monitoring or assessment	- Shallow penetration depth of the light beam
- Detection at micron-level of contaminants, presence of porphyrins due to bacterial activity, minute defects, or deposition of extremely thin superficial layers	

Most of the limitations of Raman spectroscopy technique are directly associated with the inherent weakness of the effect – approximately 1 in 10^7 photons, which requires usually longer measurement times. The potential of damaging the sample through heating due to a longer laser exposure, which always depends on the excitation wavelength, the applied power on the measured spot and the type of the examined sample (whether it is biological, organic, or mineral) must be always considered for the planning of the measurements.

3.4 – Sample heating

An important limiting factor that should be seriously considered, before applying the probe *in-vivo,* is the sample local heating, which can result in irreversible damage of both hard (enamel and dentine) and soft (pulp, cement, nerves, and gingiva) oral tissues. To minimize the risk of temporary temperature increase, which might cause a critical or irreversible condition of the enamel and surrounding and inner tissues of a vital tooth, it must be established the limit for the duration of spectral acquisition time, in order to obtain high-quality spectra without affecting the sample, depending on the combination of excitation laser monochromatic beam wavelength and incident radiation power on the sample [33, 34].

This must be in accordance with the specific heat values of the examined inorganic material or organic tissue, enamel, and dentine, expressed in $J \cdot kg^{-1} \cdot K^{-1}$ [33, 34]. These values, according to Magalhaes et al. [34], are 1750 $J\ kg^{-1}\ K^{-1}$ for enamel, and 1420 $J\ kg^{-1}\ K^{-1}$ for dentine. It is also worth mentioning that the temperature rise for which irreversible damage is caused is about 6 temperature degrees superior to the body temperature in normal conditions – 37 °C (Celsius degree). Therefore, if we examine an enamel specimen or tooth portion that weighs about 0.01 kg, the Raman device or Raman instrumental setup (fiber-optic remote probe coupled to the benchtop equipment) should be optimized for obtaining sharp, intense and well-defined spectra, allowing for the observation of the bands of interest with good spectral-resolution, for a laser power of maximum 90 mW with an overall acquisition duration of 20s (it should not exceed 30s, to avoid heating superior to 1K in short time). If the used power was around 50 mW, the acquisition duration can be increased up until 60s, in order to obtain a Raman spectrum with good SNR, with well-defined and sharp spectral peaks. The lesser the incident power - greater the measurement time and exposure. Also, an additional solution could be repetitive alternating measurements: with short duration of 10s – laser incident on enamel surface, followed by 10s interruption - with no laser beam applied to the sample surface [34].

For this reason, in order to avoid burn, injury, denaturation or irreversible damage by heating of the biological organic samples, especially in case of *in-vivo* direct measurements of vital tissue, these are often investigated using preferentially a low-energy near-infrared wavelength for excitation (mainly 785 nm or 830 nm) [33].

3.5 - Fluorescence

A main problem in Raman spectroscopy/microscopy represents the fluorescence of the sample, which can severely affect or completely mask the spectra of the obtained Raman signals. The efficiency of Raman scattering is proportional to λ^{-4} (Raman intensity is proportional to the 4th power of the laser frequency ~ ν^4 [21]). Consequently, it is strongly enhanced at shorter wavelengths (higher frequencies) of incident light, resulting in a significant intensity decrease of 15 times going from blue to an infrared laser. At the same time, the excitation in the visible region causes strong fluorescence of real biological (organic) samples [35]. If the incident photon has sufficient energy, electrons in the sample are excited to higher states of energy and during relaxation to their ground state they emit light of longer wavelengths than that of the incident light. This means that together with the Raman scattered photons, these fluorescence wavelengths are also able to overpass the edge or long pass filters that are specially designed to block the incident light and Rayleigh radiation. Critically, fluorescence is up to several orders of magnitude more efficient than Raman scattering, so an organic sample, or one that contains strong fluorophores (mixed compound, defects, inclusions, or contaminants) will emit fluorescence that would clearly overwhelm the weak Raman signals. There are two major solutions for solving the fluorescence problem. First is the removal of it during spectral processing. There are several fluorescence rejection or correction algorithms that can effectively remove or, at least, avoid and significantly minimize the fluorescence levels regardless of the laser wavelength used. Secondly, since fluorescence has very specific excitation and emission parameters, the excitation wavelength of the incident laser beam can be chosen to minimize fluorescence. By increasing the laser wavelength, the energy is consequently reduced so as not to promote fluorescence, with insufficient energy to excite/stimulate the electrons to higher energy levels. Typically, longer wavelength, ranging from red to NIR, with over 700 nm do not cause or lowers considerably fluorescence in organic samples. Therefore, a proper choice of the laser wavelength for a certain measurement of a specific sample has a great impact on the needed trade-off between Raman efficiency and fluorescence effect. The longer the wavelength of the employed laser source, such as NIR, greater the possibility for the avoidance of the fluorescence [21, 23, 33].

According to Buchwald et al. [36], laser-induced fluorescence can be clearly detected and seen in the Raman spectrum background, which was often reported to be very problematic. Biological tissues, including teeth, exhibit strong fluorescence emission during Raman spectra measurements, making the spectral analysis more difficult. Nevertheless, the obtained information

that results from the background of the Raman spectrum is considered very useful for caries detection. The background intensity can reveal the fluorescent compounds in the enamel, such as bacterial porphyrins, which usually appear in the caries lesion or organic compounds located in plaque or calculus. During their studies, these authors observed substantially increased fluorescence levels in Raman spectra acquired at the natural caries lesion in accordance with their own predictions [36].

3.6 - Raman spectral parameters

There are several important spectral parameters that can be extracted from a Raman spectrum, as shown in Figure 3.3, acquired from either an enamel sample, or other materials, according to the specific case, that can be used not only to detect a certain molecule or identify a specific compound, but also to characterize a surface layer according to the biochemical composition, molecular structure, structural arrangement and orientation, phase and degree of crystallinity, which helps to detect and differentiate between similar molecular species, and classify distinct and/or more complex compounds, mixtures or biologic sample groups.

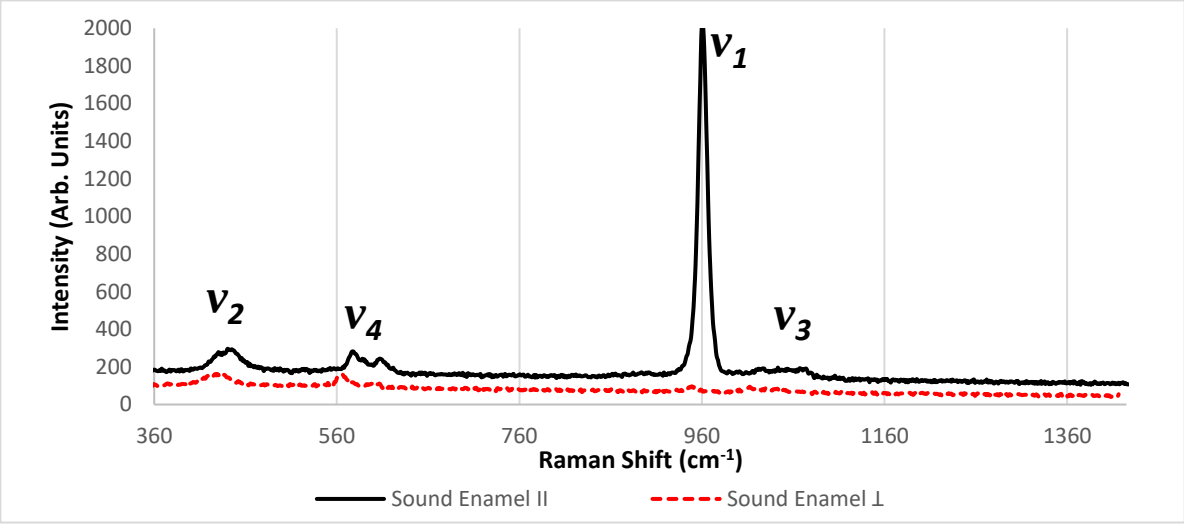

Figure 3.3 – Representation of two Raman spectra, obtained with parallel and cross-polarized configurations, acquired from dental sound enamel. Raman peaks ν_2 at approximately 430-433 cm^{-1}, and ν_4 at ~590 cm^{-1}, with shoulders at 448 and 610 cm^{-1} were attributed to PO_4^{-3} groups in symmetric ν_2 and asymmetric ν_4 bending vibrations, respectively. Peak ν_1 is assigned to symmetric stretching band of phosphate at ~959 cm^{-1}, while ν_3 corresponds to a band at ~1043 cm^{-1}, which is also attributed to PO_4^{-3} groups in the asymmetric stretching vibration of hydroxyapatite. The peak at 1070 cm^{-1} is assigned to B-type carbonate. [Spectra obtained using Horiba XploRA confocal microscope equipped with a NIR laser diode source operating at a wavelength of 785 nm].

Hence, the main spectral parameters are the following:

- Raman band/peak intensity provides information on material relative concentration and distribution, the polarizability factor of the chemical bond, and additionally, material traceability or detectability (defined as the capability of being detectable to certain extent). In the case of enamel, the amplitude of the phosphate peak in the Raman spectrum is directly proportional to the amount of mineral content [5], also to the examined enamel layer thickness.
- Raman band position (as a function of frequency, expressed in wavenumbers, specific to a certain molecule, compound, material, or tissue) yields unique information on the examined material composition (fingerprint). The bands of interest, for each molecule or compound, that are assigned to different vibrational modes and/or groups, are detected at specific positions.
- Raman band shift (band position increase or decrease) can reveal structural changes, phase, as well as material stress/strain. It shows if the sample was prone to certain significant alterations at conformational and compositional level, such as phase transition, or deformation, elongation, increased pressure, stress and/or temperature.
- Raman band width is a precise characteristic of crystallinity (degree), amorphousness, molecular orientation, molecular alignment and material phase, a parameter often used for the detection of defects, impurities, contaminants and/or doping content.
- Raman band polarization provides relevant information on the material' molecular orientation, crystal orientation and alignment, crystallinity, structural arrangement and/or symmetry.

  In the case of dental enamel, by using the ~959 cm^{-1} phosphate band intensities obtained with different polarizations, one can calculate the depolarization ratio and anisotropy values [4, 38, 39].

3.7 – Polarized Raman spectroscopy

Polarized Raman spectra (Figure 3.3) are measured with different polarization conditions of the incident and scattered light, controlling the polarization of outgoing and incoming signal (Figure 3.4). In order to control the polarization state of the incident light, a rotating half-wave plate (HWP) controlled mechanically is placed in the laser path. Another polarizer, called analyzer (PA), is positioned before spectrometer to enable the selection of the desired polarization component of the scattered light. In this way, by rotating the HWP, the laser polarization is varied in relation to that of the analyzer, obtaining different angles of the polarization direction of the linearly polarized (LP) laser light with respect to that of the polarization analyzer. By changing the analyzer (PA) angle only photons with a specific polarization can pass. Linear parallel-polarized and cross-polarized spectra can be obtained with the analyzer (PA) polarization oriented parallel (||) and perpendicular (⊥) to that of the linearly polarized (LP) laser light, respectively [17, 21, 31, 37-39]. Polarized Raman spectroscopy is regarded as a useful technique for studying molecular structure. For randomly oriented molecules in solution, the depolarization ratio (ρ) is mainly dependent on

vibrational symmetry and therefore can aid in peaks assignments. While in solid samples such as crystals, when molecular orientation is known relative to the polarization of the laser beam's electric field, the depolarization ratio (ρ) is strongly influenced by molecular alignment, thus providing additional important structural information [39].

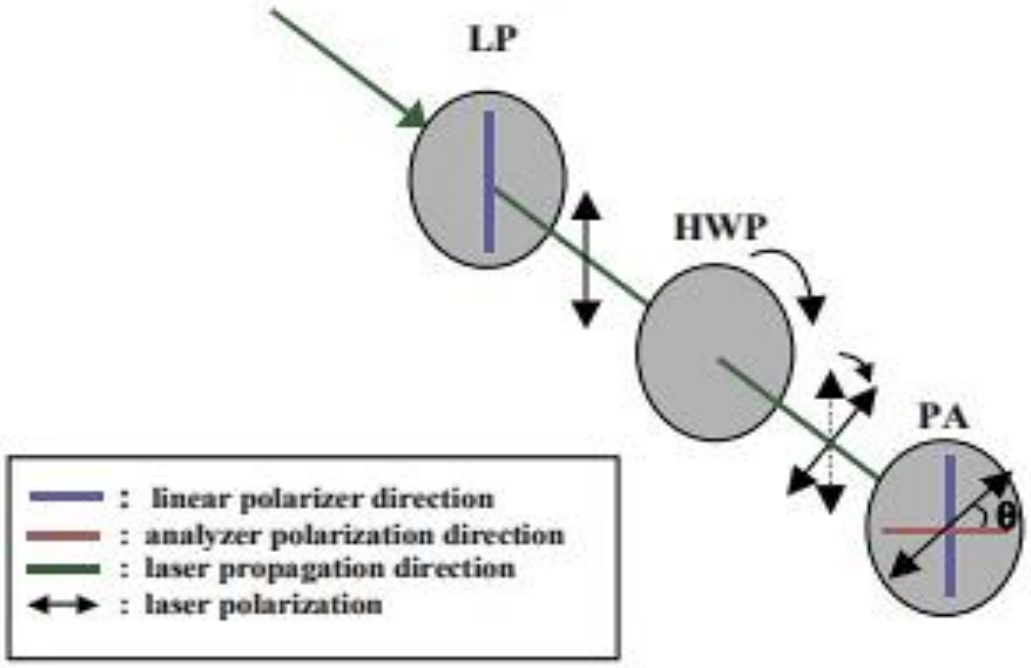

Figure 3.4 – Schematic representation of the polarized Raman system, indicating the definition of angle (θ) between the laser polarization direction and the analyzer polarization direction (PA) [39].

Therefore, Raman spectroscopy does not only identify with great accuracy and precision the examined material. This technique can also detect changes in its chemical composition, conformation/physical form, including morphology (biologic samples) and crystallinity variations (minerals), amorphousness, polymorphism (polymers), material phase (solids), primary and secondary structural modifications and can detect other general molecular backbone or structural changes due to compressive, tensile or shear deforming stresses, or erosive action of different acids.

Thus, the Raman spectral parameters can provide specific molecular fingerprint information and can reveal the sample sound or pathological state in label-free manner. In the case of enamel, the main parameters used for mineralization assessment or early carious detection are the band intensity (amplitude), band integrated area, bandwidth (FWHM) and band position (shift) of the $\boldsymbol{\nu_1}$ – phosphate symmetric stretching band. The information on the crystalline state of the dental enamel can be provided by the determination of the depolarization ratio and polarization anisotropy of the $\boldsymbol{\nu_1}$ symmetric stretching band of phosphate (at 959 cm^{-1}), while the determination of the depolarization ratio of phosphate is achieved by acquiring and comparing two different Raman

measurements (Figure 3.3) of the same observed region/spot obtained with parallel and cross-polarized configurations of the spectrometer [1, 5, 13, 17, 37-40]. The vibrational modes of dental enamel's main component - hydroxyapatite affected by caries are shown in Table 3.2 [13].

Table 3.2 - Vibrational modes that are affected by caries [4, 13, 38].

Functional group vibrations	**Raman Band Shift**
O-P-O bending modes	430-433 and 589-593 cm^{-1}
P-O symmetric stretching– most significant	~959-960 cm^{-1}
P-O asymmetric stretching vibration mode	1042-1043 or 1046 cm^{-1}
C-O symmetric stretching bands (B-type, A-type)	1069-1072, 1103-1107 cm^{-1}
C-H stretching bands (associated with organic matter)	1450, 2700-2880 cm^{-1}
O-H hydroxyl environment vibrational modes of phosphate spectra	3513 and 3573 cm^{-1}

4

RAMAN INSTRUMENTATION

4.1 – Context

Due to most recent developments of the used analytical software for the acquired Raman spectra from single or multiple points of interest, as well as the implementation of more sophisticated components and accessories in Raman instrumentation, such as sensitive high-resolution detectors and fiber-optics, respectively, were improved even more its sensitivity, information content, together with remote, automated, real-time, non-invasive and non-destructive features, and also imaging or mapping options, Raman technique is no longer confined only to research and development. Thus, it has become one of the most powerful tools for a wide range of research and clinical studies. This technique is progressively more employed for qualitative examination and quantitative analysis, including the identification of certain compounds of interest, process and control monitoring, inspection of impurities, contaminants, or structural defects, mechanical stability, as well as quality assurance and quality control. Moreover, any Raman user - researcher or student, regardless of the training level or expertise, has direct access to spectral libraries or databases in thousands of compounds that are now available for a direct compound identification or comparison, enabling a quick search by peak, spectrum, compound's name or mixt, turning out to be useful for a fast characterization and quantification of the obtained data [17, 21, 22].

Regarding the equipment of a typical Raman microscope, there are few major basic components (commercially available) that are relevant to a Raman spectroscopy instrumentation setup, as follows: **1) excitation source**, consisting in an incident laser that provides the monochromatic light beam; **2) light delivery and collection**, with additional sample illumination (since the Raman scattering is weak, the excitation laser can take advantage of an optical microscopy system that focuses properly the light beam onto the sample, allowing an efficient collection of the scattered radiation for sample surface observations) and collection system (spectrometer that collects the scattered signal, consisting usually in an achromatic lens system with a collecting lens and a focusing lens); **3) dispersive devices** – gratings for dispersive

Raman systems, or wavelength selectors for FT-Raman; **4) detection system** – usually a sensitive, low noise detector is necessary to detect the Raman scattered light. For UV-NIR excitation scan, cooled charged couple device (CCD) cameras are the typical detectors of choice. The main reason of using cooled CCDs is that cooling process reduces the array's dark current, resulting in an improvement of the sensitivity of the CCD to low light/signal intensities, even for ultraviolet and visible wavelengths. These detectors can be air-cooled or cooled and maintained with liquid nitrogen to reduce the dark current, and therefore thermal noise, to insignificant levels, leading to a substantial rise in the SNR. Such a detector, however, will normally represent a costly component of a Raman spectroscopy system. For some applications it may be possible to employ a point detector or a simple array detector which, by detecting more limited spectral information, will be less expensive; and **5) computer automated control and spectral analysis system** [2, 17, 25-28].

A typical Raman spectroscopic measurement usually consists in directing a focused laser beam onto the sample (Figure 4.1) and recording the energy profile of the light that is scattered (Stokes scattering). Every compound or chemical element gives a unique spectrum and for mixed samples the spectra are a superposition of the signals from each of the constituents [2, 27, 29].

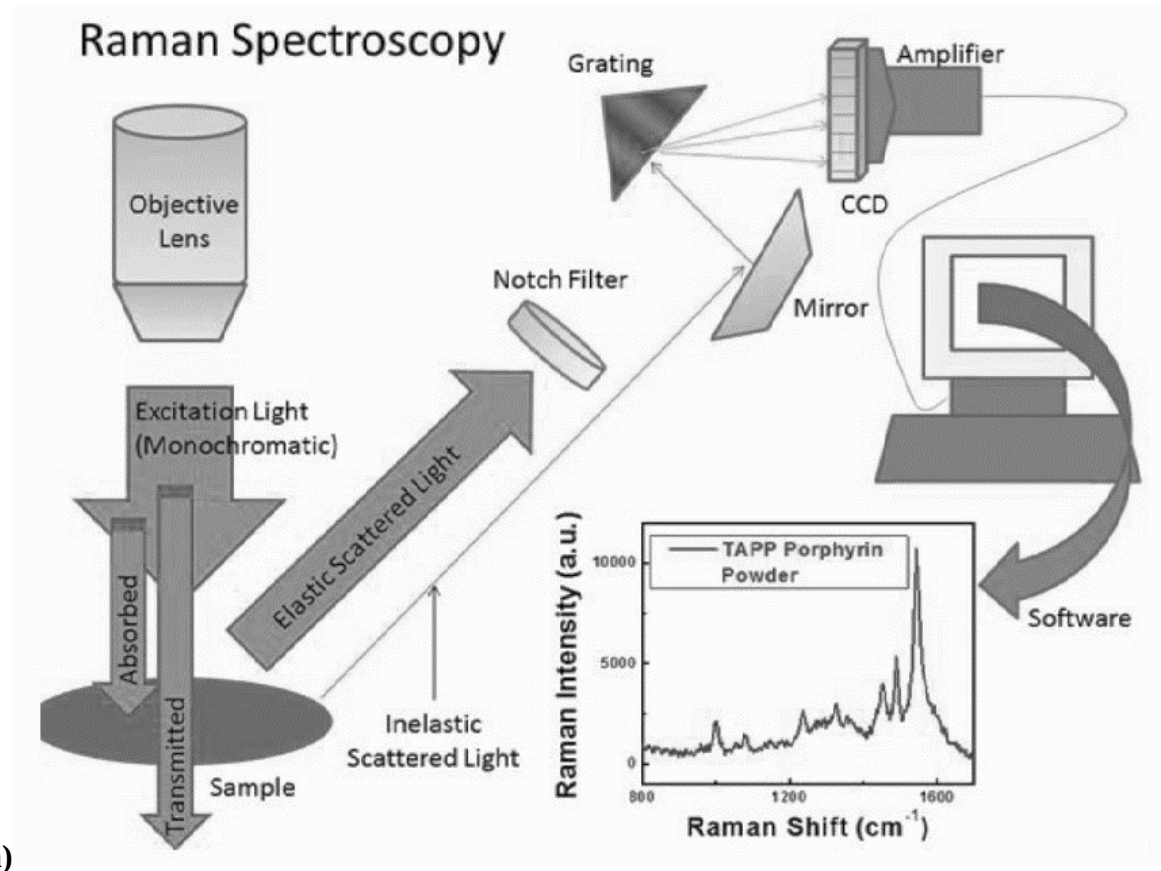

a)

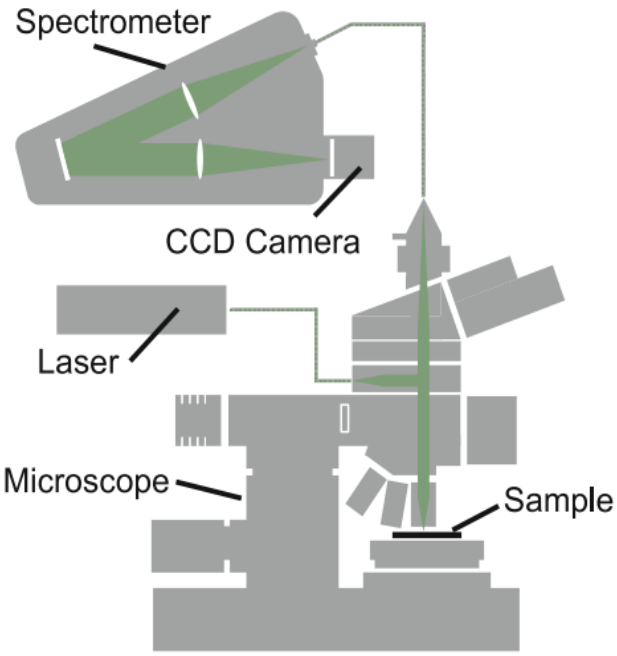

b)

Figure 4.1 – **a)** Schematic representation of a Raman spectroscopy system, including the major components, applied to a specific sample (porphyrin compound in this case), yielding unique characteristic Raman spectrum represented with peak positions expressed in wavenumbers as a function of intensity [41]; **b)** Schematic layout of a Raman microscope system coupled to laser source through optical fibers [23].

4.2 - Excitation sources

A laser ("light amplification through stimulated emission of radiation") is an intense monochromatic light source that is commonly used for Raman spectroscopy [21]. Excitation is a process achieved by delivering the light from a certain laser source to the tissue or sample of interest, directly through a microscope objective or remotely by means of fiber-optics.

The main advantages provided by laser excitation sources are (1) monochromatic light, with (2) high degree of collimation (small divergence), (3) intense beam (high intensity), with (4) phase coherence, (5) frequency stability and (6) polarized radiation. In the case of pulsed lasers, these have a (7) very short pulse duration [2, 21, 23, 25, 27, 42, 43].

Although conventional light sources have been initially used for absorption analyses, lasers were increasingly used in luminescence and Raman measurements. Lasers are considered an ideal excitation source for Raman spectroscopy technique due to the following features of the laser beam: single lines from large continuous wave lasers can easily provide up to 2 W of power, while pulsed lasers can generate great peak powers (on the order of 10 W-100 MW); the laser beams for Raman are monochromatic, and extraneous lines are significantly weaker; the majority of the used laser beams have small diameters, reduced also by simple lens systems;

laser beams are almost completely linearly polarized (ideal for depolarization ratios measurements); laser beams can be generated in a wide wavelength variety by means of dye lasers or other instruments [2, 27, 28].

Given the weak nature of Raman scattering, it is essential to deliver enough power to the examined sample to generate Raman scattered photons for detection in a reasonable integration time pertinent to the clinical setting under investigation. Also, Raman scattering is affected by other competing optical phenomena within the sample – fluorescence, which can surpass and overlay the spectral bands or even swamp the signal, turning the spectral analysis very difficult. Moreover, it is relevant to consider issues such as maximum permissible exposure (determined by ANSI – American National Standards Institute or similar organizations) and temperature rise (in the case of *in-vivo* examinations, it is extremely important to keep patients' comfort and minimize tissue damage). Consequently, laser power setup depends on several factors, such as: used laser wavelength, type of sample, signal to noise ratio (SNR), patient safety and comfort, and instrumentation considerations. Selection of laser is also ruled by other features such as laser stability, especially when using a multimode laser [2, 23, 27, 28].

The choice of laser excitation sources relies on the properties of the samples under examination, including scattering and total attenuation coefficients as well as excitation, emission, and yield properties for any endogenous fluorophores present in the sample, which are critical factors that must be considered. The influence of each of these parameters is a function of wavelength. Samples that reveal a high attenuation coefficient will limit the capacity to deliver and collect the light beyond very superficial layers. Additionally, highly absorbing molecules in a sample can also generate an excess heat deposition in the tissue, which can lead to serious damage with high irradiance. Similarly, the presence of strong fluorophores can produce signals that overwhelm the weak Raman peaks that are concurrently detected. Due to the associated decrease in total attenuation coefficient for the major absorbing molecules in many biological tissues (water, melanin, oxy- and deoxy-haemoglobin), NIR excitation sources are frequently and increasingly employed for clinical instruments [2, 27, 28].

An appropriate laser source for Raman microscopy should have the following wavelength characteristics:

- Gaussian beam shape (single longitudinal mode, TEM00), so that it can be focused onto a diffraction-limited or most concentrated spot;

- a narrow line shape of high spectral resolution (below 1 cm^{-1}), to avoid broadening of the Raman lines;
- very stable in frequency (lesser variations than 0.01 cm^{-1}), to allow temperature variations, tensile or compressive stress measurements with high accuracy;
- very stable in intensity (ideally, power fluctuations inferior to 1-2%), to allow accurate and comparable measurements of different compound concentrations;
- linear polarization, to allow the observation of polarization-dependent sample properties [23, 42].

The employed laser excitation wavelength has a strong impact on the measurement outcome and the obtainable information, since it influences:

- the Raman signal: Raman scattering intensity is proportional to the frequency and intensity of the excitation laser radiation, meaning that a lower excitation wavelength results in higher Raman signals. The scattering intensity is proportional to $\mathbf{\nu^4}$, where $\mathbf{\nu}$ is the frequency of the exciting laser radiation. Therefore, an excitation at 400 nm results in a Raman signal that is 16 times higher than excitation at 800 nm [23, 42].
- the fluorescence signal: many of the samples, especially biologic, exhibit stronger fluorescence (whose interference in Raman spectroscopy is originated intrinsically - from the analyzed compound own composition or from fluorescent impurities in the examined sample) when excited in the UV or blue region and lower fluorescence when excited in the red (638 nm) or NIR (from 785 to 1064 nm) region of the spectrum. The fluorescence signal is comparatively strong (up to several orders greater) and could obscure the weaker Raman signal, turning difficult or even impossible the precise identification of Raman peaks [21, 23].
- the spectral resolution: the shorter the excitation wavelength, the lower the spectral resolution. However, at longer wavelengths, the spectral resolution increases while the spatial lateral resolution decreases, with Raman efficiency falling significantly, together with as strong reduction of fluorescence background [23].
- The sample damage: for short wavelengths, the high photon energy can cause significant and irreversible sample damage at a lower laser power than for longer wavelengths (see section 3.4 – Sample heating) [23, 25, 34, 42].

Regarding the laser power, the Raman signal is directly proportional to the excitation power, which should be chosen well below the point where absorption leads to thermal decomposition of the sample. The selection of laser power depends on laser wavelength, sample properties (absorption, thermal conductivity), and other measurement conditions, such as laser spot diameter [23].

There is a great variety of choices, comprising different wavelengths that are frequently used in Raman Spectroscopy at present, ranging from the UV, over the visible, and reaching the near infra-red (NIR). The selection of the best excitation laser wavelength and /or power for a more specific application is not always obvious or easy. During a given experiment that employs Raman spectroscopic measurements and data acquisition, there are many system variables that must be thoroughly considered to optimize the quality of acquired spectral data, and several of them are directly connected to the wavelength selection. Shorter wavelength gives usually (much) stronger Raman signal, when compared with longer wavelengths. Shorter wavelengths are also advantageous by allowing the use of cost-efficient, rapid, and low-noise CCD detectors (up to approximately 800 nm). This type of wavelength is frequently used as it enables higher resolution in imaging. Nonetheless, the main limitation is that spectra acquisition can be significantly affected by the much higher background noise from fluorescence, depending on the investigated samples. Consequently, with all these considerations, many of Raman applications require for a longer wavelength, which is about 780-790 nm, while for highly fluorescent materials it might be necessary to choose even longer wavelengths in the NIR region, such as 1064 nm [2, 23, 27, 29, 42, 43].

For Raman specific applications, there are several requirements that must be achieved [21]:

• frequency stability: laser wavelength must not change significantly between two or more measurements;

• narrow bandwidth: for most applications a narrow laser line (monochromatic) is required, typically smaller than 1 cm^{-1}. The bandwidth of the laser line also influences the spectral resolution of the established spectrum;

• few sidebands (implies the use of band pass filters) - gas lasers emit atomic emission lines of the present gases, while solid state lasers can emit luminescence radiation. This radiation can interfere with the sample and cause fluorescence among others;

• low divergence: especially when no optical fibers are used - very important criterion [21].

The laser wavelengths that are typically used for Raman measurements are next:

1 - Ultra-violet (UV): 244 - 364 nm.

2 - Visible (VIS): 457 - 660 nm.

3 - Near infra-red (NIR): 785 - 1064 nm.

The most frequently used are the **Argon-Ion laser** (514.5 nm) and **Diode laser** (785 nm).

There are 3 main categories of dye lasers that are widely used for Raman spectroscopic measurements: continuous wave gas laser, pulsed laser and flashlamp lasers. In many cases, tunable lasers are usually utilized to provide a range of different wavelengths for Raman excitation process.

Undeniably, one of the most frequently used lasers in the modern Raman spectrometer is certainly the diode laser operating at ~785 nm. Diode lasers do not reveal some of the advantages of gas lasers, such as inherent wavelength stability and beam profile. However, most of these differences are reduced in modern diode laser designs by using active temperature stabilization, dispersive intra- or extra-cavity optical elements, and beam-shaping optics. Still, there are many other practical advantages that recommend the use of diode lasers in Raman applications. Even though fluorescence is not entirely eliminated at ~785 nm, it is significantly decreased. Another aspect is that the most common silicon-based detectors have a maximum detection efficiency in the region of 800–1100 nm, usually a region in which most of the Raman signal of interest is generated. The depth of penetration of NIR light into biological tissue (few millimeters or more) can also be a significant advantage over visible excitation especially for the detection, identification, and visualization of the subsurface layers of tissues or materials [2, 27, 28].

4.3 - Sample illumination and light collecting system

There are several types of illumination configuration, such as point, line, or global illumination: top and side illumination for back-scattered, or bottom – for transmission illumination designs. In the case of confocal Raman microscopes (CRM), these allow the laser source to be simply and easily focused on a small sample area and the emitted radiation efficiently focused on a slit. The term ‘confocal’ means ‘having the same focus’, and in the context of light microscopy, it refers to all image information that arrives from the same focal plane.

The main functions of a confocal microscope are to create a single point source of light and reject out-of-focus light, which makes possible to image deep into tissues with high resolution, and optical sectioning for 3D reconstructions of the examined samples. The basic principle of confocal microscopy is that both illumination and detection optics are focused on the same diffraction-limited spot, which is moved over the sample in order to build a complete image on the detector. While the entire field of view is illuminated during confocal imaging, anything outside the focal plane that contributes even little to the image, is rejected together with out-of-focus light. Therefore, confocal microscopy provides a means of rejecting the out-of-focus light from the detector such that it does not affect the images that are collected. The confocal technique allows for high-resolution imaging in thick tissues [44].

By using a pinhole in the back-focal plane of the microscope, it results that instead of illuminating the entire sample at the same time, the laser light beam is highly focused onto a well-defined spot at a specific depth within the sample.

By using confocal microscopes combined with Raman spectroscopy components, is enabled the visualization and mapping of molecular information over a defined sample, with high spatial (lateral XY and depth Z) resolution, allowing the detection of certain compounds. Spectral information can be obtained by measuring the scattered Raman radiation from single or multiple points of interest on the sample under examination. This way, small surface structural and conformation details on the spatial distribution and association of components or mineral phases, or chemical variation could be easily observed, with high accuracy degree, providing an extremely useful information that contributes significantly to the understanding of a sample's complexity and biochemical composition. Moreover, this combination provides a precise identification of their characteristics that can be evaluated from large scale scans in the centimeter range to the finest detail with sub-micron resolution. Therefore, very small samples can be examined [2, 23, 27-29].

To obtain the highest possible efficiency for the scattered signal, in combination with the best spatial resolution, it must be used an objective with the highest numerical aperture applicable under the measurement conditions, also considering the specific transmission characteristics of the microscope objective at a certain excitation wavelength. A good microscope objective could have 80–90% transmission at a certain - 500 nm wavelength, but only 40% or even less at a different one - 900 nm. The main reason for this is the anti-reflection coating characteristics. For example, coatings that have less than 0.5% reflectivity in the visible (VIS) can be significantly more reflective in the infra-red (IR). This is particularly important since the light

must pass through the objective twice: incident laser beam and collected scattered signal. Another important detail is the sample flatness and uniformity, that needs to be considered as well when selecting the proper objective, since a high NA objective will provide a good depth resolution and collect from only a narrow height in the Z direction [23].

4.4 – Dispersion systems

According to [21], all Raman spectrometers need a system to disperse the incoming light, depending on their wavelength. Raman instruments utilize principally two types of wavelength selection mechanisms, **(1) dispersive** and **(2) non-dispersive**, which means that radiation of different wavelengths can be separated in two different ways: (**1) either as function of space,** or **(2) in function of time**. Dispersive spectrometers use the principle of diffraction of light (space), whereas non-dispersive FT-Raman devices use Fourier-transformations (time) to obtain the spectra. A dispersive spectrometer uses diffraction gratings (Figure 4.2) or prisms, which represent the major component of a dispersive system. A diffraction grating consists in a linear repetition of reflecting or transmitting elements, according to the case. The distance between the reflecting elements (typically known as grooves or lines) is comparable to the wavelength of the dispersed light. The periodic variation in the diffraction grating leads to constructive or destructive interference of the scattered (or transmitted) light, in function of the wavelength of the incoming light and the angle under which this is scattered. Consequently, it is obtained a spatial resolution of the light directly proportional to its wavelength. Dispersive systems usually employ one of two main types of gratings: reflection or transmission grating. In the past two decades, several types of gratings (planar, concave, constant or varied line space gratings) were designed and installed in miniaturized spectrometers. Therefore, specific design considerations for a certain type of grating can be implemented according to the fabrication details, improving the dispersion performance [2, 21, 27].

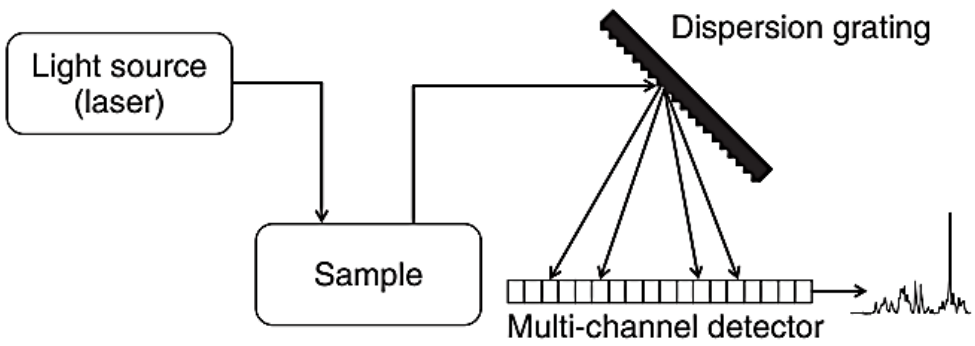

a)

b)

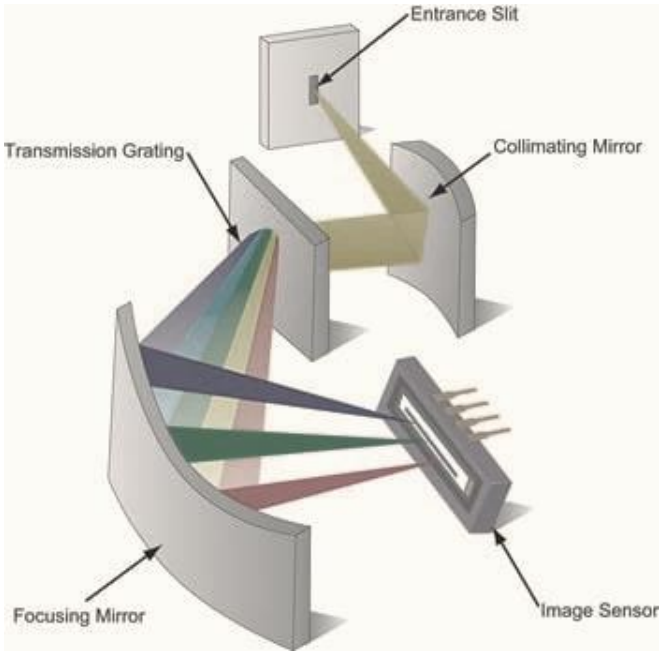

Figure 4.2 – a) General diagram of dispersive Raman spectrometer [21]; **b)** Schematic representation of a possible signal path from the entrance slit until the detector [45].

Two relevant parameters rely on the chosen grating and its dispersion properties: 1) the wavelength range and 2) spectral resolution – which, by definition, can be interpreted as how close two separated energies can be resolved (how finely a thin spectral band/peak can be identified from another situated extremely close). The number of grooves per millimeter determines the dispersion characteristics, meaning that a high number of grooves/mm (lines/mm) will lead to a high dispersion and an increased spectral resolution. On the other hand, this results in a reduced spectral range and distributes the incoming signal over a larger number of CCD pixels, requiring for a greater detector size. High spectral resolution is fundamental, since it is required to resolve less intensive or weak Raman peaks, together with existent "shoulders" originated from the same vibrational modes, proper band assignment and distinction between human tooth enamel, hydroxyapatite (HAp) and synthetic hydroxyapatite (OHAp), as well as to precisely identify a slight shift of a certain band [2, 4, 21, 23, 27, 38].

4.5 – Detectors - Charge Coupled Device (CCDs)

The detector is one of the main components of a Raman microscope, which has a strong impact on the performance of the instrument. In dispersive Raman devices, is widely used a specific type of multi-channel detector - the charge-coupled device (CCD), which consists of a 2-

dimensional array of light-sensitive elements. Usually, the acquired Raman spectrum is projected along one of the dimensions of the CCD, and pixels of the other direction are combined through a method called "binning". Nevertheless, many of the existing Raman instruments make use of the full 2-dimensional properties of a CCD, to incorporate spatial information in the analysis [21, 23].

A CCD detector consists of an array of light-sensitive photodiodes made of silicon. Every photodiode is connected to a capacitor, and in each of them, every detected photon creates an electron-hole pair which is separated by the internal electric field and the electrons are stored in the capacitor. An example of detector size for a spectroscopic detector is 1024 × 127 (pixels per line × pixels per column), with a pixel size of 26μm × 26μm. For pixels that are reverse-biased, depletion regions are formed, and charges are detained and stored within the potential well up to the full well when illumination is applied. In contrast, those zero-biased pixels are transparent to the incoming photons. The number of charges generated is directly proportional to the intensity of the incident light flux, and the full well capacity regulates the maximum light intensity that is possible to detect. Each element (or pixel) of the detector array is a photoactive capacitor that will collect and hold charge determined by the number of photons that arrive to it. Each pixel is a component with specific resolution for a certain wavelength, with a varying quantity of incoming light photons. Several relevant performance parameters can be inferred from this form of operation, such as noise level associated with each detector element, noise amount that is generated during shifting/reading, the efficiency of the array in detecting individual photons, and the rapidity to read out the detector [2, 23, 27].

CCD detectors are available in a great variety of sizes, uncooled or cooled, with Peltier or liquid nitrogen (LN) cooling, front- or back illuminated, as deep depletion models, with anti-reflective coating or a UV-absorbing coating, among many numerous variations [23].

There are a few main differences between front- and back-illuminated CCDs. The front of a CCD is considered as the side where the electrical circuit is printed, and a front-illuminated CCD is illuminated from the front side. The detector's electric circuit covers approximately half the area and is not photon-sensitive, therefore the maximum quantum efficiency is about 50%. On the other hand, the back of a regular front-illuminated CCD can be partially etched (back-thinned), resulting in a thickness of only about 15 μm. Thus, the electrons resulted from the irradiation of the back can migrate through the chip to the potential drains at the front of the detector. Since the electric circuit does not cover the CCD in this case, the quantum efficiency (QE) is much higher compared to the front-illuminated CCD (typically up to 80–95%,

ca. 1.6-1.8 more efficient). Furthermore, the back-illuminated detector is more sensitive in the UV area, compared with a front-illuminated CCD [21].

Although back-illuminated CCDs have a much higher sensitivity than front-illuminated CCDs, there are a few relevant disadvantages [21]:

- Back-illuminated CCDs are more expensive than front-illuminated CCDs.
- Back-illuminated CCDs are thinner and therefore more fragile than front-illuminated CCDs.
- With back-illuminated CCDs light passes through a thin layer of silica and therefore an interference phenomenon can occur, which will have a significant impact on the sensitivity, leading to substantial variations, being even more pronounced with the use of longer laser wavelengths.

The most important characteristic of a detector is the quantum efficiency (QE), which is the percentage of detected photons from the total incoming photons. Given that the light-sensitive area of a CCD is partially blocked by electrical interconnection lines, the QE of a typical (front-illuminated) detector is approximately 45% at 500 nm. For a higher detection efficiency, it is also used a different type of detectors - back-illuminated devices, which means that the incident light irradiates from the backside. With this technique and a proper anti-reflection (AR) coating, it can be achieved a QE higher than 90% (at 500 nm) [23].

CCD detectors represent a major advance in detector instrumentation from the UV to NIR spectral range. These are increasingly used due to their high quantum yield, two-dimensional imaging capability, and extremely low dark current (low noise), and additionally, due to the unique combination of sensitivity, speed, and durability in a relatively compact and small volume package [2, 23, 27].

4.6 - Filters for Raman scattered photons

For an efficient detection of the Raman signal (which is an intrinsically weak effect), Rayleigh scattered photons must be suppressed, rejected, or attenuated. The collected scattered light needs to be filtered to remove the Rayleigh scattered component otherwise this signal would mask or overwhelm the Raman signal. For an efficient suppression of the Rayleigh photons, one should use an edge or notch filter that will reduce the laser line intensity by several orders of magnitude while allowing an overall throughput of > 95% for the Stokes-shifted Raman.

Most of the available commercial spectrometers are equipped with filters for Rayleigh light attenuation and/or rejection. [2, 23, 27, 29, 46].

A Raman instrument contains several types of filters. Every component has its own characteristics. Generally, the filters are divided into different categories:

• Neutral density filters (grey filters): these function by absorbing the light with a quasi-constant value over the entire wavelength area.

• Long pass (edge) filters: these filters reflect the incoming radiation with a wavelength under a certain limiting value; above this limiting value there is transmission.

• Low pass filters: these filters are the opposite of long pass filters. The incident light with a wavelength shorter than a certain limiting value will be transmitted, whereas the remaining light with a longer wavelength is (ideally) totally reflected.

• Band pass filters: these filters transmit only signal of a certain wavelength (limited within a well-defined wavelength interval), the remaining light – with wavelengths inferior, or superior to this range limiting values is reflected.

• Band block (notch and holographic) filters: these filters block signal from a certain wavelength but let pass through a majority of signal of other wavelengths. They can be used to remove a single wavelength, or a narrow band of wavelengths, according to the case [21].

5

STATE OF THE ART - USE OF RAMAN TECHNIQUE IN DENTISTRY

In 1997, Tsuda and Arends [28] published a review paper on an upcoming subject of Raman applications, the study of dental hard tissues. More recently, Ramakrishnaiah et al. [3] updated this analysis with the review of Raman spectroscopy for the analysis of tooth structure and applications for oral hard tissues pathologies, such as, diagnosis of early dental caries and developmental disorders of enamel and dentin, identification of oral microbial flora and characterization of dental biomaterials.

Several research studies reported that Raman spectroscopy is a precise technique for the analysis of tooth structure and applications for oral hard tissues pathologies, such as, diagnosis of early dental caries and developmental disorders of enamel and dentin, identification of oral microbial flora and characterization of dental biomaterials. Raman spectroscopy has shown to be a very suitable method for the characterization of dental tissues, from caries detection to the evaluation of demineralization caused by acidic external agents [1, 3-5, 8, 17, 22].

The spectral bands of interest in a Raman spectrum acquired from human dental enamel are the bands assigned to the phosphate group, associated with apatite crystals, which has four internal vibration modes, namely the ν_1 symmetric stretching (~959-960 cm^{-1}) [4, 13, 38], which represents the totally symmetric P-O stretching vibration of the phosphate ions (PO_4^{3-}) and ν_3 anti-symmetric stretching (~1043-1046 cm^{-1}) bands [13, 38]. The other two markers of the mineral component are ν_2 O-P-O symmetric bending (~430-433 cm^{-1}) [13, 38] and ν_4 asymmetric bending (~589-591 cm^{-1}) bands [4, 13, 38]. The sensitivity of this spectroscopic technique for alterations in the ν_1 symmetric stretching band of phosphate ions in hydroxyapatite matrix can be used as a powerful tool for early diagnostics, even before signs of demineralization are detected by conventional methods [2, 3-6, 27, 28]. In addition, the carbonate bands can also reveal significant changes of enamel tissue. The internal modes of the CO_3^{2-} group are identified near 1069-1072 cm^{-1} (ν_1 mode of B-type carbonate) and 1103-1107 cm^{-1} (mode of A-type carbonate), respectively [4, 13, 38]. The intensity of carbonate bands assigned to CO_3^{2-}

group indicates the overall carbonate content in the enamel and their substitutions in apatite lattice either for the hydroxyl - OH^- group (A-type) or for the phosphate - PO_4^{3-} group (B-type) [4, 13, 38].

According to Ko et al., which performed several studies by means of polarized Raman spectroscopy [17, 38-40] by examining *ex-vivo* extracted teeth with early carious lesion, for measuring the polarization dependence of Raman spectra of tooth enamel, a series of spectra were acquired at different angles of the polarization direction of the linearly polarized laser light with respect to that of the polarization analyzer. By mechanically rotating a half-wave plate placed in the laser path, laser polarization was varied in relation to that of the analyzer.

Parallel-polarized and cross-polarized spectra were obtained with the analyzer polarization oriented parallel (||) and perpendicular (⊥) to that of the linearly polarized laser light, respectively. The depolarization ratio ρ_{959} and polarization anisotropy A_{959} were calculated according to conventional definitions:

$$\boldsymbol{\rho}_{959} = \frac{\mathbf{I}_{959}(\perp)}{\mathbf{I}_{959}(||)} \qquad \textbf{(5.1)}$$

$$\boldsymbol{A}_{959} = \frac{\mathbf{I}_{959}(||) - \mathbf{I}_{959}(\perp)}{\mathbf{I}_{959}(||) + \mathbf{2x}\, \mathbf{I}_{959}(\perp)} \qquad \textbf{(5.2)}$$

where $I_{959}(\perp)$ and $I_{959}(||)$ are the integrated peak intensities of the ~959 cm^{-1} band detected with the analyzer oriented perpendicular to (⊥) and parallel to (||) the polarization direction of the linearly polarized laser light, respectively. Polarization dependence was found evident for Raman peaks at 590 cm^{-1}, 608 cm^{-1}, 959 cm^{-1}, 1069 cm^{-1} and 1104 cm^{-1} as a function of angle (θ), being this dependence most noticeable for the phosphate symmetric mode at 959 cm^{-1} [39].

Using Raman spectroscopy, Bulatov et al. [13] performed in 2008 a comparison study of healthy and carious teeth and established that the carious process can affect the phosphate and carbonate phases of enamel. The mineral component – HAp, has a hexagonal symmetry and the apatite crystalline structure is adaptable to various additions; for example, dental apatite contains a substantial amount of carbonate groups, which substitute for the OH^- groups (A-type CO_3) or for the phosphate tetrahedral (B-type CO_3). In this study, four stages of dental caries were determined, according to their severity: normal enamel (no caries at all), fissure carries, moderate caries, and advanced caries, providing sufficient information on a variety of chemical bonds and vibrational modes potentially affected by caries (described in Table 3.2, section 3.4). During their work, images and corresponding spectra were obtained from several

different tooth sites, demonstrating that different groups, containing normal enamel, white opaque, brown discolored, and pitted tooth surfaces all have different and distinctive spectral features which characterize distinct severity degrees of dental caries. Furthermore, by performing spectral analysis can be obtained an accurate detection and identification of early changes in the enamel surfaces of (incipient) carious teeth, while the associated mapping feature allows for localization and morphological characterization. The authors concluded that the emission peak at ~960 cm^{-1}, which corresponds to phosphate symmetric stretching vibrational mode, is the most significant Raman spectral band and can be certainly used for caries detection. According to these authors, RSI could be an appropriate method for estimating the extent of tooth caries and providing imaging information. This non-destructive optical method was considered able to characterize and differentiate between normal enamel tooth surface, as well as initial and advanced tooth caries. Hence, the obtained results strongly suggest that Raman technique may be further developed, enhanced, and applied for clinical diagnosis and monitoring of (early) initial and more advanced demineralization, and subsequently, decay processes of the enamel tooth surface [13].

A similar approach was followed by Ionita et al. [47], while examining extracted natural teeth with questionable caries, reporting an increased depolarization ratio at 959 cm^{-1} vibrational mode, both at the external surface of the carious enamel and in sectioned enamel. Moreover, a thorough examination of the intensities of several different PO_4^{3-} vibration modes (situated at 1043, 590, and 431 cm^{-1}, respectively) have revealed a consistent variation in the intensities of spectra of carious lesions when compared to healthy normal enamel. Furthermore, the Raman spectrum of the diseased enamel showed a high-level background, reported to be frequently higher than the most intense Raman peak of sound enamel – $\boldsymbol{\nu_1}$, which means that two specific phenomena occur: 1) the decrease of the phosphate peak intensity due to local structural disorder produced by enamel mineral loss and consequently decay process, and 2) simultaneously a strong increase of the background due to fluorescence process (mostly caused by a rise in organic elements/waste of bacteria). It was found that during the early-stage decay of the tooth the enamel crystals' orientation is changed, affecting the results in polarization of the symmetric stretching vibrational mode assigned to 959 cm^{-1} Raman band. Demineralization causes a more porous outer enamel structure, which increases the overall (Rayleigh + Stokes) scattering of the incident light, while the decay process provides a higher amount of unorganized material, which promotes an increased level of fluorescence, and given these fluorescence conditions, the researcher affirmed that was more difficult to measure the Raman spectrum [47].

Timchenko et al. [48, 49], conducted several studies using Raman spectroscopy. In their first study [48], the authors applied this technique for the diagnosis of caries and weakening of tooth tissues in its early or more advanced stages, by using parallel-polarized and cross-polarized configurations to collect Raman spectra at 959 cm^{-1} peak intensity. Different parts of tooth areas (enamel, dentin, cement), both in normal and in caries cases, were considered as object areas for examination. The key finding of this work was that dental caries can be characterized by intensity changes of spectrum at 959 cm^{-1} and 1069 cm^{-1} wavenumbers (peak positions), corresponding to the phosphate and carbonate bands, respectively (assessing the substitution of PO_4^{3-} ions to CO_3^{2-}, B type), and 1241 cm^{-1}, 1660 cm^{-1}, assigned to collagen III and collagen I, respectively. The authors established that carious lesions are characterized by a strong decrease of PO_4^{3-} ions and collagen I in dental tissues. The reliability of the research results was confirmed by means of an additional technique - scanning electron microscopy.

In their second and most recent study [49], it was shown mainly the specific spectral features of hard dental tissues with progressive periapical periodontitis, a pathology that leads to crack lines on tooth cementum surface with depth depending on severity and progression of the disease, which can result in severe damage and/or further tooth loss. The obtained results revealed that the main spectral differences of teeth with periapical periodontitis are observed by assessing the phosphate symmetric stretching mode assigned to the most intense band of dental tissues at 956 cm^{-1} (PO_4^{3-}), when compared to all existing vibrational modes of mineral components of dental tissues, as well as on the peaks of 1230-1270 cm^{-1} (Amide III), 1665 cm^{-1} (Amide I), related to organic components of dental tissues. This work revealed that the major changes that were detected were predominantly caused by the destruction of collagen fibers in case of periapical periodontitis and significant reduction of mineral components (mineral loss) during the illness progression. More precisely, the main alterations that indicated the destruction of hard dental tissues were the detection of collagen matrix presence and the identification of hydroxyapatite salts [49].

In a research study performed by Monteiro et al. [1], it has been demonstrated the suitability of confocal Raman microscopy for the examination of carious dental tissues and mineral loss in depth by analyzing tooth cross/sections. Since the analysis of the PO_4^{3-} symmetric stretching band and its polarization anisotropy are reported to be sensitive markers of demineralization, and at the same time, precise identifiers of early caries detection, samples of enamel and dentine, with carious lesions in different stages of progression, were assessed by comparing the depolarization ratio of the PO_4^{3-} symmetric stretching band at 959 cm^{-1} in different sound and

carious tissues carefully chosen by an expert and the selection criteria were represented by the presence of lesions, cavitated or not, including white spots. Raman spectra of samples were acquired by means of a Horiba XploRA confocal microscope using a near infrared laser (785nm). To determine the depolarization ratio of the most intense band in the Raman spectrum, spectra were recorded in two orthogonal polarizations of scattered light (perpendicular and parallel to the polarization of the incident laser beam). Raman mappings were performed as well and found to be extremely useful in the delimitation of carious tissues, however, the analysis of a representative area is a time consuming and complex process, since the areas should be scanned twice with different polarizations, also with a major risk of defocusing.

By performing this work, it has been shown the appropriateness of utilizing Raman spectroscopy, namely by means of the depolarization ratio of the vibrational symmetric stretching mode of the phosphate band, as a powerful tool for mineral loss and carious detection even in early stages. Moreover, spectral mappings proved to be extremely useful in the delimitation of carious tissues; however, according to the authors the analysis of representative surface enamel areas was very time consuming [1].

A research group led by Buchwald et al. [4, 36, 50-51] have recently performed several research studies in order to investigate the effectiveness of Raman spectroscopy technique in the determination of changes in chemical composition, structural arrangement, crystal rod orientation and/or morphology of human tooth enamel affected by caries. They have used spectral parameters such as Raman band position, peak intensities obtained by using different excitation laser wavelengths, the full width at half maximum of Raman band (FWHM) and line shape of Raman band. Additionally, they have also used the depolarization ratio and polarization anisotropy, parameters derived from the intensities of the symmetric stretching vibrational mode assigned to the phosphate band recorded with two different orthogonal polarizations of the scattered light, since in sound enamel, Raman signal is highly polarized in the direction parallel to that of the incident light (monochromatic excitation laser beam), and the value of the depolarization ratio is low and polarization anisotropy is high [4].

In the first study [4], they assessed Raman spectroscopy as a tool for early caries detection, using this technique to study permanent teeth. As the results have shown, it was confirmed that parameters such as depolarization ratio (ρ_{959}), anisotropy (A_{959}), phosphate band position and line shape are precise indicatives of enamel caries changes. Likewise, it is possible to detect early caries by analysis of background in the Raman scattering spectrum related to the Rayleigh scattering and fluorescence emission. The overall findings of their studies [4, 36, 50, 51],

obtained by means of RS, indicate precisely and reliably the occurrence of early caries, characterizing sound and demineralized enamel, enamel with incipient caries and enamel affected by advanced caries. The results of their studies allowed them to statistically correlate the parameters values and the severity of dental caries.

Also, recently, Pankrushina et al. [8] conducted a study in which they applied Raman spectroscopy. Being mainly motivated by the fact that Raman technique is widely used in helping to better understand the impact of the structure and composition of enamel and dentine layers on their chemical resistance, mechanical properties, protein alteration and the effects of de-/remineralization processes, as well as different types of tooth diseases, this research group decided to investigate the teeth affected by hypoplasia lesions with different severity degrees, and to compare these results with those obtained from eroded and intact sound teeth. For this study, three types of dental samples were examined: 1 – tooth with hypoplasia lesions of different severity degrees, such as white, yellow, and brown spots; 2 – eroded and 3 – intact sound tooth. The authors have performed a hyper-spectral Raman imaging with a high spatial resolution, obtaining results that detected, identified, emphasized, and differentiated the structural variations of affected teeth according to the degree of bioapatite disorder. Moreover, in order to increase the accuracy levels of the obtained results, the authors constructed a different distribution map based on a novel parameter – mineral distribution correlation, which represents a values based on the calculation of the autocorrelation function, which allows to parameterize the effective linewidth of individual Raman bands or specific groups in bands in the recorded spectra and to determine precisely and efficiently the regions of various critical or affected regions of interest (by demineralization, hypo-mineralization, erosion or incipient caries) and other critical phenomena. The authors also mentioned the relevance of "zonality" (neighborhood) and "zonal distribution" of both organic and mineral component distribution, managing to indicate in the presented maps a clear separation between the enamel and dentine layers and obvious boundary at the dentine-enamel junction level.

And lastly, in a recent research work published in 2021 by Prikule et al. [52] were presented comparative studies with a slightly different approach, that were carried out using scanning Raman micro-spectroscopy with several sources of laser excitation with wavelengths of 532 nm, 785 nm, and 1064 nm, obtaining different spectra of tooth enamel according to the used radiation, with different levels of fluorescence background and SNR, also revealing that the intensity of Raman scattering of enamel is directly proportional to the enamel layer' thickness. These comparative studies provided relevant data obtained from vital and removed teeth,

showing an obvious difference in the optical response during the measurements of the vital teeth surface with an in-vivo approach compared to the in-vitro approach applied to the removed teeth, under the same conditions of signal registration. The main reported difference was that due to the standard oral hygiene procedure carried out by each of the patients, microbial plaque remains on the surface of their teeth, which effectively absorbs and scatters visible high-frequency laser radiation. Additionally, it must be considered that the presence of fluid circulation in the dentine tubules of vital teeth may lead to significant differences in the obtained indicators during Raman diagnostics on vital and removed teeth.

In conclusion, the authors stated that Raman spectroscopy represents a promising method for the differential diagnosis of teeth predisposition to early caries. The implementation of such developed research methods will increase the effectiveness of not only the diagnosis, but also the prevention of dental hard tissue diseases development. Moreover, Raman scattering provides an opportunity to determine both the static value of the dental tissues' mineralization degree, and the effect of remineralization in dynamics [52].

6

POLARIZED RAMAN MICROSCOPY FOR DENTAL ENAMEL ASSESSMENT

6.1 – Introduction

In this chapter are described three different case studies on dental enamel performed by means of polarized Raman spectroscopy, in order to confirm and demonstrate the utility of this method. It is known that different teeth, or distinct regions of the same tooth, can have different Raman scattering efficiency due to bio-heterogeneity. Different levels of mineralization and crystallographic orientation of the hydroxyapatite crystals result in measured Raman band intensities that vary significantly from person to person (of different ages and/or gender, known as inter-individual variability), from tooth to tooth or even from region to region (intra-individual differences). Misleading results originated by band intensity values can be avoided by using parameters such as depolarization ratio ($\boldsymbol{\rho_{959}}$) and polarization anisotropy ($\mathbf{A_{959}}$) as forms of peak ratios, which respond to the underlying structure and related changes, but not to the types of experimental variations [39, 53]. These two parameters do not respond to the environment changes, such as temperature and/or pressure increases or decreases, which can affect the detector QE, nor to slight alterations of the OWD, changes that might result in significant band intensity fluctuations. Nonetheless, despite of the $\boldsymbol{\rho_{959}}$ and $\mathbf{A_{959}}$ parameters being very sensitive to mineral content changes in composition (demineralization/remineralization) or structure (porosity, molecular alignment, crystal symmetry, or structural organization and orientation), these do not indicate the main cause, which can be a mineral loss induced by different factors, such as acid erosive challenge, bleaching product, cleaning products or other dental treatment.

Hence, by using polarized Raman measurements and comparing polarization anisotropy (A_{959}) and depolarization ratio (ρ_{959}) instead of comparing band intensities or integrated areas, potential problems caused by instrumental variations and sampling heterogeneity are avoided. Moreover, since molecular alignment may cause polarization anisotropy of certain bands in the Raman spectrum, Raman spectra collected for well-aligned molecular structure at different

polarization angles are expected to show substantial spectral variations [39, 53, 54]. Therefore, in all three presented studies, the parameters that were compared in each step of the study were the depolarization ratio ($\boldsymbol{\rho_{959}}$) and polarization anisotropy ($\mathbf{A_{959}}$) of the symmetric stretching band of phosphate (υ_1 PO_4^{3-} ~ 959 cm^{-1}). The obtained results are in agreement with the existing literature about Raman spectroscopy used for the determination of changes in composition and structure of human enamel by using the mentioned parameters [1, 4, 17, 39, 54-56].

All acquired spectra of the examined samples in the described studies were obtained with a Horiba XploRA Raman device (Horiba, Jobin Yvon, France), optically coupled to an Olympus BX41 confocal microscope, employing a laser diode source operating at 785 nm, using a 1200 lines/mm grating. This way, the spectral range investigated was from 300 cm^{-1} to 1800 cm^{-1}, resulting in a spectral resolution of 4-6 cm^{-1}. Using an entrance slit of 200 μm, and a confocal hole of 300 μm, the scattered light collected by the objective was dispersed onto the air-cooled CCD array of an Andor iDus detector. A 100x objective (NA = 0.9) was used to focus on the surface of enamel, as well as a 50% neutral density filter rendering an incident power on the sample of 9.0 ± 0.4 mW (Lasercheck®, Edmund optics). For each of the analyzed samples, an average of 20 to 30 measurements was performed (10 different points measured with no polarization – in some cases, 10 points with parallel polarization between the incident radiation and the scattered Raman radiation, followed by other 10 with cross polarization). The exposure time for each measurement was between 15-20 s with at least 3 accumulations, depending on the specific requirements, phosphate band intensity and spectral signal quality (SNR) for each of the studies. Spectra deconvolution was achieved by means of LabSpec software (v5.58.25, Horiba, France), making use of a linear baseline correction to remove the spectral background due to fluorescence, improving the SNR and enhancing the accuracy of the analyzed parameter ratios. The band intensities were determined by integrating the area under the bands.

6.2 - Use of polarized Raman spectroscopy – case studies

6.2.1 - *In-vitro* study on the protective suitability of a dental fluorinated varnish

6.2.1.1 - Context and goals

Dental erosion is a multifactorial condition associated with chemical, biological, and behavioral factors whereby a non-bacterial chemical process leads to an irreversible loss of dental structure [57-58]. Based on the origin of the erosion-causing acids, a distinction between endogenous and exogenous erosions is made. Intrinsic erosion most often affects the palatal and

occlusal tooth surfaces, while extrinsically triggered erosion is initially localized on the labial surfaces of the anterior teeth. Consequences of this erosive process include painful sensitivity, susceptibility to further erosion, mechanical wear, changes in occlusion, exposure of dental pulp, and poor esthetics [57-59]. Fluoride plays an important role in dental protection, as it strengthens teeth and prevents their decay by turning the surface enamel layers more resistant to the action of acids while accelerating the build-up of healthy minerals in the enamel. This protective role occurs by allowing the formation of hydroxy-fluorapatite or calcium fluoride, forms of hydroxyapatite more resistant to bacterial demineralization. According to Ismail et al. [19] and Medjedovic et al. [60], the presence of fluoride in the oral environment and its subsequent incorporation can even prevent the already started tooth decay and demineralization process by rebuilding (through remineralization) the weakened or damaged tooth enamel. Thus, fluoride can be considered highly anticariogenic since it reduces and slows down significantly the loss of minerals from tooth enamel and enhances the remineralization, reversing in this way the early signs of tooth decay and delaying or arresting the existing dental caries. Floride prevents the growth and inhibits the metabolism of harmful oral bacteria. The described *in-vitro* study [53] was performed in order to assess the protective effect of fluorinated varnish on human enamel samples, after enduring a citric acid erosive challenge. To accomplish this evaluation, it was performed a direct analysis on 10 dental samples before and after the application of a fluorinated varnish; and then again after an acid erosive procedure which was similar to the intraoral environment. The evaluation of the soundness of enamel specimens was undertaken by means of polarized Raman spectroscopy. More precisely, the depolarization ratio (ρ_{959}) of the symmetric stretching band of phosphate in Raman spectra was used to evaluate the loss of mineralization of the hydroxyapatite matrix.

6.2.1.2 - Materials and methods

Specimen selection and sample preparation

Twenty healthy (non-carious and non-restored) human teeth (incisive, canine, pre-molar, and molar) previously extracted for periodontal or orthodontic reasons and preserved in a 0.5% (w/w) chloramine $T_3 – H_2O$ solution, at 4 °C, were carefully selected and evaluated by research dentists having as exclusion criteria the presence of superficial lesions observed employing a stereomicroscope (Meiji Techno EMZ 8RT, Japan). Afterwards, teeth were cut with a precision diamond saw (Buehler Isomet 1000, USA) to obtain enamel specimens app. 8 mm x 2 mm,

according to the cutting sequences shown in Figure 6.1. Afterwards, the examined samples were stored in properly identified storage vials in a new chloramine solution until the beginning of measurements. Before measurements, each sample was brushed with a non-fluorinated toothpaste Couto (Pasta Dentifrica Medicinal Couto, Couto S.A., Portugal) rinsed with distilled water, cleaned and air dried.

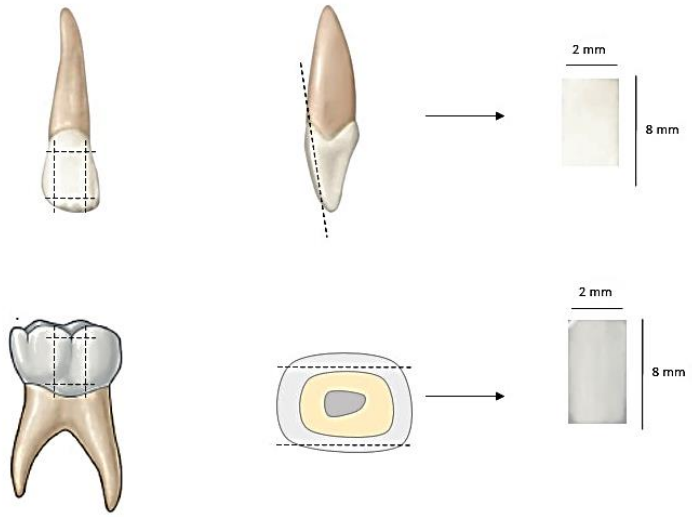

Figure 6.1 – Representation of the enamel sample preparation procedure, illustrating the section of the sample in incisors and molars.

Methodology and experimental groups

Two experimental groups of human dental enamel samples, control (C) and treatment (T), each containing 10 tooth samples, were subjected to 5-immersion acidic cycle. Before the erosive challenge, the T group was brushed with Couto toothpaste and treated with Fluoride containing dental varnish - VOCO Profluorid while group C was only brushed with Couto toothpaste. All sets of samples were analyzed using Raman spectroscopy technique during three distinct stages: 1 - before any treatment, 2 - after application of dental varnish and/or toothpaste and 3 - after citric acid erosive attack procedure. Between applications and treatment procedures, all teeth samples were brushed with a mild toothbrush and stored in renewed human saliva, to better simulate in vivo conditions. Figure 6.2 illustrates the erosive protocol. All dental enamel samples included in our study (N = 20) were kept and maintained in chloramine solution, and then carefully prepared and submitted to acidic erosive attack, as follows: acid erosive challenge (0.3% citric acid, pH 2.6,) for 5 minutes, human saliva (during 2 h), and afterwards thoroughly washed, cleaned, and maintained in chloramine solution [61].

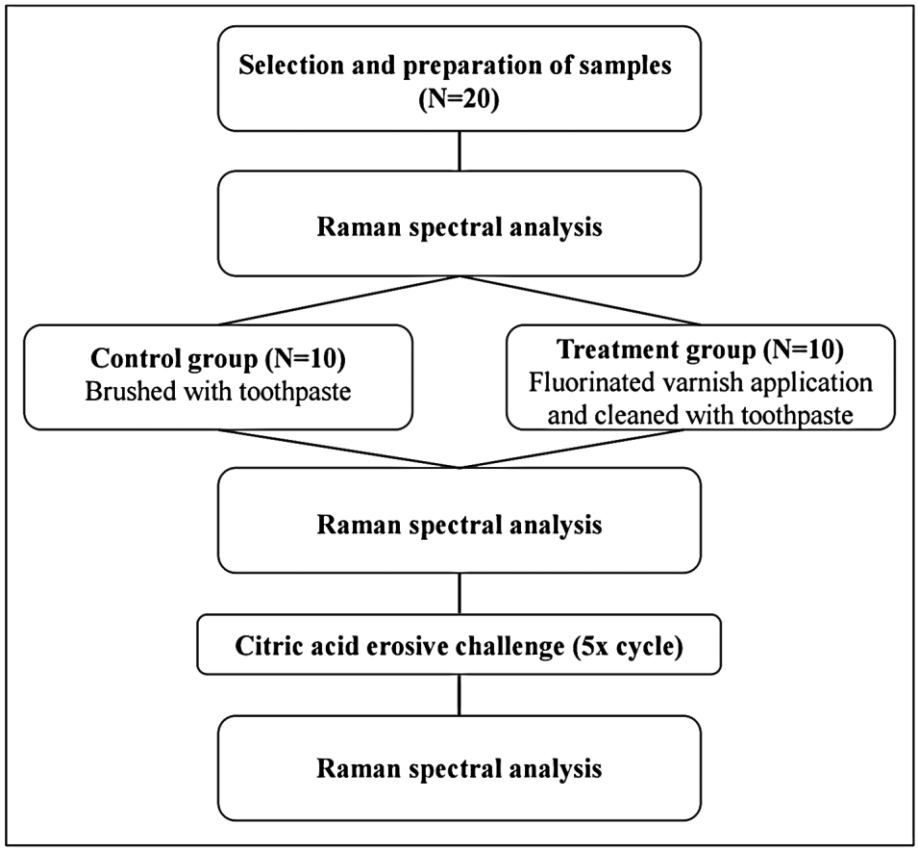

Figure 6.2 – Flowchart of the methodology employed in the surface enamel sample examination, during all study stages [Adapted from 53].

Experimental setup – Raman spectroscopy

For each sample, an average of 20 measurements (10 different points with parallel polarization between the incident radiation and the scattered one, always followed by other 10 with cross polarization) was performed. The exposure time for each measurement was 20 s with 4 accumulations.

6.2.1.3 – Statistical Analysis

All data collected was analyzed using IBM SPSS v25.0 software (IBM Statistics, Inc. Chicago, IL, USA). Parametric tests were used since the study had a sufficiently large sample size (all variables with 100 measurements for each sample) according to the central limit theorem [62]. ANOVA tests with Tukey post hoc were performed to analyze intergroup differences at each study stage, while paired t-student tests were performed to analyze intragroup differences between study stages, to determine the mean difference between every two sets of observations – 1st and 2nd stage, and 2nd and 3rd stage. It was considered a statistical significance level of p=0.05 (the smaller the p-value < 0.05, the more likely it is the rejection of the null hypothesis).

6.2.1.4 – Results

Ten teeth per study group were analyzed without any drop-out during all proceedings. After analysis, were obtained results comprising the mean values and standard deviations. Results are presented for each group regarding the three treatment stages: Stage 1 – before any treatment, Stage 2 – after dental varnish and/or toothpaste application and Stage 3 – after citric acid attack procedure. Depolarization ratio (ρ_{959}) values were compared for control and treatment groups, during all study stages, as shown in Figure 6.3. Independent t-student test showed no significant differences between the two groups at Stage 1 of the study; however, significant differences were found between control and treatment group after 2nd stage, due to the application of the fluorinated varnish ($p<0.01$). In fact, there was a significant decrease of this parameter in the treatment group, from 0.07 ± 0.06 to 0.03 ± 0.02 ($p<0.01$ post hoc) and no significant change in the control group. Similarly, the depolarization ratio between control and treatment groups after 3rd stage - acidic cycle of the study presented significant differences ($p<0.01$). Regarding the anisotropy parameter (A_{959}), there were also no significant differences among the 3 stages of the study for the control group. This parameter was also similar between groups at stage 1 of the study. However, after the application of the fluorinated varnish there was a significant increase for the treatment group, from 0.9 ± 0.1 to 0.93 ± 0.04 ($p<0.01$ post hoc) towards the initial values in Stage 1 - 0.90 ± 0.04.

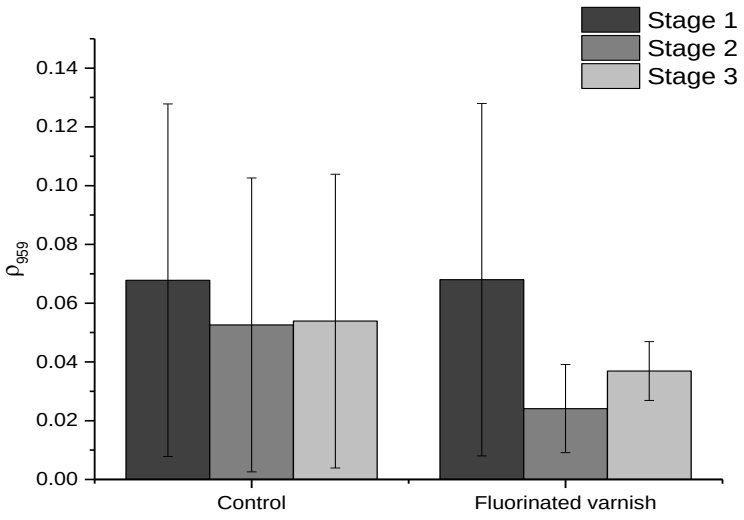

Figure 6.3 – Mean depolarization ratio obtained for both groups during the different stages of the study (1 – no treatment, 2 – dental varnish and/or toothpaste application, and 3 – erosive cycle) [53].

6.2.1.5 – Discussion

This study intended to assess the protective effect of a dental varnish against the demineralizing effect of an erosive attack cycle. The obtained data indicates a significant loss of mineral content, namely calcium, after performing the tested erosive cycle. Moreover, this reduction in mineral content is more prominent in control group for which enamel samples were just brushed with fluorine-free toothpaste thus reinforcing the protective effect of topical fluoride application, with surface adherent remineralizing capacity. Regarding the polarized Raman measurements, the assessment of protective effect of the varnish against acid challenge was overwhelmed by the effect that the application of the fluorinated varnish had on the enamel, namely, with the significant decrease of the depolarization ratio and increase of anisotropy in Stage 2. After application of the protective varnish and toothpaste, the decrease of ρ_{959} is more significant, corresponding to a substantially greater alteration of the structure of enamel. Sound human enamel is composed of carbonated hydroxyapatite crystals bundled in a highly ordered structure; most enamel rods have one orientation. However, the orientation of rod arrangement changes in a demineralized/remineralized region causing an increase/decrease of depolarization ratio and concomitant decrease/increase of anisotropy, respectively [38, 39]. Mineralization of enamel after use of fluorinated whitening product was already determined by Bollineni et al. [63] after application of 10% carbamide peroxide gel with 0.463 % of F. Similar decrease of depolarization ratio, although in lesser extent, also was verified in the samples in the control group, brushed with Ca and P containing toothpaste. There is again evidence that the toothpaste plays a role in mineralizing enamel, here more evident because of the reduced probed volume in a Raman measurement, within 1 micrometer, hence more sensitive to superficial changes.

6.2.2 - Assessment of human dental enamel samples with different caries severity degrees

6.2.2.1 – Context and goals

In this section I will describe an *ex-vivo* study performed on two different study groups, each with 10 human dental samples, which resulted in three main distinct spectral data groups: **A** – sound teeth (white-white opaque, not affected by caries); **B** – intact (white opaque or yellow), mild-affected tissue from a healthier and non-cavitated region of carious teeth; and **C** – edge of cavities and cracked carious tissue - moderate to severely affected, of the carious teeth from group B (selected points for measurement from the edge of carious lesions and/or cavities).

6.2.2.2 - Materials and methods

Specimen selection and sample preparation

Twenty human teeth (incisive, canine, pre-molar, and molar), divided in 10 non-carious and 10 carious, non-restored, previously extracted for periodontal or orthodontic reasons and preserved in a 0.5% (w/w) chloramine T_3 – H_2O solution, at 4 °C, were carefully selected and evaluated by research dentists, employing a stereomicroscope (Meiji Techno EMZ 8RT, Japan). Samples were stored in properly identified storage vials in a new chloramine solution until the beginning of measurements.

Methodology and experimental groups

In this work were analyzed three experimental groups of human dental enamel samples, each containing 10 tooth samples, **A** – sound and intact teeth; **B** – sound regions from carious teeth; **C** – cavity edge of carious and /or cracked teeth, as shown in Figures 6.4 and 6.5. All sets of samples were analyzed using the Raman polarized spectroscopy technique. Between applications and during the measurement procedures, all examined teeth samples were not brushed, treated, nor kept in human saliva, or other solutions, to maintain the same experimental conditions – dry environment. Nevertheless, there was no significant dehydration of the sample enamel surface. This was avoided since all Raman measurements, for both of approaches, were performed within a few days.

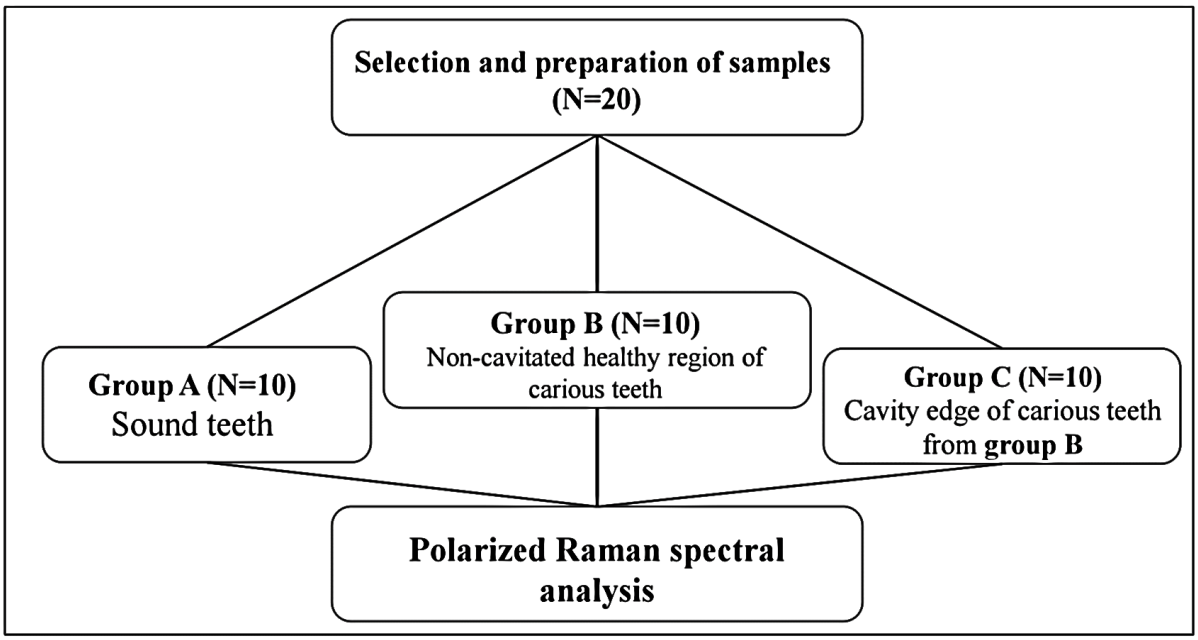

Figure 6.4 - Flowchart of the methodology used for the assessment of mineral content of the examined samples.

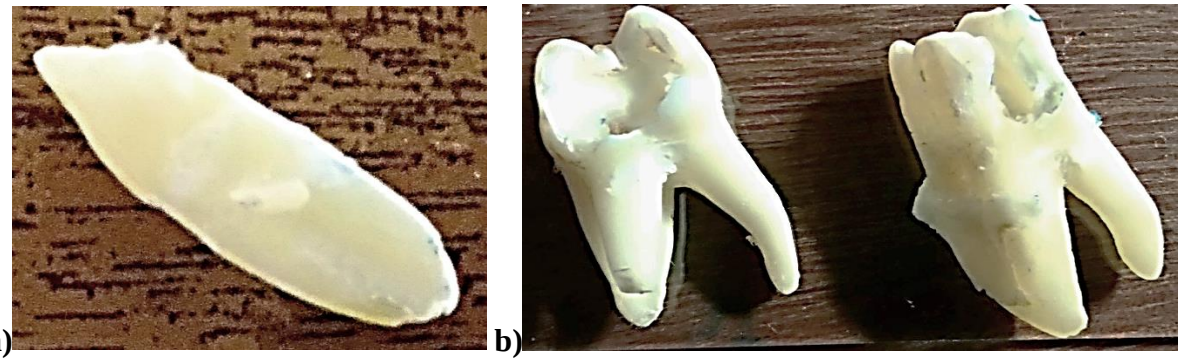

Figure 6.5 – Representation of three of the examined enamel samples from: a) Group A and b) Groups B and C.

Experimental setup – Raman microscope

All acquired Raman spectra of the examined samples during this study were obtained using the same equipment – Horiba XploRA Raman microscope (Horiba, Jobin Yvon, France), with the configuration described in section 6.1. For each tooth sample, an average of 30 measurements was performed: 10 different randomized points – to reduce bias, with no polarization, parallel polarization between the incident radiation and the scattered one, always followed by other 10 with cross polarization. The exposure time for each measurement was 15 s with 3 accumulations (resulting in an overall acquisition time of 45 s). The analyzed parameters were the depolarization ratio ($\boldsymbol{\rho_{959}}$) and polarization anisotropy ($\mathbf{A_{959}}$) of the symmetric stretching band of phosphate ($\boldsymbol{\upsilon_1}$ PO_4^{3-} ~ 959 cm^{-1}), similar to [1, 4, 17, 39, 47, 53, 64].

6.2.3.2 - Statistical analysis

All spectral parameters were analyzed using IBM SPSS v27.0 software (IBM Statistics, Inc. Chicago, IL, USA). Parametric tests were used since the study had a sufficiently large sample size (all analyzed variables with N ≈ 300, with N ≈ 100 per group; in some cases, the numbers were slightly inferior to N=100, since the extreme outliers were excluded from the analysis) according to the central limit theorem [62]. ANOVA tests with Tukey post hoc were performed to analyze differences between the groups, for each of the calculated or obtained spectral parameter, since all groups were considered as independent study groups. Even if the groups B and C were originated from the same dental samples, these included spectra obtained from different regions of the teeth, B – sound region and C – cavity edge from carious teeth. It was considered a statistical significance level of p=0.05 (pre-specified significance value is <0.05).

6.2.2.3 – Results

The acquired Raman spectra, with different polarizations, are represented below in Figure 6.6.

a)

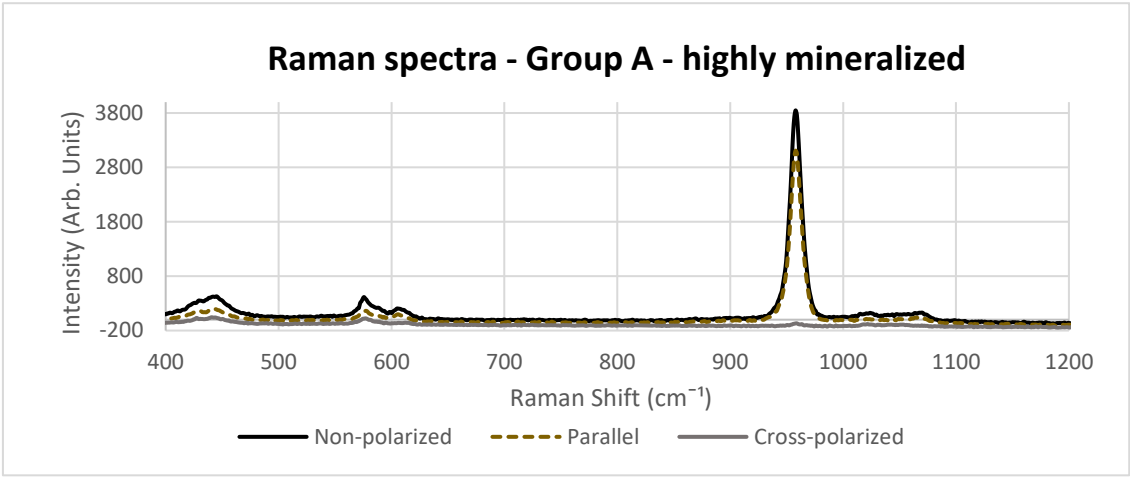

b)

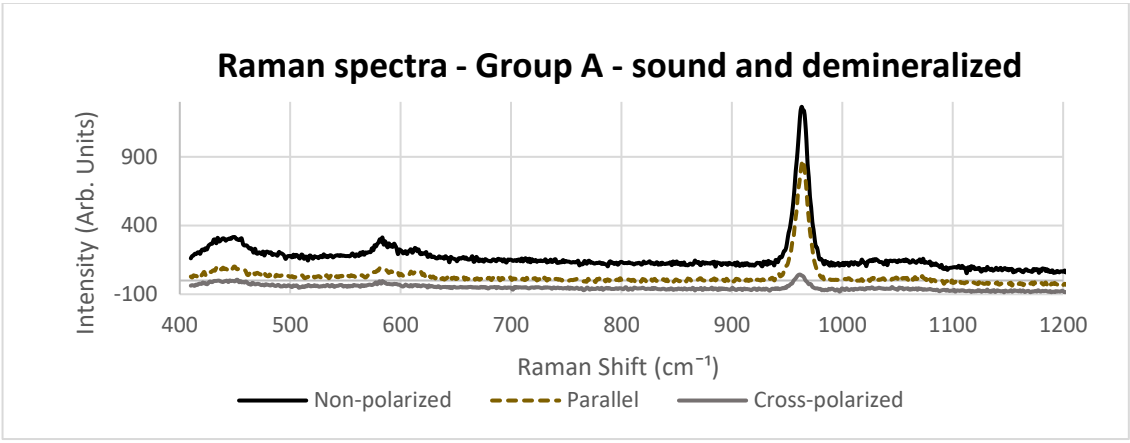

c)

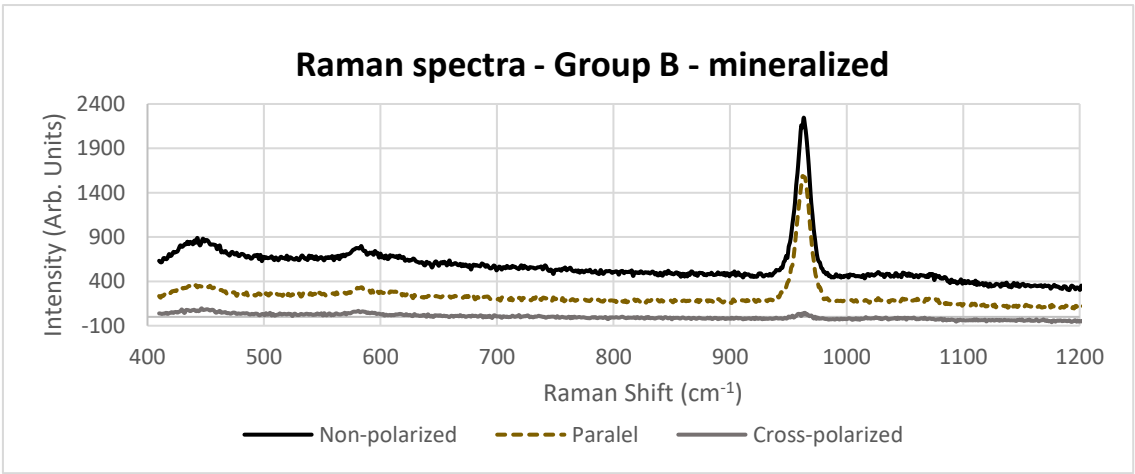

d)

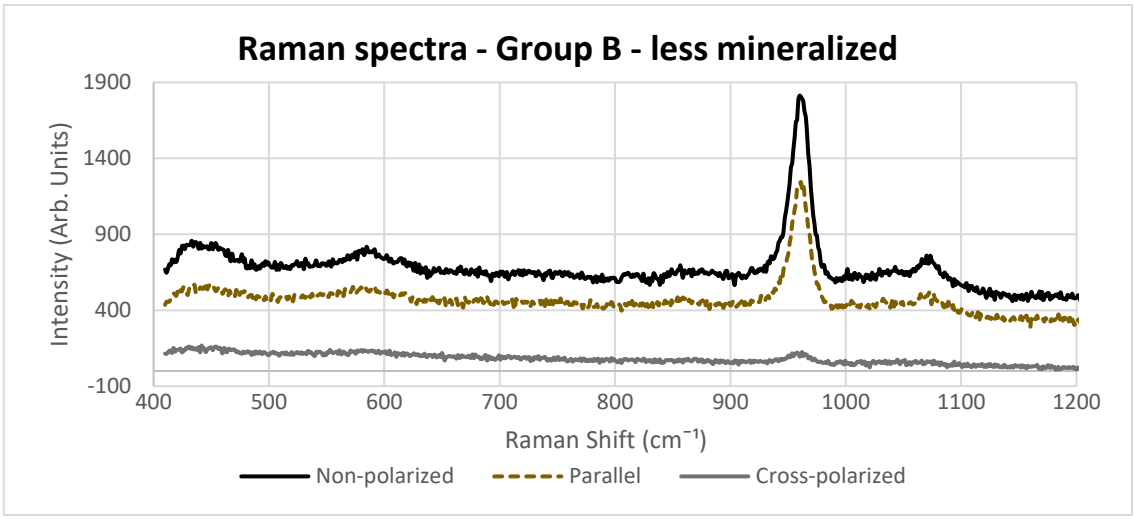

e)

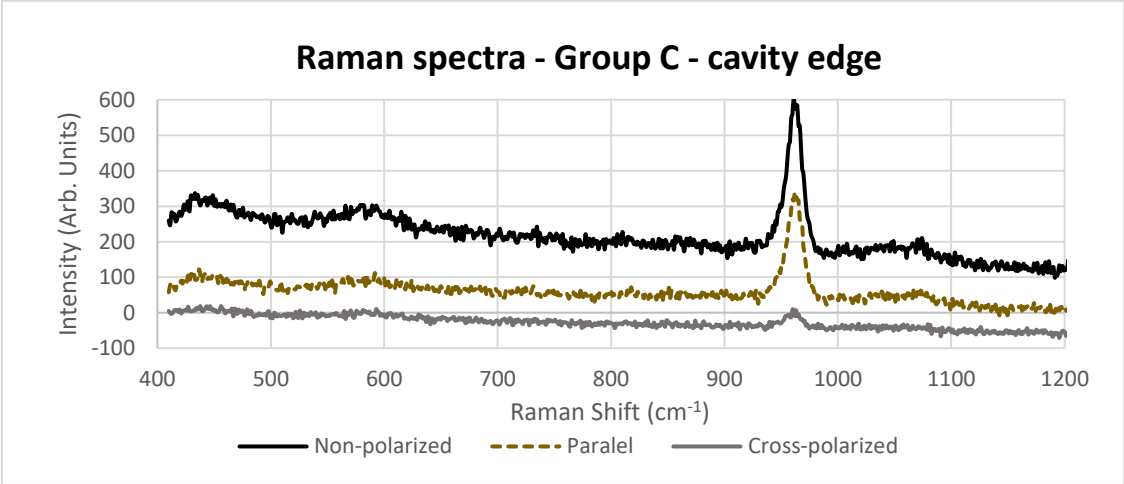

f)

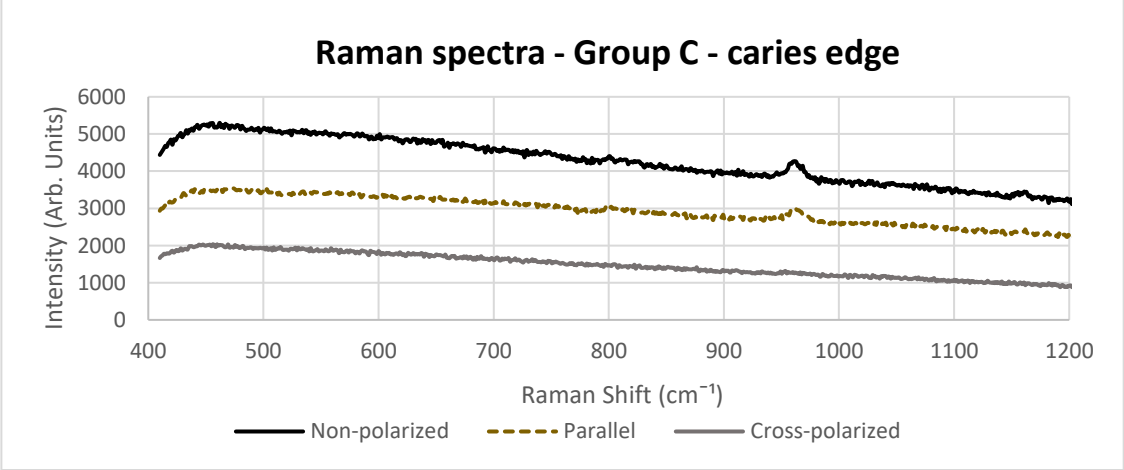

Figure 6.6 – Graphs representing the Raman raw spectra, without background removal, obtained during benchtop measurements, using the Horiba XploRA confocal microscope, with different configurations of the polarizer, for **a)** and **b)** sound enamel samples, with high and low mineralization degrees, respectively; **c)** and **d)** healthy and non-affected region from distinct carious tooth samples; **e)** and **f)** cavity and caries edges from different carious dental samples.

After spectral data processing and analysis, all obtained results comprising the mean values and st. deviations for each of the parameters are graphically represented in Figure 6.7, showing the main differences between the study groups. Both parameters, ρ_{959} and A_{959}, have revealed statistically significant differences between the three groups, with $p<0.01$ Tukey post hoc.

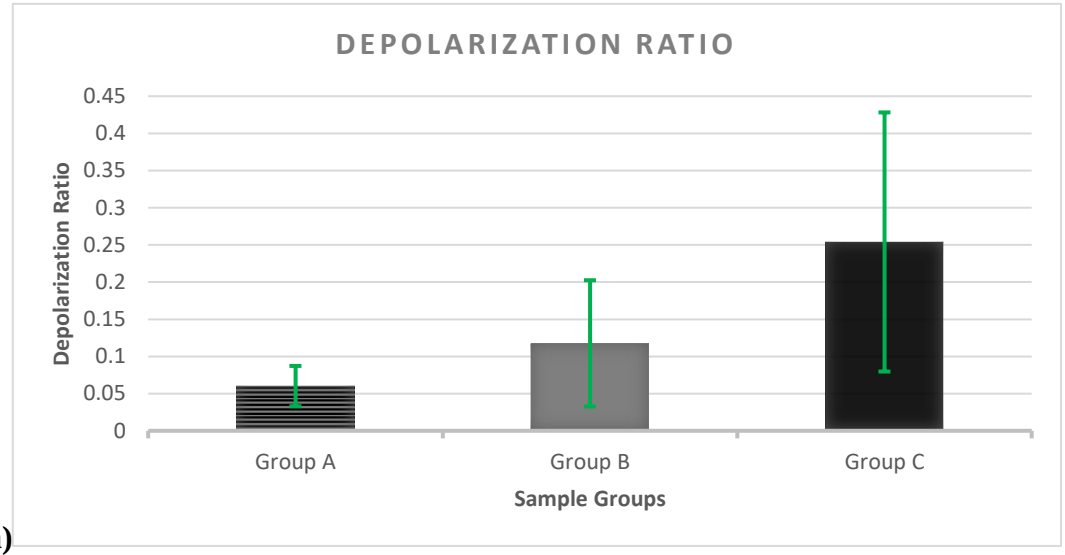

a)

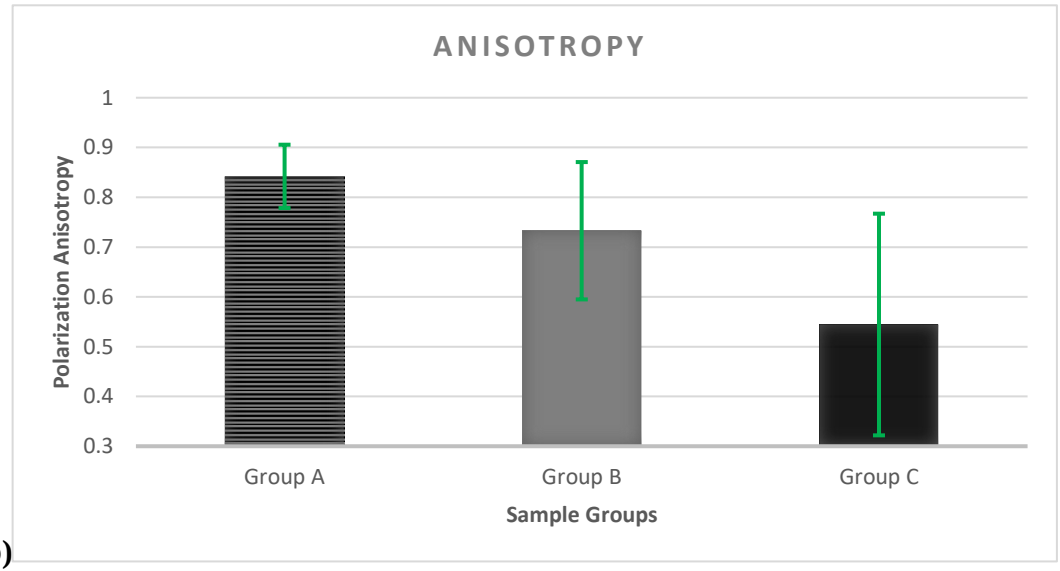

b)

Figure 6.7 – Bar-charts, with columns representing the mean values, with the error bars showing the uncertainty range (standard deviation), for **a)** depolarization ratio (ρ_{959}) and **b)** polarization anisotropy (A_{959}) parameters, for each study group.

6.2.2.4 – Discussion

This work, performed *ex-vivo*, by means of polarized Raman spectroscopy, was conducted to distinguish between three main groups of enamel samples**: A – sound** (white-white opaque, not affected by caries); **B – intact** (white opaque or yellow) tissue from a healthier and non-

cavitated region of **carious teeth**; and **C – edge of carious tissue and cavities,** and cracked regions of the carious teeth from group B (selected points for measurement from the edge of carious lesions and/or cavities).

The obtained data has revealed strong evidence of an overall significant loss in mineral content of the carious samples, particularly in the regions near the non-cavitated lesion margins or cavity edges. Therefore, this reduction in mineral content is the most prominent in Group C, resulting in significantly higher depolarization ratios (ρ_{959}), and markedly decreased anisotropy values (A_{959}).

6.2.3 – Study of oral hygiene and cleaning dental products effect on enamel

6.2.3.1 – Context and goals

According to Janiszewska-Olszowska et al. [65], periodic consultations and the patient's oral hygiene habits helps to maintain the biofilm control and leads to a decrease in the incidence of caries and maintenance of periodontal health. On the other hand, and according to the afore-mentioned work, it is also known that ineffective biofilm control is at the origin of the main oral diseases mentioned above. In this way, it is essential to carry out periodic oral hygiene consultations that include biofilm control and tartar removal [65].

The oral hygiene consultation comprises a set of commonly applied procedures that include the use of ultrasonic and manual instruments to remove tartar and a bicarbonate jet to eliminate biofilm and extrinsic pigmentation [66-68]. One of the objectives of the mentioned procedures is a minimally invasive treatment, preserving as much as possible the integrity of the surfaces on which they are used, guaranteeing the effectiveness for which they are performed [69, 70]. In this way, the use of the jet has become an alternative for biofilm removal, complementing and facilitating oral hygiene consultations due to the advantages it presents for the professional and the patient. This procedure allows for faster treatment, less fatigue for the professional and better and easier access to difficult surfaces [65, 70, 71]. The main objective of the present work is to study the effect of using two different cleaning products: sodium bicarbonate and erythritol jet on enamel surfaces, under *in-vitro* conditions.

Polarized Raman measurements were performed on two groups of sound enamel samples, during two study stages: before and after being subjected to dental hygiene products, in order to assess the mineral composition changes of the examined enamel samples, after the treatment.

6.2.3.2 – Research design and methodology

Sample selection and sample preparation

Twenty-six enamel samples were obtained from healthy anterior teeth stored in a 1.0 % chloramine solution. The teeth were extracted for surgical reasons to place implants and were preserved for a maximum period of 3 months. The samples were observed with a stereoscopic magnifying glass in order to identify possible irregularities on their surfaces. In cases where irregularities were identified, the samples were rejected and replaced by others. Each of the substrates was randomly divided into two groups, one group undergoing intervention with erythritol – group A, and the other with sodium bicarbonate – group B (Figure 6.7). Enamel samples were taken from sound teeth, ensuring that a smooth surface of enamel and dentin alone was obtained, separately. Samples were cut to a size of 8 mm x 2 mm x 2 mm according to the cutting sequences shown in Figure 6.1. After cutting, samples were kept in 1.0% chloramine.

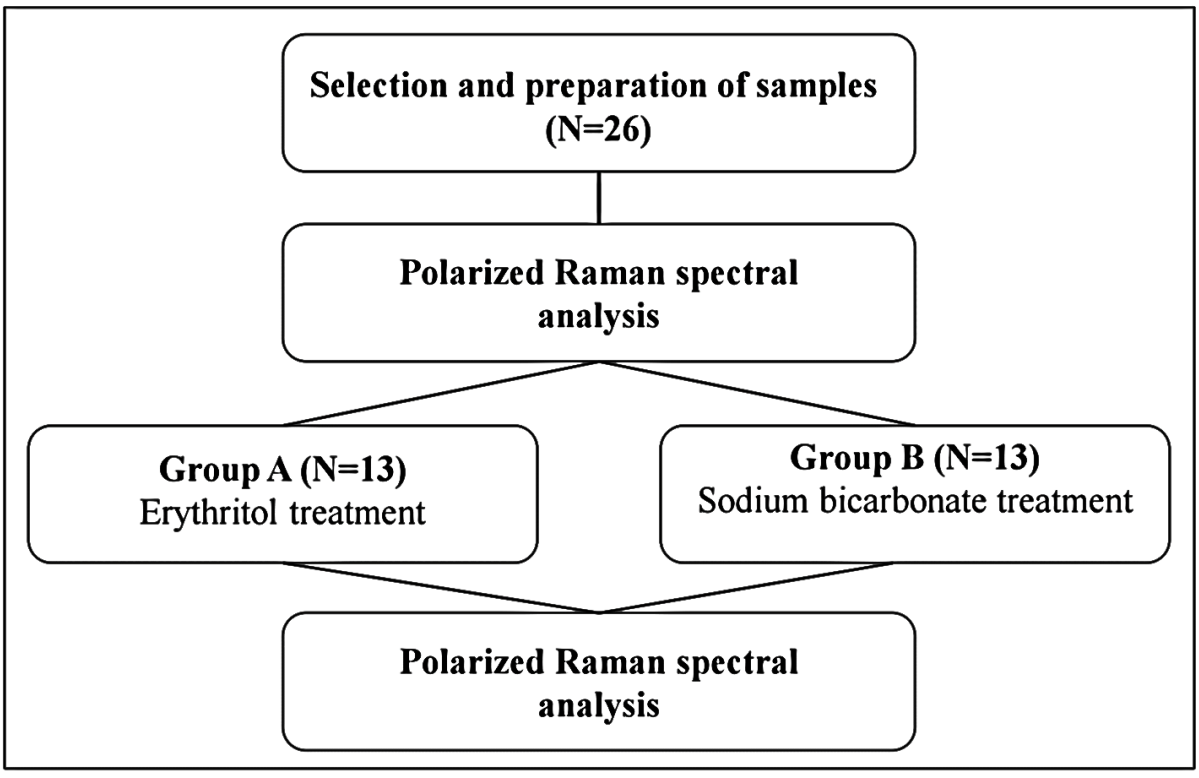

Figure 6.8 - Flowchart of the methodology used for the assessment of mineral content before and after the application of cleaning products.

Dental products

The sample treatment was carried out using two types of products: erythritol and sodium bicarbonate. The characteristics and composition for each of the dental cleaning products are presented in Table 6.1.

Table 6.1 – Dental products characteristics.

Commercial designation/ reference	Producer/Country	Composition	Particle dimension
Classic (DV-048/ LEM/65)	EMS SA/ Switzerland	Sodium bicarbonate Amorphous silica	~65 μm
Plus (DV-082)	EMS SA/ Switzerland	Erythritol Chlorhexidine 0.3% Amorphous silica	~14 μm

Experimental setup - Raman Microscope

Raman spectra of samples were obtained using the same equipment described in section 6.1. Each spectrum was obtained by 3 accumulations of 20 s each, completing an average of 20 measurements per sample (10 distinct points). In each spot, Raman spectra were recorded with two orthogonal polarization configurations of scattered light (perpendicular and parallel to the polarization of the incident laser).

6.2.3.3 - Statistical Analysis

All data collected was analyzed using IBM SPSS v27.0 software (IBM Statistics, Inc. Chicago, IL, USA). Parametric tests were used since the study had a sufficiently large sample size (all analyzed variables with $N \approx 260$, with $N \approx 130$ per study group) according to the central limit theorem [62]. Independent t-student tests were performed to analyze differences between the two groups – A and B, for each spectral parameter, since these groups were considered independent. Paired t-student tests were used to compare the obtained data, for each of the groups, before and after the jet treatments. It was considered a significance level of $p=0.05$.

6.2.3.4 – Results

Thirteen enamel samples per study group were analyzed by means of polarized Raman spectroscopy, before and after applying the dental products for jet cleaning. The paired t-student tests have not revealed any significant difference between the study phases, while independent t-student tests have shown statistically significant differences for the depolarization ratio - ρ_{959} between the study groups only after the treatment, with a significance of $p<0.01$. The obtained mean values of the depolarization ratio are shown below in Figure 6.9.

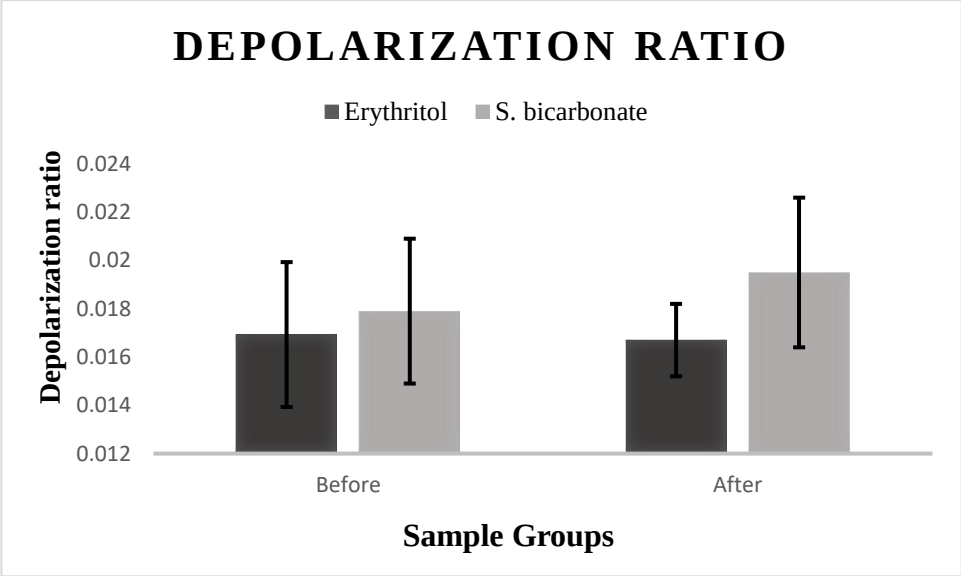

Figure 6.9 – Mean values of the depolarization ratio obtained for both groups during the different stages of the study (before and after jet cleaning).

6.3 – Overall conclusion on performed studies

The 1st study demonstrated that erosive acid procedures result in mineral loss, while control enamel samples treated only with dental toothpaste are more prone to demineralization and acid erosion. Dental varnish products used according to manufacturer instructions seem to preserve enamel integrity and structure of enamel surface layers, as well as the elemental Ca concentration, promoting remineralization and preventing the demineralization process. Dental fluorinated products efficiently incorporate fluoride in the surface aprismatic enamel crystalline structures. This study confirmed that Raman spectroscopy, can be successfully applied, *in-vitro,* to monitor the mineral content alteration in mineralization/demineralization processes, by assessing the behavior of phosphate group [53].

The 2nd study, similar to the previously described studies, is in agreement with the revised literature and has confirmed, once again, that polarized Raman spectroscopy can be successfully applied, ***ex-vivo***, to assess and monitor the mineral content alteration in mineralization/demineralization processes, as well as to distinguish and compare the results from distinct groups of tooth samples, with different conditions – varying from sound and highly mineralized to carious, demineralized with cavities and/or hypo-mineralized specimens.

The 3rd study also yielded important results, showing no significant differences between product application phases, as expected. Moreover, it was clearly shown that before the treatment, the sample groups were not significantly different, showing a statistically significant discrepancy only after the treatment, confirming that sound and highly mineralized enamel samples differ between them only after undergoing a different treatment or distinct product application.

Hence, all described studies that were conducted with polarized Raman spectroscopy have confirmed that this method can be certainly applied, *in-vitro*, or *ex-vivo*, to assess and monitor the surface mineral content changes before and after the application of protecting fluorinated products, bleaching products or during different treatments and/or procedures, such as acid erosive challenges or jet cleaning procedure with different dental cleaning products, as well as to distinguish and compare the results from distinct groups of enamel samples, subjected to distinct treatments and/or product applications. Therefore, polarized Raman technique can be regarded as a sensitive analytical technique in the biomedical field, providing specific parameters – $\boldsymbol{\rho_{959}}$ and $\mathbf{A_{959}}$, that characterize the overall mineral condition of the tooth which can bring improved solutions and new imminent bright perspectives for diagnostic spectroscopy, imaging, and image guided treatment in dentistry in the close future.

7

ALTERNATIVE METHODS FOR RAMAN SPECTRA EVALUATION

In the previous chapter were described several case studies performed by means of polarized RS, by analyzing and comparing the depolarization ratio (**ρ959**), and polarization anisotropy (**A959**) ratios, which, can yield precise information about the chemical composition – presence of HAp phosphate ions and relative amount - degree of mineralization, structural arrangement, HAp rods orientation and degree of crystallinity. These parameters, especially the **ρ959**, were already repeatedly proven, according to the existing literature [1, 4, 17, 37, 47, 53, 64] to be relevant characteristics for the assessment of the mineralization/demineralization degree of hydroxyapatite surface layers. In this chapter are described alternative methods to the polarized Raman technique, such as the combination of Raman-PCA, as well as additional parameters that can be extracted from the acquired spectra, such as band position, band width (FWHM) and the b-type carbonate ratio, which is a ratio between the band assigned to b-type carbonate located at 1070 cm^{-1} and υ_1 symmetric stretching band of phosphate group at ~959 cm^{-1} [72].

7.1 - Application of unsupervised MVA methods to Raman spectroscopic assessment of human dental enamel

7.1.1 – Context

In this chapter, I will describe a latter study, performed during my PhD research, in which the obtained Raman data from an initial study [53] described in section 6.2, was divided in three main groups: 1) numerical parameters extracted from Raman spectra; 2) average baseline corrected Raman spectra; and 3) average raw Raman spectra. The 2nd approach was implemented for reducing as much as possible the fluorescence background and enhance the SNR.

All these data sets were analyzed and characterized by using mainly two different unsupervised multivariate methods: 1) Principal component analysis (PCA) and 2) Hierarchical clustering. From this work resulted two papers, namely: “Application of machine learning methods to

Raman spectroscopy technique in dentistry" [73] and "Application of unsupervised multivariate analysis methods to Raman spectroscopic assessment of human dental enamel" [74], which are interconnected and share mostly the same Raman data and analytical results.

7.1.2 – Introduction – Principal Component Analysis

Principal component analysis (PCA) method represents the unsupervised multivariate statistical tool most extensively used, which is widely applied especially when vast spectral data must be transformed into a smaller number of independent variations known as principal components (PCs), while contributions of these components are known as scores, which are extensively used as parameters for classification. PCA algorithms are frequently applied directly to collected (Raman) spectra within a certain data set to reduce the original dimensionality into a linear combination of orthogonal basis spectra known as principal components (PCs), resulting afterwards in derived loading plots represented as plots of first three PCs as function of the wave number. Generally, the first PC is the most important and accounts for the spectral features with highest variation, while subsequent secondary and tertiary PCs represent features with progressively lower variance. PCA method is typically used to characterize and distinguish the Raman spectra of a specific "calibration set" of samples that contain at least two distinct features/chemical components, as determined by pathology under study. In the case of Raman measurements, PCs represent an orthogonal set of spectral data (with varying spectral parameters), a linear numerical combination of which can accurately provide valuable insights on each of the existent spectra in the sample set. By correlating the mentioned fitting coefficients "scores" of the analyzed spectra in the data set with their established classifications, an accurate diagnostic algorithm can be easily obtained. However, its main disadvantage lies on the fact that PCs are pure mathematical concepts, without any direct physical significance or meaning [73, 74].

When Raman spectroscopy is used in combination with PCA or other MVA methods [73, 74], it is possible to obtain unique spectral characteristics extracted from raw acquired spectra, which can be used for the identification of similar areas, specific features, or certain types of samples, along with differentiation and classification of a different sample or tissue condition, according to the case. Raman spectroscopy and PCA can be used to distinguish control from treated enamel samples [53], as well as to discriminate sound enamel from severe dental fluorosis samples with high levels of sensitivity and specificity [75]. Furthermore, Raman

spectroscopy and PCA can be used to differentiate healthy (sound) from demineralized enamel, as well as identify and assess enamel remineralization with different fluoride solutions [76]. RS-PCA method was also used for the analysis of human dental enamel surfaces from sound, affected (cavitated), and highly affected tooth samples, revealing that exists a predisposition in individual teeth to caries that can be directly correlated with the structural/compositional enamel changes that occur mainly along the main c-axis of hydroxyapatite crystals [77].

Therefore, MVA unsupervised methods, such as PCA, applied to Raman technique can provide a baseline for methodological development designed for clinical diagnostics of different pathologic conditions, being of a great utility for data analysis in several relevant fields of dentistry diagnostics and research [73, 74], as follows: (1) early detection and recognition of carious lesions; (2) differentiation between normal (sound, intact, healthy or control) and affected samples (by several conditions such as caries, tooth decay, demineralization, hypo-mineralization, fluorosis, Amelogenesis Imperfecta); (3) bleaching products performance; (4) assessment of dental pharmaceutical products, for example fluorinated dental protecting varnish; (5) demineralization induced by acid erosive challenges, low pH foods, and acidic beverages; (6) proteomic differences between different types of human teeth; (7) remineralization agents and other related treatments; and (8) cleaning products or procedures, such as jet cleaning or dental laser treatments.

7.1.3 – Methods and materials

In this work were applied PCA algorithms to the spectral data obtained in the previous study, in order to differentiate the samples of the Control from Treatment group, aiming to establish the most suitable methodologies for the treatment of Raman spectra and evaluation of the collected data. Multivariate analysis methods were applied to Raman spectra, acquired in our laboratory, from 20 enamel samples, as shown in Figure 7.1. In order to establish the most efficient method for Raman data analysis and evaluation, and to distinguish between enamel sample groups, three different approaches were undertaken: A—principal component analysis (PCA) of the numerical spectral parameters derived from Raman spectra deconvolution, namely, depolarization ratio, polarization anisotropy, band width (FWHM) and band shift for the symmetric stretching band of phosphate.; B—PCA of the average Raman spectra after baseline correction using polynomial function; and C—PCA of average raw Raman spectra.

These three approaches were applied on control and treatment group samples, before and after application of fluorinated varnish (treatment group) and acidic erosive cycle.

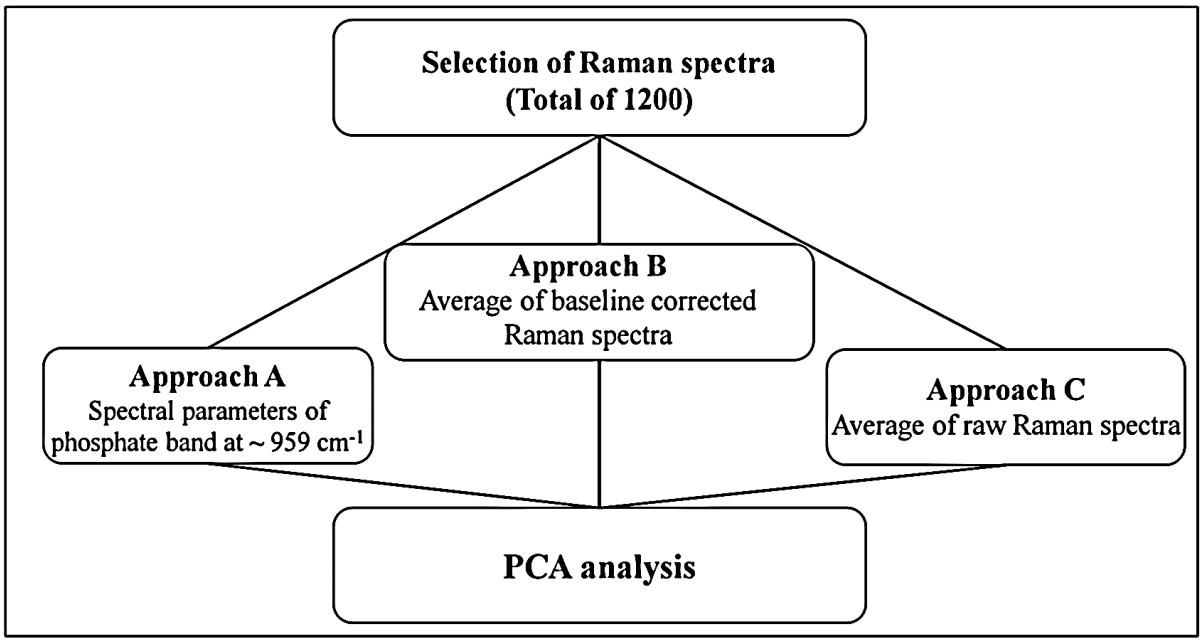

Figure 7.1 – Schematic diagram showing the used methodology for the Raman-PCA alternative method.

7.1.4 – Results

The score plots obtained for Approach A, and for all three types of approaches are represented in Figures 7.2-7.3, and Figure 7.4, respectively. These score plots were used to identify, distinguish, and categorize two small clusters: control and fluorinated varnish treated sample groups. Regarding approach A, making use of derived numerical parameters, PC1 scores account for the majority of variance within all analyzed data set. The first three principal components were extracted from the spectral parameters of all enamel samples and were used to identify, distinguish, and categorize two small clusters: control and varnish treated sample groups (Figure 7.2) and to show likewise the correlation degree between these 4 different peak spectral features, namely the depolarization ratio, polarization anisotropy, peak position, and FWHM, which yield useful structural and chemical information. PC1 scores account for the majority of variance within all analyzed data sets, with proportions of 50.55 %, 57.09 %, and 55.18 % for 1st, 2nd, and 3rd treatment stage, respectively. As can be seen in Figure 7.2, in the PCA - correlation scatter biplots, after 1st treatment stage the samples are randomly dispersed, revealing that there is no significant difference between the samples' overall condition within and between groups initially. After the 2nd stage, the treated samples tend to form a group in the center,

starting to separate from control samples that continue dispersed. After the 3rd stage, there is a clear separation between the two groups, with the treated samples getting spatially very close to each other, indicating that most of the varnish treated samples (8 out of 10) share almost the same biochemical characteristics, mineral content, and structural arrangement after undergoing the treatment and acid challenges, remaining equally affected. The key meaning of these biplots representing the sample distribution is that all analyzed spectral parameters, especially band position and depolarization ratio, are strongly influenced by the chemical environment, which has a great impact on hydroxyapatite chemical bonds, and inter- and intramolecular forces of outer enamel layers.

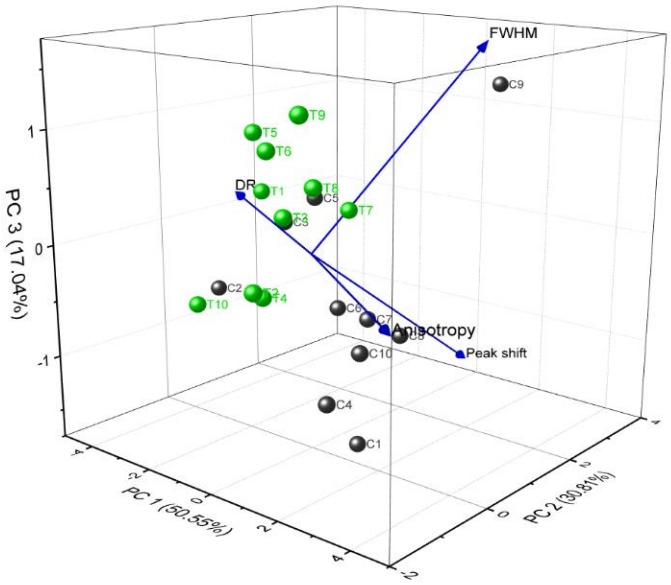

a)

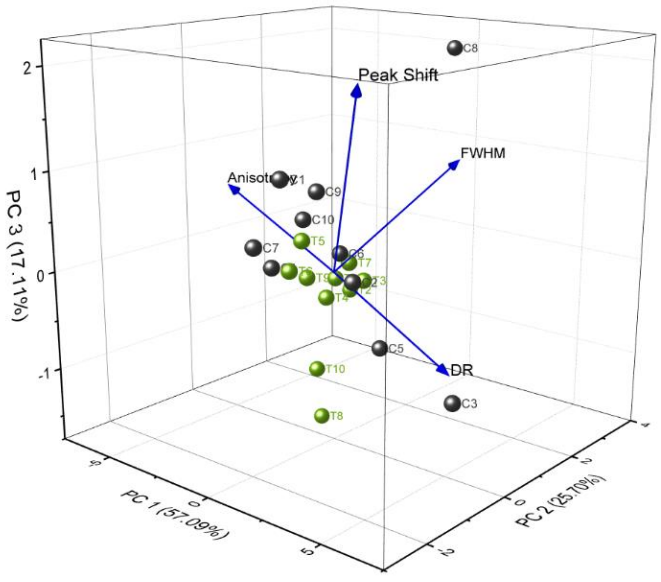

b)

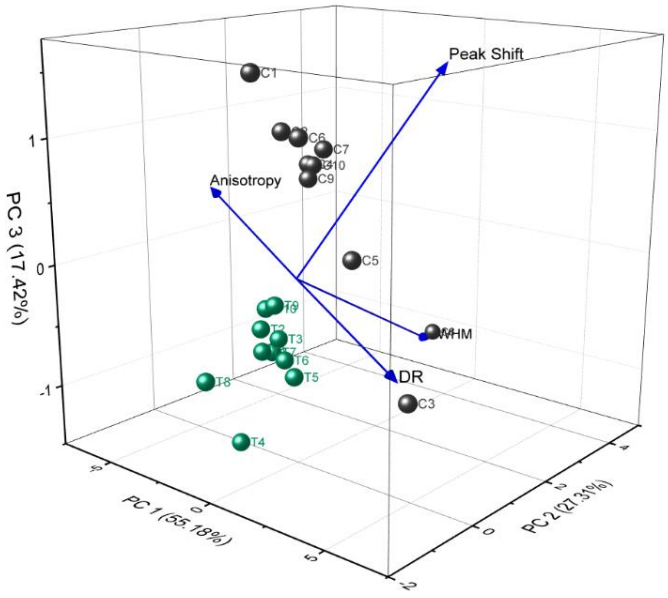

c)

Figure 7.2 – 3D representation of PCA-correlation scatter biplots of analyzed Raman parameter vectors (blue) and differentiation between examined control (black) and dental varnish treated (green) sample groups, corresponding to the following study phases: **a)** 1st – before any treatment; **b)** 2nd – after dental products application; **c)** 3rd – after acid exposure [73].

The exposed results show that PCA can distinguish and separate two different sample groups, according to the main three PC scores extracted from spectral parameter analysis, with the 1st PC score accounting the most. In this study, were chosen the first three most representative components since their summed scores represent all together the greatest majority, varying between 98% and 99,9 %, maintaining the most important information at a significant level. The exposed results confirm that Raman-PCA methods combination has a strong capability for an early detection and evolution monitoring and assessment of dental incipient caries and demineralization/remineralization processes.

Figure 7.3 shows in a different type of graph - score plots, that before treatment, the samples are randomly dispersed, indicating that there is no significant difference between the samples' overall condition within and between groups initially. After 3rd study stage - the erosive challenge, there is a clear separation between the two groups, with the varnish treated samples getting spatially very close to each other, indicating that most of the varnish treated samples (8 out of 10) share almost the same biochemical characteristics, mineral content, and structural arrangement after undergoing the treatment and acid challenges, remaining equally affected.

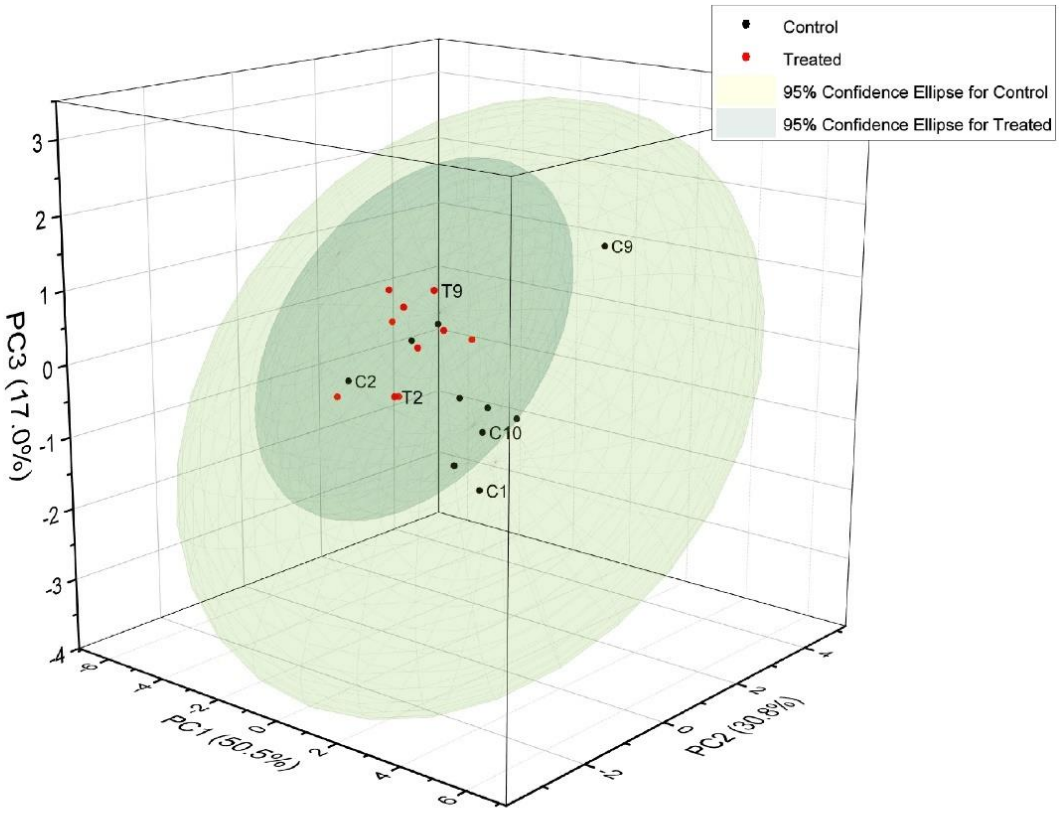
Control
Treated
95% Confidence Ellipse for Control
95% Confidence Ellipse for Treated
C9
T9
C2
T2
C10
C1
PC3 (17.0%)
PC1 (50.5%)
PC2 (30.8%)

a)

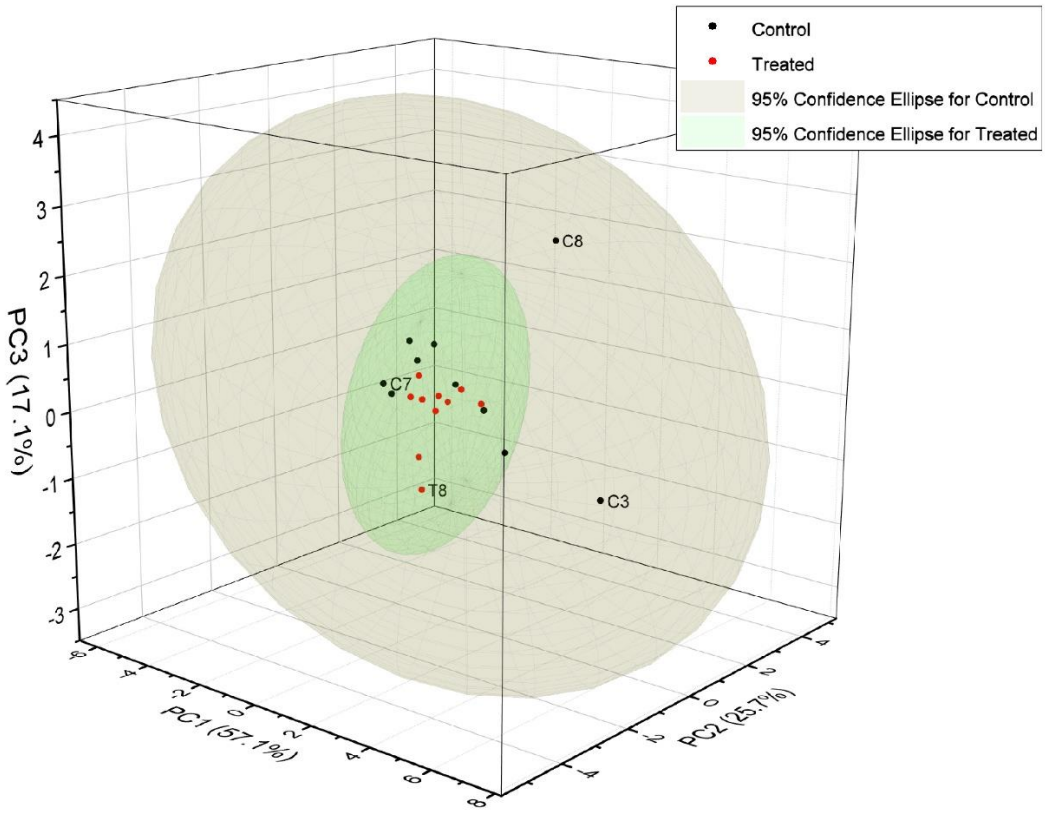
Control
Treated
95% Confidence Ellipse for Control
95% Confidence Ellipse for Treated
C8
C7
T8
C3
PC3 (17.1%)
PC1 (57.1%)
PC2 (25.7%)

b)

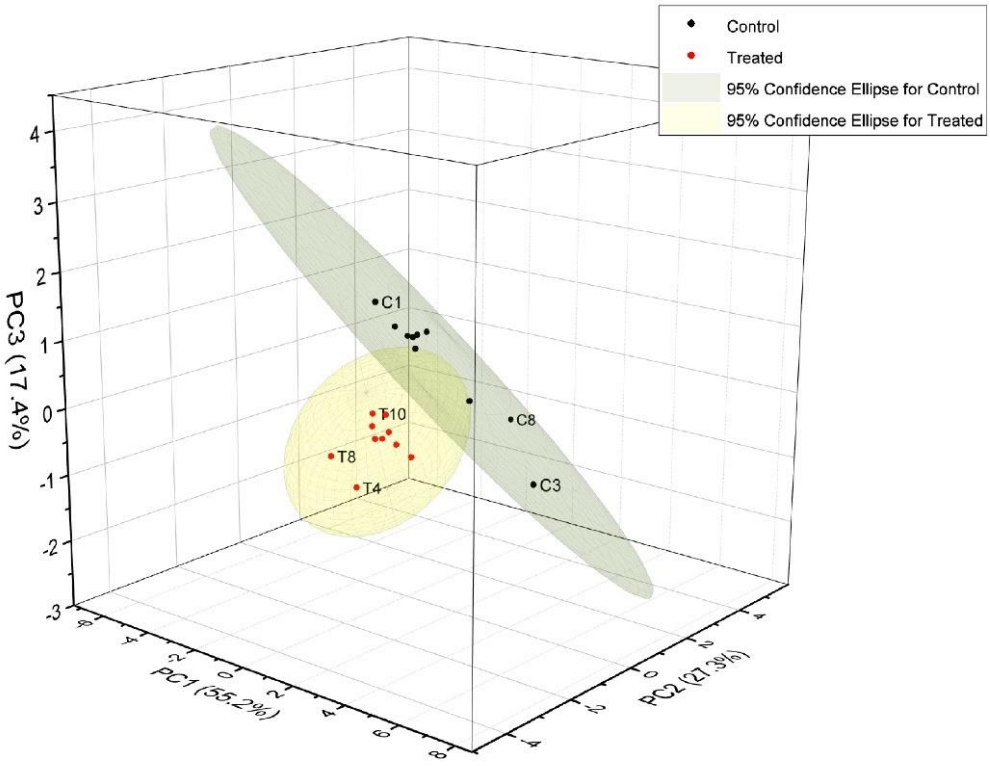

c)

Figure 7.3 – Schematic representation of 3D graphs, illustrating the PCA score plots resulted from approach A, with confidence ellipses of 95 % significance delimiting the distribution of the examined samples, control (black) and treated (red), according to PC scores obtained from the same analyzed spectral parameters after **a)** 1st stage; **b)** 2nd stage; and **c)** 3rd stage of the study [74].

Figure 7.4 shows with more precision the difference between the results obtained with three distinct analytical PCA approaches, during all treatment stages. Nonetheless, these results are still considered preliminary, confirming, that RS-PCA techniques combination has a strong capability to be a non-invasive real-time tool for (early) detection and monitoring evolution of dental caries and demineralization/remineralization processes. Therefore, PCA can be certainly used to recognize similar features within the analyzed enamel samples, as well as to compare and differentiate between different spectral parameters for a precise distinction and classification of the sample groups under examination.

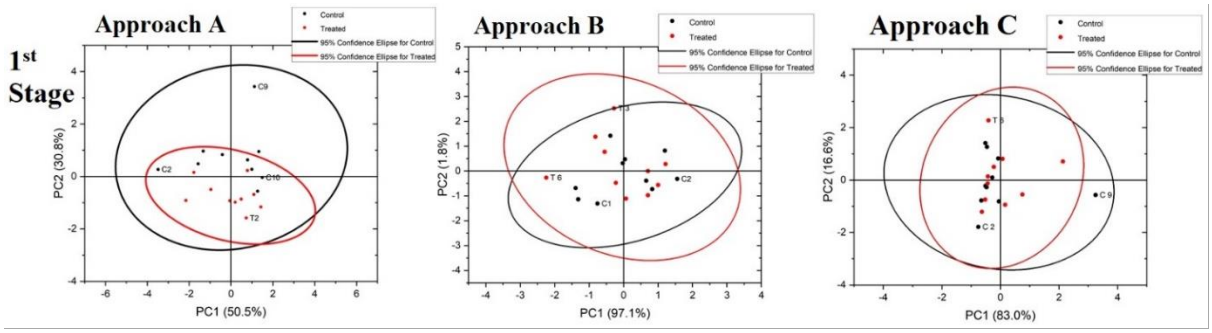

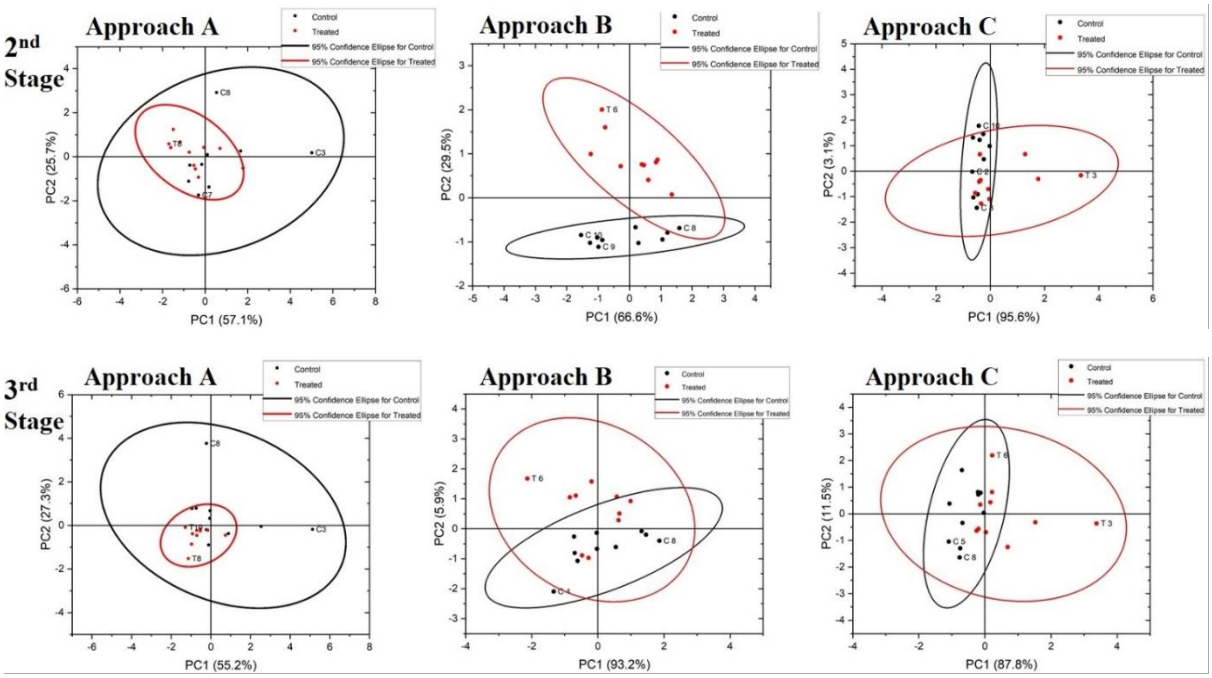

Figure 7.4 – Schematic representation of PC score plots in 2D, obtained by applying PCA algorithm in three different approaches: A, B, and C, respectively. The shown PC score plots for the first two principal components correspond to the 1st, 2nd, and 3rd study stages, respectively.

Thus, the key result of this study is represented by the sample distribution obtained with Approach A, which indicates that all analyzed spectral parameters, especially band position and depolarization ratio, are strongly influenced by the chemical environment, which has a great impact on hydroxyapatite chemical bonds, and inter- and intramolecular forces of outer enamel layers. These parameters will consequently influence dramatically the sample distribution and group separation [73, 74].

7.1.5 – Conclusion

Raman spectroscopy has confirmed to be a specific and sensitive analytical technique in the biomedical field, providing precise spectral results and accurate specific spectral band parameters that characterize the overall condition of the tooth (mineralization degree, caries and/or lesions presence, crystalline orientation, and structural arrangement of both surface and inner morphologic layers). Regarding the data evaluation approach, Approach C has revealed to be less suitable for this kind of study, rendering sample distributions and group separations that could not be discriminated or classified. Approach A showed a clear group separation at the end of the acidic challenge, while Approach B showed a clear group separation and sample differentiation after the 2nd stage – sample treatment, distinguishing the control group from the

dental varnish treated group. The obtained results must be considered preliminary, confirming, that Raman-PCA technique has a strong capability to be a non-invasive real-time tool for (early) detection and monitoring the evolution of dental caries and demineralization/remineralization processes. Therefore, PCA can be certainly used to recognize similar features within the analyzed enamel samples, as well as to compare and differentiate between different spectral parameters for a precise distinction and classification of the sample groups under examination. This study proves that the Raman spectroscopy technique combined with the PCA method has a strong potential to discriminate healthy teeth with sound enamel from demineralized ones, control from treated samples, as well as spectral measurements performed with different laser wavelengths, with good sensitivity and specificity levels. The RS-PCA technique can certainly be employed to monitor the evolution of dental samples during different dental product applications and acid challenges, since it requires no or minimal sample preparation and can provide objective, accurate, real-time, specific, and fast results, reducing subjectivity to human error. There is a high probability that in the next few years, Raman spectroscopy could be routinely used in hospitals, applied particularly to *in-vivo* examinations for diagnosing and surveying several diseases, producing each time quicker and more accurate results, decreasing waiting times and, subsequently, improving investigation efficiency, accuracy, and confidence, along with the efficacy of treatments [73, 74].

7.2 – Alternative spectral parameters: phosphate band width (FWHM), band position and b-type carbonate ratio

7.2.1 - Introduction

In this section is described an additional study, performed, *ex-vivo,* on human enamel samples, using the benchtop equipment - Horiba XploRA BX41 microscope. To accomplish this evaluation, it was performed a Raman analysis, using the same methodology described in Section 6.2.2, including examined sample groups and the Raman equipment, with the same instrumental set-up (1200 grooves/mm dispersive grating, 200µm slit and 300µm confocal hole, NIR 785 nm laser wavelength with the same 50% laser filter, maintaining the same incident beam power, microscope objective, and sample exposure time). Three experimental groups of human dental enamel samples, each containing 10 tooth samples, **A** – sound and intact teeth; **B** – sound regions from carious teeth; **C** – edge of cavitated caries of cracked teeth. Between applications and during the measurement procedures, all examined teeth samples were not brushed, treated,

nor kept in human saliva, or other solutions, to maintain the same experimental conditions – dry environment. The analyzed parameters that were extracted from the acquired spectra are the phosphate band width (FWHM), band position and b-type carbonate ratio, obtained from the ratio between the integrated area of the b-type carbonate band at 1070 cm^{-1}, assigned to the b-type carbonate group, and the integrated area of the phosphate band, located at 959 cm^{-1}.

7.2.2 - Statistical analysis

All spectral parameters were analyzed using IBM SPSS v27.0 software (IBM Statistics, Inc. Chicago, IL, USA). Parametric tests were used since the study had a sufficiently large sample size (all analyzed variables with $N \approx 300$, with $N \approx 100$ per group) according to the central limit theorem [62]. ANOVA tests with Tukey post hoc were performed to analyze differences between the groups, for each of the calculated or obtained spectral parameter, since all groups were considered as independent study groups. Even if the groups B and C were originated from the same dental samples, these included spectra obtained from different regions of the teeth, B – sound region and C – cavity edge from carious teeth. It was considered a significance level of $p=0.05$.

7.2.3 – Results

Three study groups – A, B, and C, with ten teeth per group were analyzed. After analysis, all obtained results comprising the mean values and standard deviations for each of the parameters are graphically represented below in Figure 7.5. The results are presented to show the differences between the study groups.

The parameters that have shown significant differences between the groups were the b-type carbonate ratio and the band width parameters, which have revealed significant differences only between the Group C and the other two groups, with $p<0.01$ Tukey post hoc. No significant differences were observed between the Groups A and B.

These results are further commented and discussed in Chapter 9, which contains a comparative study performed by means of benchtop and probe measurements, analyzing the spectral parameters that characterize the Raman bands assigned to phosphate group (at ~959 cm^{-1}), and additionally, the b-type carbonate group (at 1070 cm^{-1}).

a)

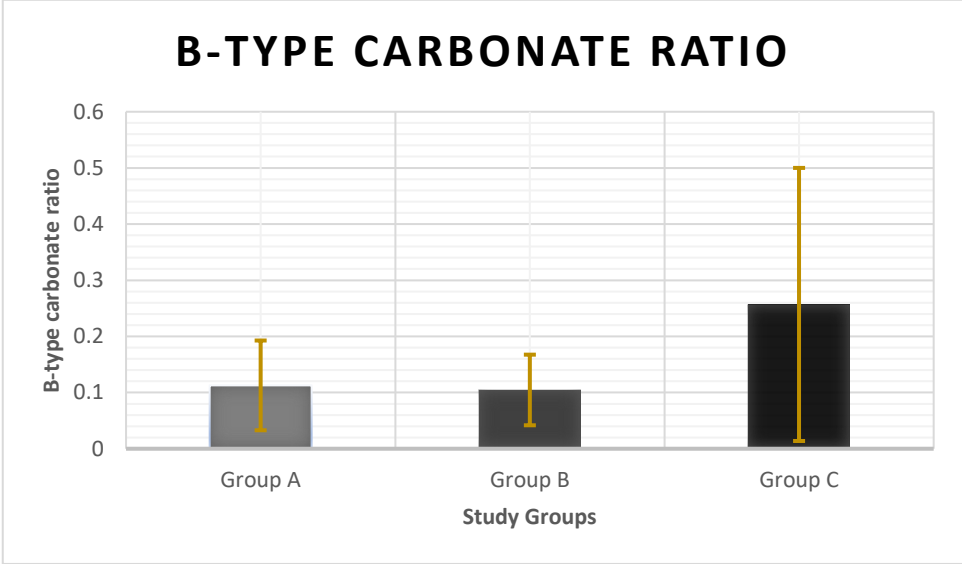

b)

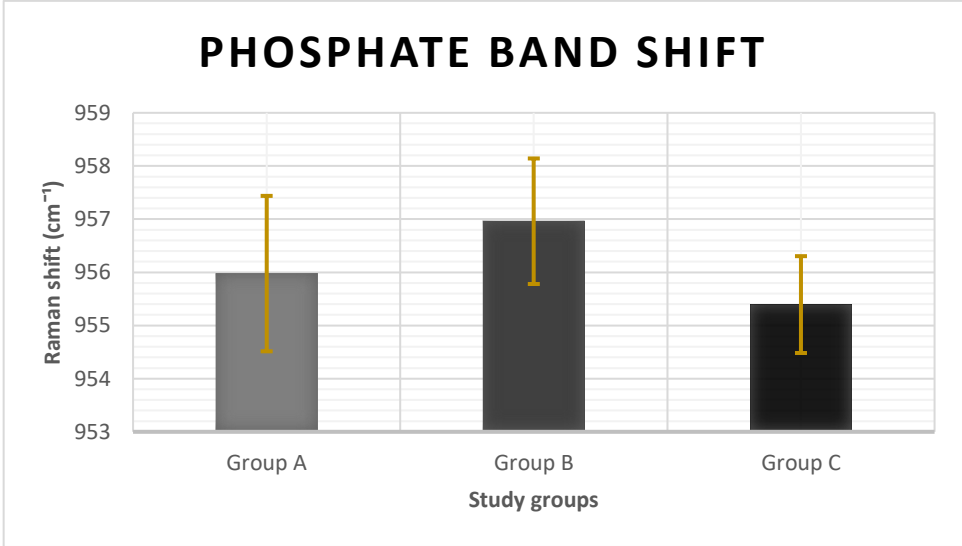

c)

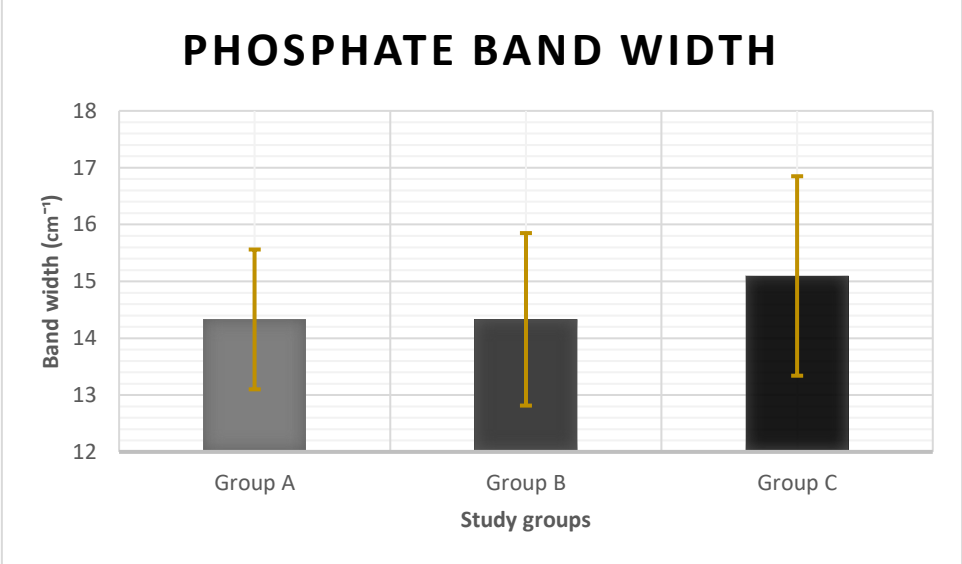

Figure 7.5 - Bar-charts, with the columns representing the mean values and the error bars showing the uncertainty variations, for **a)** b-type carbonate ratio, **b)** phosphate band position and **c)** phosphate band width parameters, for each of the study groups – A, B and C, respectively. Data was obtained by means of benchtop measurements.

In Table 7.1 are represented the individual and overall predicted values (in %) for the **sensitivity** (ratio of true positives to total existing positives in the data), **specificity** (ratio of true negatives to total real negatives in the data), and **accuracy** (ratio of correctly predicted values to the total real data or entire pool of subjects) of different spectral parameters of the phosphate and carbonate bands, compared to the depolarization ratio, used for the distinction of each sample group from the others: A from B, B from C and A from C, obtained by applying the logistic regression method. As shown below, the greatest prediction accuracy is achieved by using the depolarization ratio, followed by the b-type carbonate/phosphate ratio combined with band position and bandwidth parameters.

Table 7.1 – Accuracy of the alternative spectral parameters in distinguishing the sample groups, compared to the depolarization ratio. Spectra were acquired by means of benchtop-based measurements.

Benchtop measurements - depolarization ratio (ρ959)

COMPARISON	SENSITIVITY (%)	SPECIFICITY (%)	ACCURACY (%)
Groups A-B	75	63	69
Groups B-C	84	58	72
Groups A-C	93	77	85
Overall	**84**	**66**	**75**

Benchtop measurements - b-type carbonate ratio

COMPARISON	SENSITIVITY (%)	SPECIFICITY (%)	ACCURACY (%)
Groups A-B	46	59	53
Groups B-C	85	62	74
Groups A-C	83	60	72
Overall	**71**	**61**	**66**

Benchtop measurements - b-type carbonate ratio, peak shift, and peak width (FWHM)

COMPARISON	SENSITIVITY (%)	SPECIFICITY (%)	ACCURACY (%)
Groups A-B	70	71	71
Groups B-C	80	83	82
Groups A-C	79	60	70
Overall	**76**	**71**	**74**

8

RAMAN REMOTE FIBER-OPTIC PROBE

8.1 – Context

The combination of Raman spectroscopy with portable and fiber-optics technology allows for remote and real-time examination, *in-situ* analysis, *ex-vivo* and *in-vivo* investigation, and comparison of different materials – organic, inorganic, or mixed, different compounds or mixtures of compounds, or even biological vital tissues and physiological samples, in a minimally invasive and non-destructive way. Different types of examined samples can be situated in distant, isolated, hardly accessible, contaminated, or even dangerous environments. For such reasons, Raman fiber-optic probes have found numerous applications in several fields, from process control to medicine. Therefore, these can have different designs, varying dimensions, and distinct geometrical configurations – from standard to custom-made, modified and/or adapted according to the examined sample and surrounding environment, containing specific optical components, according to the specific application – industrial use, laboratorial measurements, or clinical examination. Additionally, the remote probe must contain the necessary filters and optical components, coupled to highly efficient input and output optical fibers, in order to deliver the excitation laser beam, collect and transmit the Raman signal with a high efficiency, with minimal signal losses, low fiber spectral background and maximal SNR, yielding Raman spectra with intense and sharp peaks, in order to obtain the highest possible spectral quality, spectral resolution, and band intensities (especially for the "fingerprint" region or bands of interest).

8.2 - Raman fiber-optic probes for biomedical *in-vivo* and *in-vitro* applications – state of the art

The present chapter gives a short and reliable description of Raman fiber-optic probes together with a detailed review on recent studies that implied *in-vivo* or *in-vitro* applications of Raman spectroscopy by means of coupled fiber-optic probes in dentistry research and clinical diagnostics over the last 20 years.

In a study performed in 2005 by Izawa et al. [78], were carried out *in-vivo* trial measurements of living teeth to verify the accessibility of Raman technique by using a fiber-optic probe type multi-channel Raman spectrometer. The authors explored the possibility of dental caries diagnosis by using Raman spectroscopy and its clinical application, reporting that Raman peak intensity of hydroxyapatite at carious lesion was considerably lower compared to the healthy parts of sound enamel tissue, while the florescence intensity levels at the same portions were higher.

Another research study, performed by Ko et al. in 2008 [17], described the possibility of examining tooth enamel by using a fiber-optic coupled polarization-resolved Raman spectroscopic optimized system for an 830 nm laser excitation, which was designed and developed by this group for simultaneous collection of orthogonally polarized Raman spectra within a single measurement. Moreover, these authors demonstrated also "an application of detecting incipient dental caries based on changes observed in Raman polarization anisotropy". They managed to obtain precise results.

In a review paper published by Krafft et al., in 2012 [79], were described with a great accuracy the functioning principles of fiber-optic Raman probes along with their applications in cancer research of lung, breast, skin, bladder, brain, cervix, oral cavity and gastrointestinal tract. The applications of probes in oncology are of extreme importance, namely for the study, diagnosis, treatment, and prevention of all types of cancer. Therefore, according to these authors, dedicated fiber-optic Raman probes must be developed corresponding to the required conditions for the specific application. Handheld probes are considered appropriate for easily accessible sites such as skin or during open surgical procedures. Flexible, small diameter probes can be inserted into the working distal channel of endoscopes. Beside these specific geometrical features, the probe should structurally enable an efficient collection of Raman spectrum with a sufficiently high signal-to-noise ratio, within few seconds measure time at tissue safe power levels. This results in high scattered signal collection efficiency.

Fiber-optic probes for *in-vivo* diagnostic applications by Raman spectroscopy are necessary as optical tools for guiding surgical interventions, delineating lesion margins or for replacing random biopsies of suspicious tissues by targeted biopsies which, in turn, would reduce pathology costs and biopsy-associated risks and morbidity. Different probe geometries and structures have been designed for use by coupling with Raman spectrometers. They can be generally divided into handheld probes and miniaturized probes, planned for minimal-invasive

endoscopic applications. Four different types of Raman probe geometric arrangements are depicted in Figure 8.1 [79].

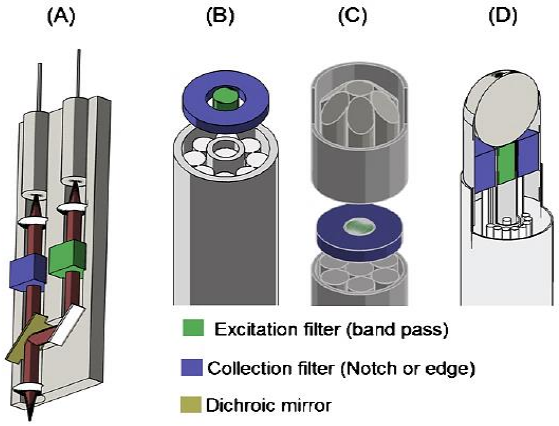

Figure 8.1 – Schematic representation of 4 different types of used geometric configurations of biomedical fiber-optic Raman probes, starting with: (A) Lensed probe with integrated filters (our developed Raman fiber-optic probe is an adaptation of this type of structure and geometrical distribution of optic components); (B) Probe with 1 excitation and a fiber round bundle consisting of 8 collection fiber with filters placed on the tip; (C) Probe with beveled fibers; and (D) ball lens for improved and more efficient Raman signal collection [79].

In a study performed by Akkus et al., in 2016 [5], were exposed important results obtained from Raman measurements, which allowed them to assess the mineral content of tooth enamel and overall mineralization level. The reference Raman measurements of dental mineral content were completed twice by means of a high-fidelity confocal Raman microscope, and following, by a fiber-optic Raman set up which was configured as non-confocal and confocal arrangements, used to collect spectral information from similar and comparable enamel area investigated by a research-grade Raman microscope. The authors reported that during this study it was used a different approach, for the first time, by which the non-confocal fiber-optic system has failed to identify significant differences in mineralization between the analyzed samples, while the combination of the in-line confocal module with the employed fiber optic system resulted successfully in determining the discrepancies in mineral content between the tooth specimens. The provided results indicated clearly that confocal aperture modification for a remote Raman probe is essential for a proper adjustment and a better control of the sampling volume of the examined enamel. Moreover, the authors reported that portable Raman systems integrated with hand-held confocal fiber probe for remote analysis are very promising for the screening and assessment of enamel content and degree of mineralization, providing elucidative results [5].

In a more recent work, performed by Sa et al., in 2017 [80], were monitored the mineral contents change of human enamel, in-vitro, by means of a portable micro-Raman spectroscopic system coupled to fiber-optic probe (B&W Tek Inc., USA), equipped with a NIR monochromatic laser source of 785 nm wavelength. The main purpose of this study, performed *in-vitro*, was to investigate the efficacy and efficiency of micro-Raman spectroscopy technique on detecting and identifying mineral content variations during several sequential demineralization and de/ remineralization cycling processes. The authors also used microhardness and chemical analysis to prove the accuracy of the micro-Raman spectroscopy, affirming that this technique could successfully monitor the human dental enamel surface mineral losses. It was concluded that due to the non-invasive, portable, and remote advantages, as well as the interference from the water, micro-Raman spectroscopy can be considered as a very promising tool and can be certainly used as a reliable, precise, and quantitative technique to detect slight changes in enamel mineral content, in real-time, in the future clinic work [80].

8.3 – Raman probes – configuration and structural components

A feasible probe design must prevent unwanted signal generated in the delivery fiber – Raman scattered, and fluorescence photons generated by the fiber inner components to the sample and avoid reflected excitation light from the incident laser and elastically scattered signal – Rayleigh photons from entering the collection fibers and generating unwanted signal. Experimental results show that significant proportions of silica signal are generated in the excitation and collection fibers, indicating the necessity to use proper filters in the excitation and collection connections of the probe. Moreover, for practical reasons light is typically delivered and collected using optical fibers made of low-OH silica, in order to reduce the inner attenuation and silica background. The main reason is that silica molecules are themselves Raman active, so the Raman and fluorescence signal, known as fiber spectral background (FSB) generated from silica during the excitation beam transmission throughout the fiber can interfere with the sample Raman signal. As a result, the spectral background caused by the FSB can overlap or completely cover the spectral bands of interest, specific for the analyzed sample.

Fiber-optic technology enables the production of small, compact, portable, and flexible devices, which can be easily combined with larger benchtop devices, or integrated into narrow-diameter medical instruments or accessories, such as catheters, endoscopes, and needles, which can be certainly implemented for clinical remote analysis. Moreover, fiber-based Raman

spectroscopy offers the possibility to perform remotely spectral measurements in-vivo, probe contaminated samples or highly toxic products in hazardous environments without compromising the safety of the operators.

The excitation laser light can be remotely delivered to the sample through a combination of structural optical components, such as mirrors and lenses, distributed internally within the probe, according to the type of used configuration, and by means of optical fibers, connected externally to the probe, which may extend up to tens of meters. The remote system focuses the monochromatic light beam onto or into the sample and collects the resulting Raman scattered light. The focused excitation laser spot diameter and intensity depend directly on the used laser power, collimation, focusing optics, as well as on the optic-fiber diameter.

Therefore, the obtention of well-defined Raman spectra, with strong signal and good SNR, with intense, distinguishable, and sharp peaks, depends directly on the power of the monochromatic laser beam, efficient transmission of the excitation beam, efficient and utmost signal collection and appropriate filtering of the Raman scattered photons. The quality of obtained Raman spectra depends also on finding the optimal working distance – a very critical parameter, with regards to collection efficiency, between the employed probe and the examined sample, for a large variety of models. The optimal distance depends on the geometrical and internal structural arrangement of components, varying according to the focusing distance of the lens, internal geometrical arrangement, and characteristics of the optical components. If the probe does not contain a focusing lens, the collection optics (optic fibers or bundle) must, hence, be positioned as close to the sample as possible and must have an aperture as large as possible to provide a large collection angle (large numerical aperture collection optics should be used for this purpose). The collected scattered light must then be spectrally filtered to remove the Rayleigh scattered component (by means of Notch or long-pass filters) otherwise this would swamp the Raman signal. Various types of optical narrow band rejection or edge filters are available to perform this function [2, 26, 27, 81-83].

Overall, fiber-optic probes represent an ideal solution for the analysis of small or large, irregular, outer abnormal and/ or surface awkwardly shaped samples, monitoring real-time kinetic reactions, *in-vivo* sampling, and any other application where it is difficult or impossible to bring the investigated sample to the spectrometer. The recent development of flexible, simple, manageable, and user-friendly fiber optic probes has made them one of the most widespread devices in modern spectroscopy [33].

Usually, when performing *in-vivo* Raman spectroscopy measurements, by means of fiber-optic probes, these can be also affected by an intense background signal, which is generated in the fused-silica fibers, in the fingerprint region of the Raman spectrum (range between 50-2000 cm^{-1}). Once again, optical filtering is necessary to acquire good quality spectra from tissues. The complexity of fiber-optic probes for fingerprint Raman spectroscopy, in combination with characteristics depending on size constraints and flexibility requirements for *in-vivo* use have been a great obstacle in the development of *in-vivo* diagnostic instruments based on Raman spectroscopy. In the past years, a wide variety of different fiber-optic probe designs for Raman spectroscopy have been tested in attempts to overwhelm the problem of the fused-silica background. There were obstacles and limitations with probe designs, with separate excitation and collection paths in order to minimize noise and background. Several of these probe designs, such as 1-fiber-in-1-fiber-out or the *n*-fibers-around-1 configurations (most common) have been reviewed in detail by different authors. Though these multi-fiber designs improve the signal-to-background ratio, they appear to have decreased signal collection efficiency compared to a bidirectional single fiber probe [2, 25-27, 81-83].

8.4 - Filters

An efficient delivery of the excitation light beam requires for a band-pass filter, which ideally allows only a selective transmission of the excitation light with the needed wavelength, attenuating incoming photons of different wavelengths, resulted from silica background (also known as fiber spectral background), originated by the internal scattering processes throughout the fiber core, such as Raman scattering or fluorescence of excited silica. For an efficient detection of the Raman signal, the elastically scattered photons (Rayleigh) from the sample and Fresnel reflected photons must be rejected or attenuated. The collected scattered light must be spectrally filtered to remove the Rayleigh scattered component otherwise this would swamp the Raman signal. This is explained by the fact that Raman peaks at higher wavenumbers are clearly visible, without significant background, while the peaks positioned at lower wavenumbers are completely covered or modified by the background emission from silica. Various types of optical narrow band rejection - long-pass (LP) or short-pass (SP) or edge filters are available to perform this function [2, 21, 27, 28].

These filters are usually contained at the fiber connections, within couplers or legs of the probe. For biomedical applications, usually is required a compact Raman probe. Moreover, in several

medical applications, the probe size, inner structural arrangement and geometric configuration must be appropriate for specific clinical use, resist to pressure, humidity, and temperature variations during surface contacts or at a certain working distance from different specimens, tissues, or corrosive chemical compounds or solutions, according to the case [2, 27-29, 46, 84].

8.5 - Optical fibers

The excitation laser beam is delivered remotely to the sample by means of fiber-optic cables, usually with low-OH core, which may extend up to tens of meters. A lens system focuses the monochromatic light beam onto the sample and collects the resulting Raman scattered light. The collection of the scattered light must be very efficient, with the fiber optics positioned at the lens optimal working distance to the sample, with a sufficiently large numerical aperture, to provide a large collection angle [2, 27, 29, 46].

Optical fibers are considered as ideal waveguides or light tubes for carrying light beams and optical signals to and from an observed sample for remote analysis. Optical fibers are classified in two main types: single-mode and multimode. They can be easily, however cautiously, bended or curved, transmitting the light beam in virtually any direction, over considerable length (in an extension of tens or hundreds of meters), delivering efficiently the outgoing (excitation) or receiving the incoming (collection) optical signals. The fibers' structure consists of a core material (glass or plastic) with a relatively high refracting index surrounded by a cladding with a much lower refraction index, as shown in Figure 8.2. The total diameter of the fiber can vary from a few micrometers to millimeters. For Raman spectroscopic studies, a single (output) excitation fiber can be employed for transferring the light beam to excite the sample under examination, and either a single or multiple optic (input) collection fibers or bundle can be used for transmitting the Raman scattered light back to the spectrometer for analysis [2, 27, 29].

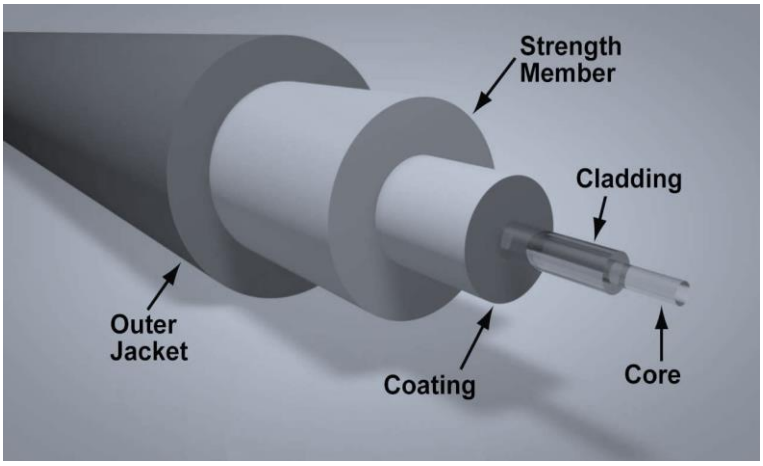

Figure 8.2 – Schematic representation of main structural components of an optical fiber, consisting of the following parts: core (silica), cladding (silica), coating (silicone, buffer jacket), strength member (Kevlar) and outer jacket [82].

Table 8.1 – Loss mechanisms in optical fibers [2].

Attenuation mechanism	**Causes**
Reflection (Fresnel losses)	Difference in index of refraction at the entrance and exit surfaces of the used optic-fiber
Scattering	Intrinsic factor — Mie, Rayleigh, Brillouin, Raman Extrinsic factor — impurities and defects
Absorption	Intrinsic factor — material Extrinsic factor — impurities
Radiation	Mode coupling

When the exciting radiation from a laser source is directed and focused into and throughout an optical fiber to a sample, a part of the radiation will be lost due to Raman scattering by the own fiber material; however, this amount is insignificant compared to the total emitted laser power. At the sample end of the fiber, the radiation will exit in a cone shape determined and influenced by the numerical aperture of the used fiber. Micro-lenses or gradient refractive index lenses are usually used to focus the laser beam onto the examined sample [2, 84].

8.6 – Design and assembly of developed remote fiber-optic probe

The present doctoral project aims to develop a sensitive Raman probe, that transmit efficiently, direct, and focus the monochromatic excitation laser beam throughout an optical excitation fiber – output signal - to the examined dental sample, and to collect efficiently the Raman scattered light and afterwards directing it by means of a collection fiber – input signal - to the spectrometer. The designed Raman probe, that was initially planned, is represented in Figure 8.3, while the final developed probe, with simplified structure and configuration, that was used for experimental remote measurements, is shown Figure 8.4.

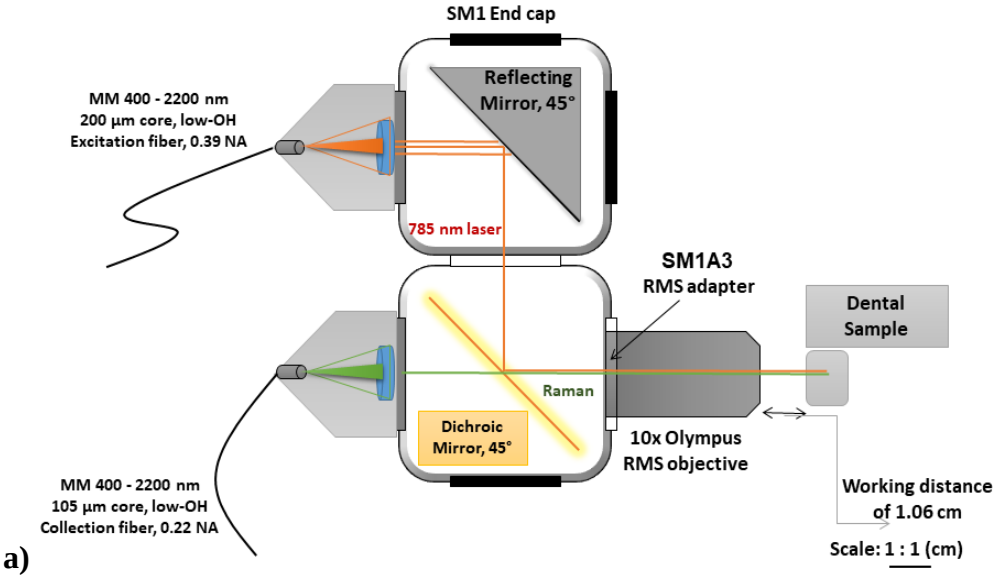

a)

b)

Figure 8.3 – Schematic representation of the **a)** the initially planned fiber-optic remote probe, adapted from [79] and **b)** depiction illustrating the constructed planned remote probe, in real dimensions, with components acquired from Thorlabs [81], and equipped with a 10x magnification Olympus objective, of 0.25 NA.

Figure 8.3 shows above the schematic representation of the initially planned probe design – 8.3a and the resulting constructed probe, equipped with a microscope objective of 10x magnification – 8.3b. The initially planned Raman probe contained the following components: focusing and collimating lenses, band-pass filter (laser transmitting filter), reflecting mirror, a dichroic mirror - 45° beam splitter (in this case the incident beam and collected signal light share a common path). The dichroic component transmits the laser light through the optics to the sample while efficiently reflecting the returning Raman-shifted signal light in direction to collection fiber). Given that the incoming Raman signal is usually extremely weak, this must be collected in normal direction to the sample surface (90^o angle), or 180^o angle in backscattering configuration.

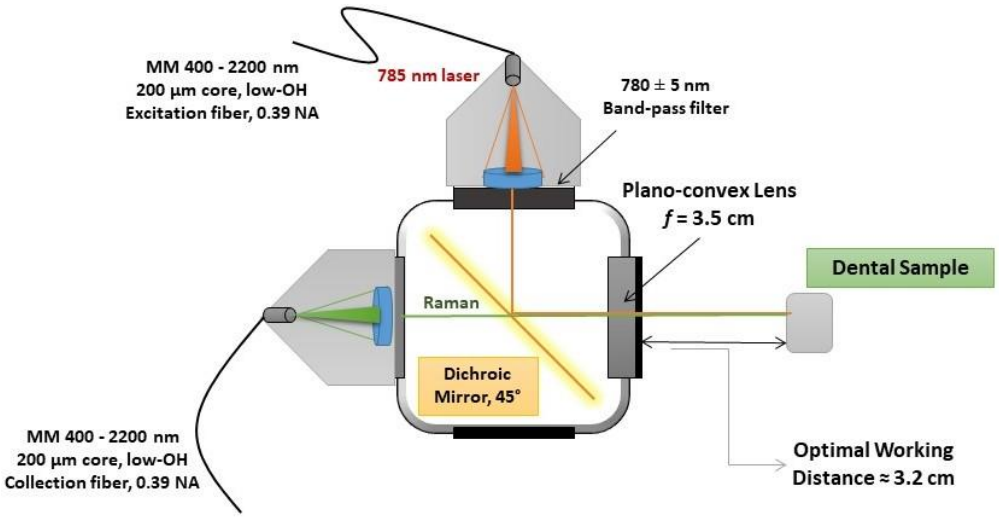

Figure 8.4 – **a)** Schematic representation of main structural components of the designed remote probe, in a simplified version, reducing the signal loss through a shorter optical path; **b)** difference between initial and final probe structural configuration, showing the removal of the 2nd main component (DFM1-PO1 cube) and the shortening of the optical path, reducing the number of couplings, connectors and inner components, diminishing the overall signal loss; **c)** the final version of the developed remote probe, with simplified configuration and reduced structure in real dimensions, equipped with a 35 mm plano-convex lens. All components were acquired from Thorlabs [81].

Figure 8.4 illustrates the schematic representation of the ultimate design version of the Raman remote probe – 8.4a, and the resulting developed probe, with simplified, compact, and more robust configuration – 8.4b and 8.4c, which was used during the experimental phase of remote spectral acquisitions, due to several practical reasons, such as: diminution of the optical path, reduction of the number of couplings, connectors and inner components, yielding more efficient results, with decreased signal loss and higher SNR due to minimized signal reflection losses. Moreover, a compact probe, with reduced dimensions, makes the remote application easier to use and simpler to handle, making Raman technique even more versatile and adaptable during its implementation.

Figure 8.5 shows the entire system and instrumental setup used for remote measurements: the fiber-coupled probe and resulting signal circuit.

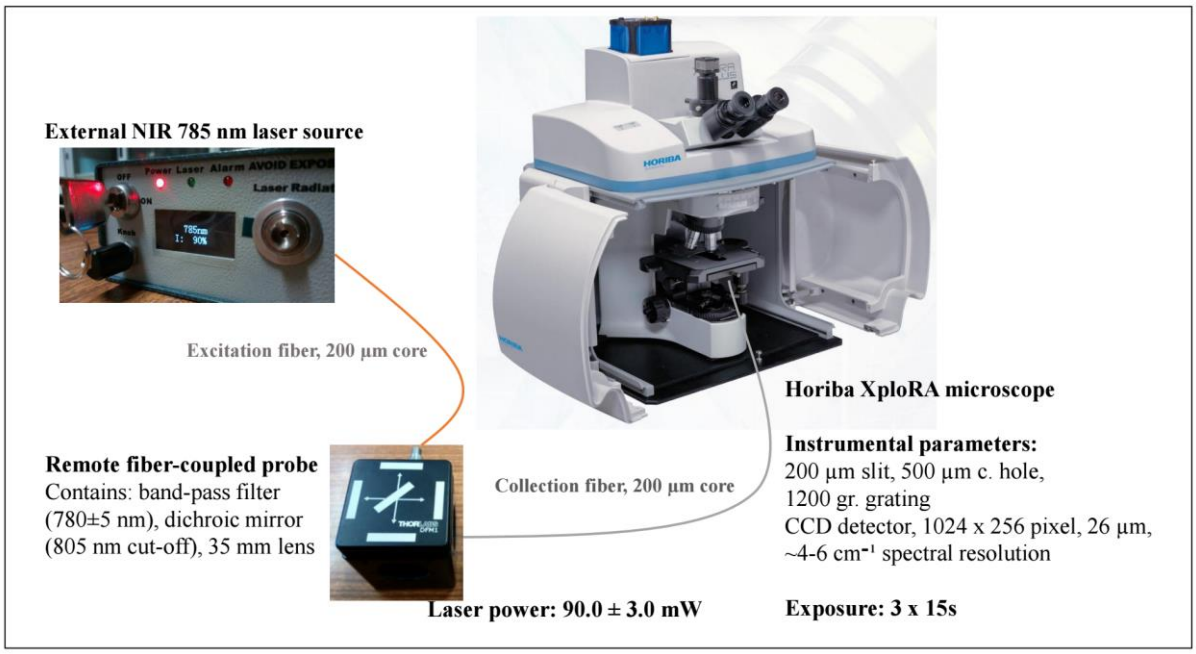

Figure 8.5 – Schematic representation of the fiber-coupled system, showing the remote probe connected to the external laser and microscope stage through optical fibers.

At the beginning, the probe was planned to contain a notch filter (which is a laser blocking filter, mostly used for the prevention of undesired reflected laser light from reaching the detector, and to suppress the Rayleigh elastically scattered radiation, while still allowing high transmission with enhanced isolation of the slightly wavelength-shifted Raman scattered signal), it was decided to exclude this component, since the dichroic mirror allowed the transmission of signal from the sample only with wavelengths superior to 805 nm, ideally blocking almost entirely – more than 99% of the reflected laser and Rayleigh scattered photons of approximately 785 nm. However, through experimental power measurements, I have discovered that the dichroic mirror transmitted app. 1% of the incoming reflected laser and Rayleigh scattered

photons, which together reached a signal power of ~0.4 ± 0.1 mW, resulting in a slight signal contamination of the Raman signal even before entering the collection fiber.

In this work, were used 2 optical fibers to connect the Raman probe, through CVH100-COL fiber adapter (collection) and a F220-FC adapter (excitation). The excitation fiber is multimode and equipped with FC/PC connectors at each fiber extremity, while the collection fiber is multimode and hybrid, with SMA905 and FC/PC connectors at the fiber endings. Initially, it was planned to use an excitation fiber with a core diameter of 105 µm. Nonetheless, since the use of another adapter – F220 FC, which connected to the FC/PC 200 µm core fiber (required for FC/PC type connectors), has shown a significantly increased efficiency for the laser signal transmission, resulting in much higher power - 171.4 ± 1.2 mW compared to 108.6 ± 0.6 mW, (almost 1.6 more efficient), it was decided to continue with the fiber with a larger core (Figure 8.6). While for the collection of Raman signal it was also used an optical fiber of 200 µm (Figure 8.6b), used due to a higher efficiency for signal transmission.

Instead of using the fiber entrance of the microscope, I have used a different configuration, employing a small plate with a tiny slit hole (Figure 8.7) to direct the Raman signal from the collection fiber directly into the microscope objective. Initially, it was planned to use a 105 µm collection fiber (Figure 8.6a), with a NA = 0.22, which corresponded to the NA value required for the fiber entrance of the microscope. Hence, since the collection fiber was coupled directly to the microscope objective, and the obtained Raman spectra through the 105 µm fiber had an increased background and decreased SNR (Figure 8.8a), I have opted for a 200 µm fiber (Figures 8.6b and 8.8b), increasing the collection efficiency about 1.8x, providing spectra with higher band intensity.

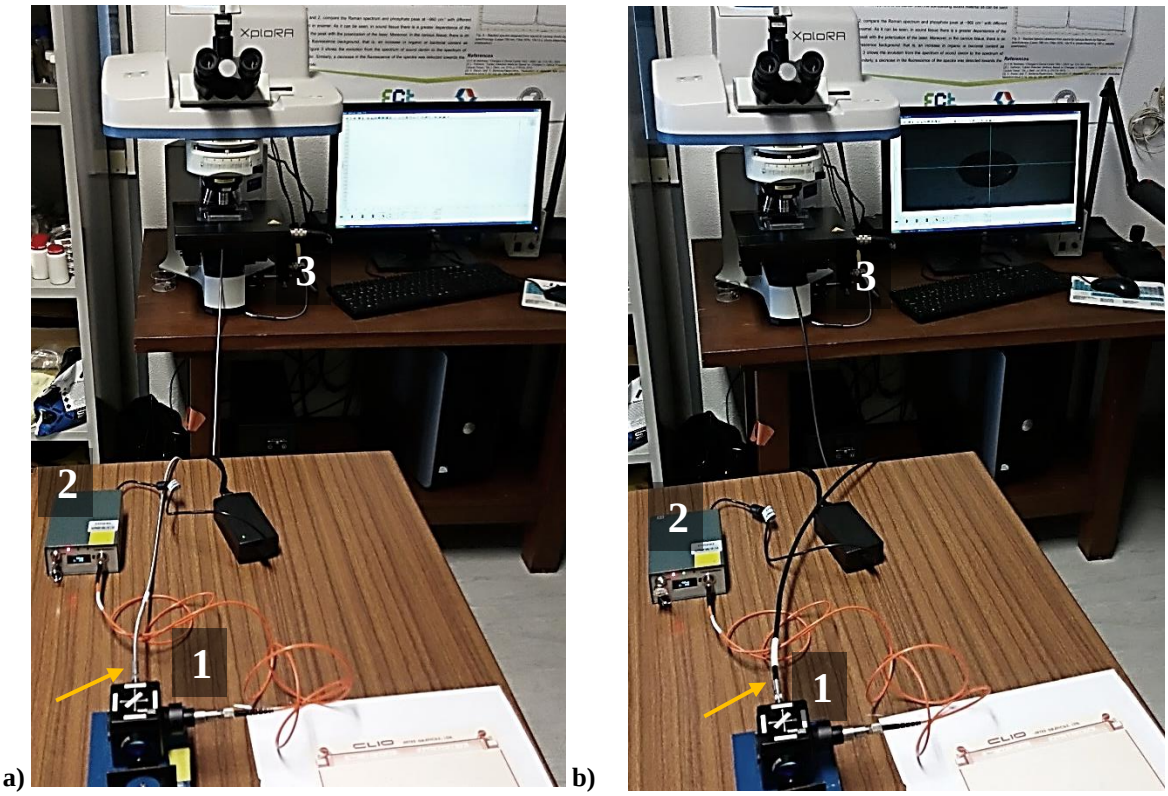

Figure 8.6 – Representation of the fiber-coupled system, showing the remote probe connected to the microscope stage with **a)** 105 µm and **b)** 200 µm collection fibers, respectively, with 1 – built remote fiber-optic probe, 2 – NIR external laser source and 3 – Horiba Xplora Raman benchtop equipment.

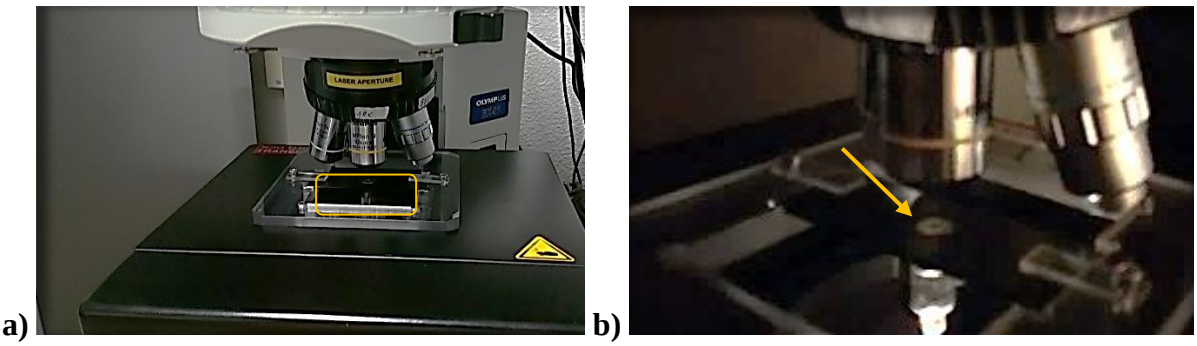

Figure 8.7 – Representation of the fiber-coupled system, showing **a)** the connection through the small plate, fixed and stabilized on the microscope motorized stage, and **b)** the collection fiber connected to the plate' slit hole (arrow) - transmitting, and directing the Raman signal to the microscope objective.

Thus, the used optical – output and input - fibers had both the same numerical aperture – NA = 0.39, the same fiber core diameters – of 200 µm, and consequently – the same acceptance/dispersion angle for both incoming and outgoing signal, respectively. The total acceptance angle of the employed fibers was 45.92°, both for the input and output signals.

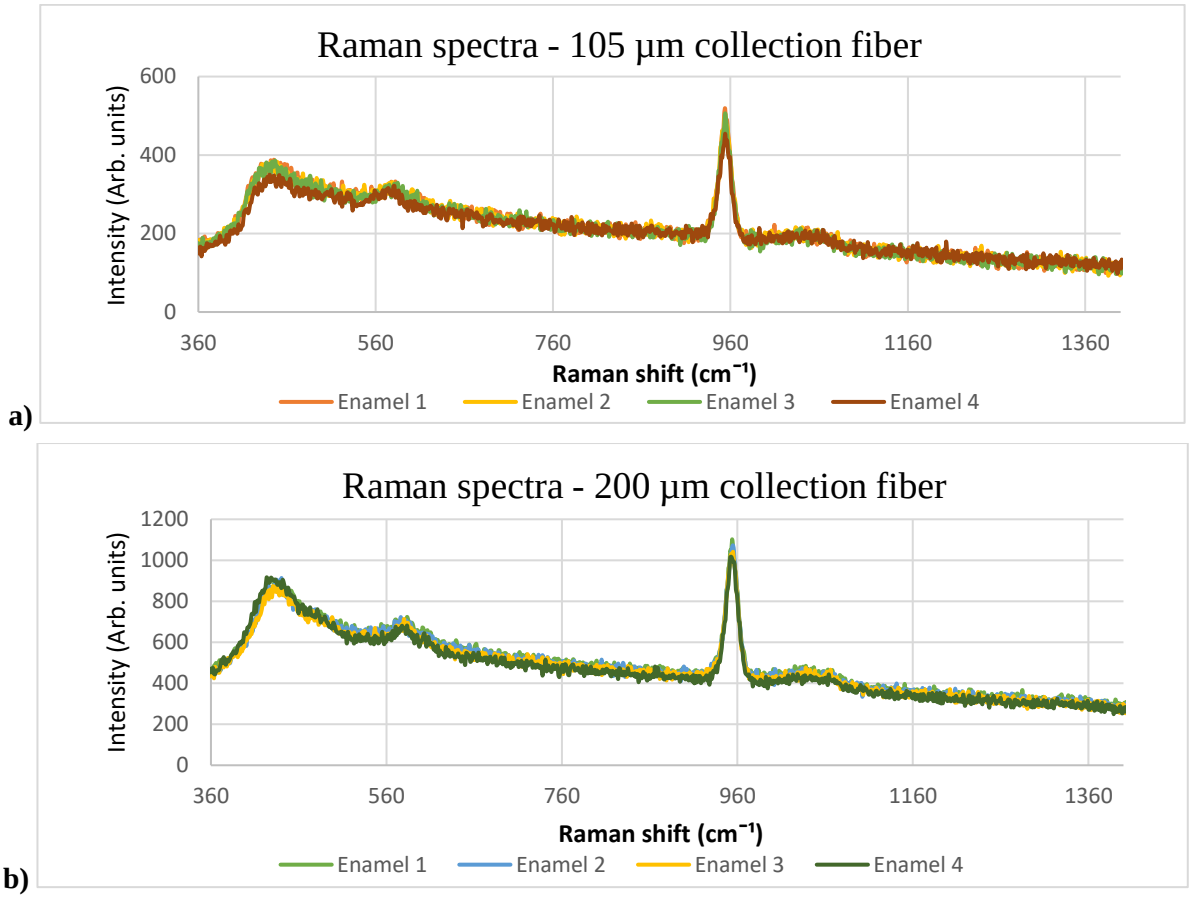

Figure 8.8 – Examples of 4 representative raw Raman spectra, obtained from a sound enamel sample, with the fiber-coupled remote probe connected to the microscope stage with **a)** 105 µm and **b)** 200 µm collection fibers.

Figure 8.9 shows distinct raw Raman spectra acquired from a silicon sample on a glass substrate, by using the remote probe. In this case, the characteristic silicon band at ~520.7 cm^{-1} specific to this material, was not possible to obtain, due to signal interference of the glass, and fiber inner background, meaning that the used configuration might require for additional improvements and components, in order to optimize the signal circuit and to increase the efficiency of filtering the Raman signal from fluorescent or inner fiber spectral background. Hollow optical fibers or with core made from a different material might be required as well. Using a different substrate, made from quartz or steel could also be an option.

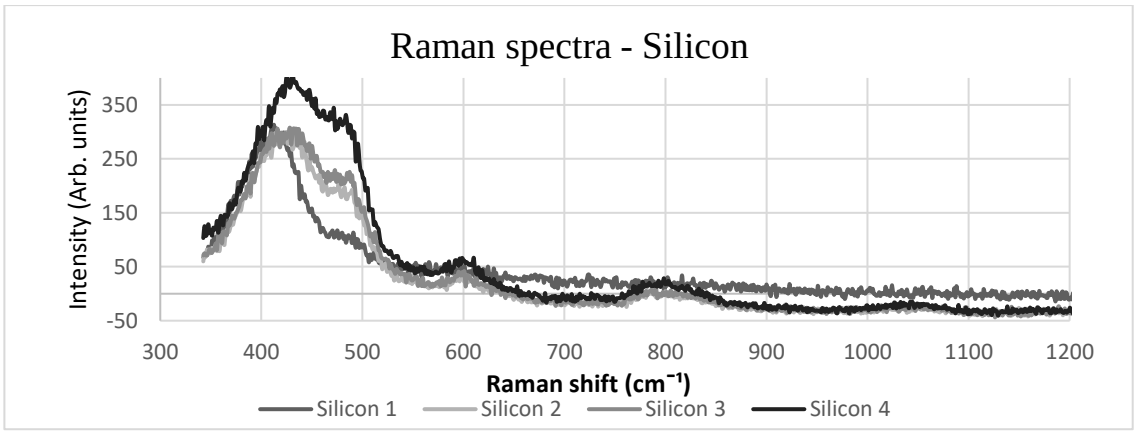

Figure 8.9 – Examples of raw Raman spectra, from 4 consecutive measurements of a silicon sample, used for calibration, with the fiber-coupled remote probe connected to the microscope stage with 200 µm collection fiber.

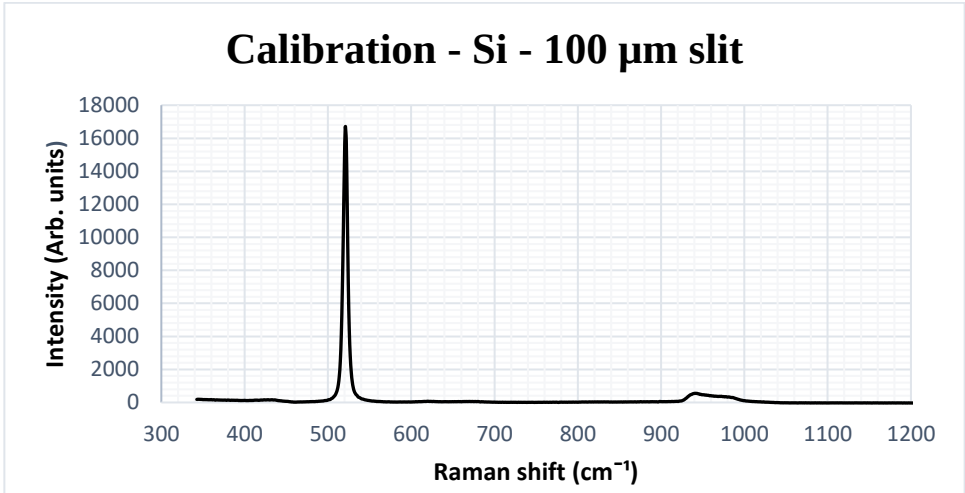

a)

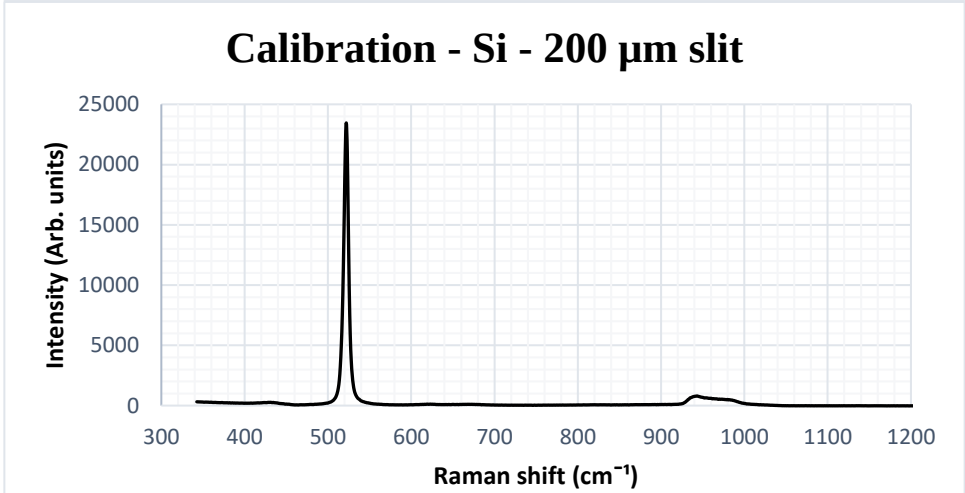

b)

Figure 8.10 – Examples of raw Raman spectra, obtained from a silicon sample, used for calibration, with the Horiba XploRA microscope, using a 100x Olympus objective, 785 nm laser, set with the 50% laser neutral density filter, rendering a 9.0 mW incident power, 1200 lines/mm grating and 300 µm confocal hole, for **a)** 100 µm and **b)** 200 µm entrance slit, providing spectral resolutions of 6.3 cm^{-1} and 6.6 cm^{-1}, respectively. [Important note: for 785 nm laser, 50 µm entrance slit, 1800 gr./mm grating and 100 µm c. hole the spectral resolution is < 1.2 cm^{-1}]

Figure 8.10 shows two different raw Raman spectra acquired from a silicon sample (usually used for calibration), obtained by means of benchtop measurements, using the Horiba XploRA confocal microscope. In this case, based on the band FWHM of the characteristic silicon band at ~520.7 cm^{-1}, it was possible to obtain experimentally the spectral resolutions of 6.3 and 6.6 cm^{-1} for 100 and 200 µm slit, respectively, which in all cases is lower than 7 cm^{-1}, slightly superior to the calculated resolution values of 4-6 cm^{-1} for 1200 gr./mm grating and 300 c. hole. The obtained value was considered for all remote probe-based measurements, since the probe was connected to the same Raman equipment, maintaining the same grating (1200 gr./mm), slit (200 µm), and laser wavelength (785 nm). The use of 90 mW laser power, x10 objective and 500 µm confocal hole did not significantly influence the spectral resolution, contributing only for a greater sample volume, higher collection efficiency and increased band intensities.

8.7 - Raman spectral measurements for the verification of the uncertainty associated to variation of the distance to sample

8.7.1 - Context and Objectives

The main objective in this section is to describe an experiment performed in order to verify the optimal working distance - D_w of the LA1027 plano-convex lens, acquired from Thorlabs, with a focal distance of f = 35 mm, the component used for laser delivery and focusing, as well as for the Raman scattered signal collection. It shows a comparison between the spectral band intensities of a silicon sample, measurements obtained using the Raman benchtop microscope, by varying the distance between the sample and the mentioned lens.

8.7.2 - Materials and Methods

Raman spectra of the sample were obtained using a Horiba XploRA confocal microscope. The lens was directly mounted on the microscope turret, and the measured initial distance – $\mathbf{D_0}$ to the sample was 2.60 ± 0.01 cm. During this experiment, the distance was gradually increased, by adding precise short distance increments along the Z-axis – in depth, by changing gradually and automatically the position of the support stage of the benchtop equipment, adding slight increases that varied between 0.005 and 0.1 cm, according to the intensity increase or reduction of the Raman band located at approximately 520.7 cm^{-1}. During this experiment it was used the 785 nm (NIR) laser. The instrumental parameters for the measurements were maintained constant (the laser intensity at 100%, entrance slit set to 200 µm, and 1200 lines mm^{-1} grating), changing only the confocal hole from 300 to 500 µm, according to the case. In this way, I have obtained 2 different groups of measurements: (1) 785 nm laser, 500 µm confocal hole (c. h.) and (2) 785 nm laser, 300 µm c. h. The typical acquisition time for the Raman single spot measurements was 10 s with 3 accumulations. Spectra deconvolution was performed using LabSpec software (v5.58.25, Horiba, France), making use of a polynomial baseline correction to remove the background due to fluorescence. The band intensities were determined by integrating the area under the bands.

8.7.3 - Results

Below, in Figure 8.11, are exposed graphs that show the variation of band intensities in function of the measured distance between the employed plano-convex lens and the examined silicon sample.

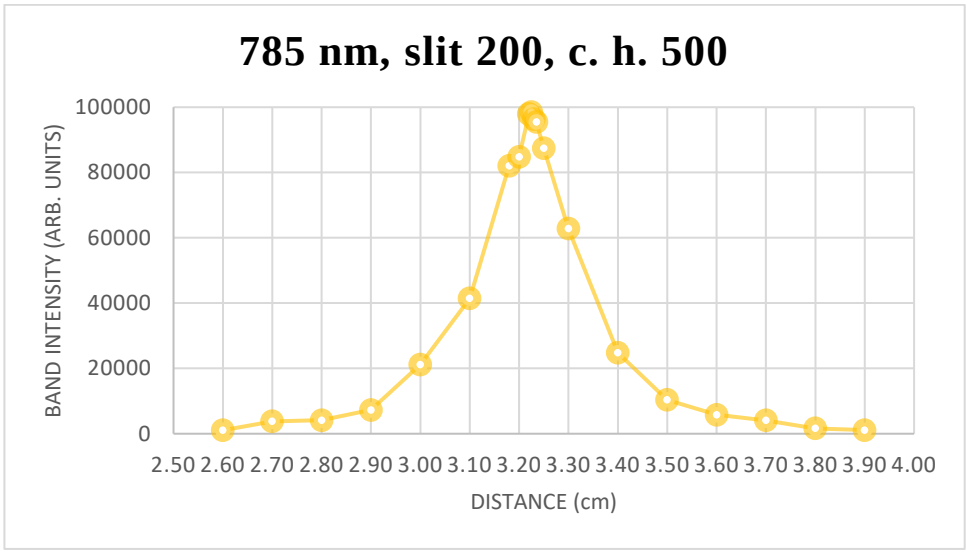

a)

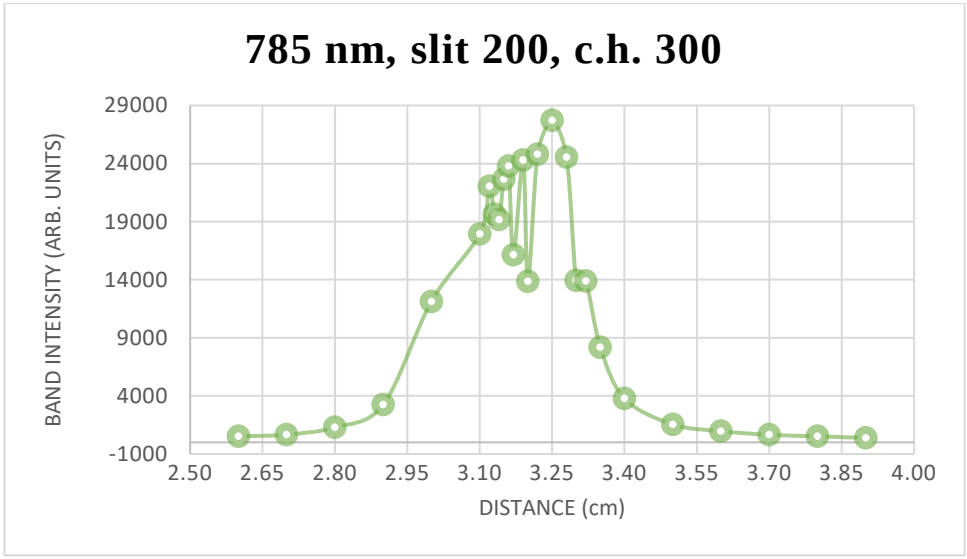

b)

Figure 8.11 – Graphs representing the intensity variation of the silica band located at 520.7, in function of distance between the mounted lens and Silicon sample, for: **a)** 785 nm laser wavelength and 500 µm confocal hole; and **b)** 785 nm laser wavelength and 300 µm confocal hole. The remaining parameters, such as grating, entrance slit, and laser filter were maintained constant.

8.7.4 - Discussion

As revealed in Figure 8.11, the intensities of the silicon band vary substantially according to the distance between the mounted plano-convex lens and the examined sample. Due to inconstant and unpredictably fluctuating fluorescence background, the band intensity values do not follow a constant increase or decrease trend. For an increased background, after the baseline correction of each spectrum, the integrated area of the band located at 520.7 cm^{-1} can have a lower value due to the total background removal.

8.7.5 - Conclusion

The optimal working distance of the LA 1027 plano-convex lens can vary to some extent according to the used parameters during the single-spot spectral measurements. For the 1st and 2nd groups of measurements – with the 785 nm laser and confocal holes of 500 and 300 µm, the obtained working distances were 3.23 ± 0.01 cm and 3.25 ± 0.01 cm, respectively. Since most of remote measuring experiments on enamel samples were performed by using the 785 nm wavelength, and 500 µm confocal hole set, the optimal working distance considered for remote acquisitions was 3.23 ± 0.01 cm. The percentual error for the intensity of the phosphate band at ~959 cm^{-1}, associated with a 0.1 cm change of the optimal distance, measured with the 785 nm laser, was estimated at 7.4 %.

8.8 – Remote probe measurements for the verification of angle dependence on enamel samples

The main objectives of this additional experiment were to verify and validate the angle dependence for the incident laser beam onto the examined enamel sample, during remote measurements, using the fiber-optic probe in a 180° backscattering configuration, relative to the sample surface (Figure 8.12 a). It is well known that for samples with flat surfaces, if placing the probe lens at the optimal working distance, at a 90° angle between the incident beam and sample surface (which corresponds to 0° between the main collection axis and surface normal), the signal collection efficiency and, consequently, the measured spectral intensity of the scattered Raman signal are the highest possible. In Figure 8.12 b) is shown the obtained graph of phosphate symmetric stretching band intensity (at ~959 cm^{-1}), in function of the collection angle with regards to the surface normal direction to the enamel sample surface (which is not perfectly flat/plane, being instead unevenly round-shaped with small superficial irregularities).

As shown below, in Figure 8.12 b), by adding small increases and gradually varying the angle between the lens collection axis and surface normal to the sample, we can observe a clear tendency of the phosphate band intensity to decrease, with certain fluctuations. The varying and non-linear decreasing slope, which is closer to 6th order polynomial trendline, might be due to several factors, such as:

- the enamel sample's outer surface is not perfectly flat, is unevenly and round shaped, and may contain disproportional irregularities and porosities in certain demineralized regions.

- the incident laser spot during all measurements is not exactly the same, since the sample rotation was performed manually, as the used external stage does not execute automatic movements or rotations.
- slight variations of the working distance between the lens and sample, by changing the sample angle and position during measurements, might have occurred as well.

In conclusion, this additional experiment has shown that fiber-coupled remote measurements are more complex than expected, and always depend on several factors, such as optimal working distance of the probe lens and angle of laser incidence and signal collection. These experiments are of extreme importance, since during dental Raman measurements of the enamel, performed *in-vivo*, by means of an enhanced and more compact probe, the Raman operator (user with different knowledge and training levels – beginner - student, or proficient – experienced researcher, or dentist) must hold the Raman probe by hand, and direct manually the laser beam onto the vital tooth, which might cause possible slight alterations of the measurement spot position, and minute to more significant variations of distance to sample and the angle of incidence with regards to the surface normal.

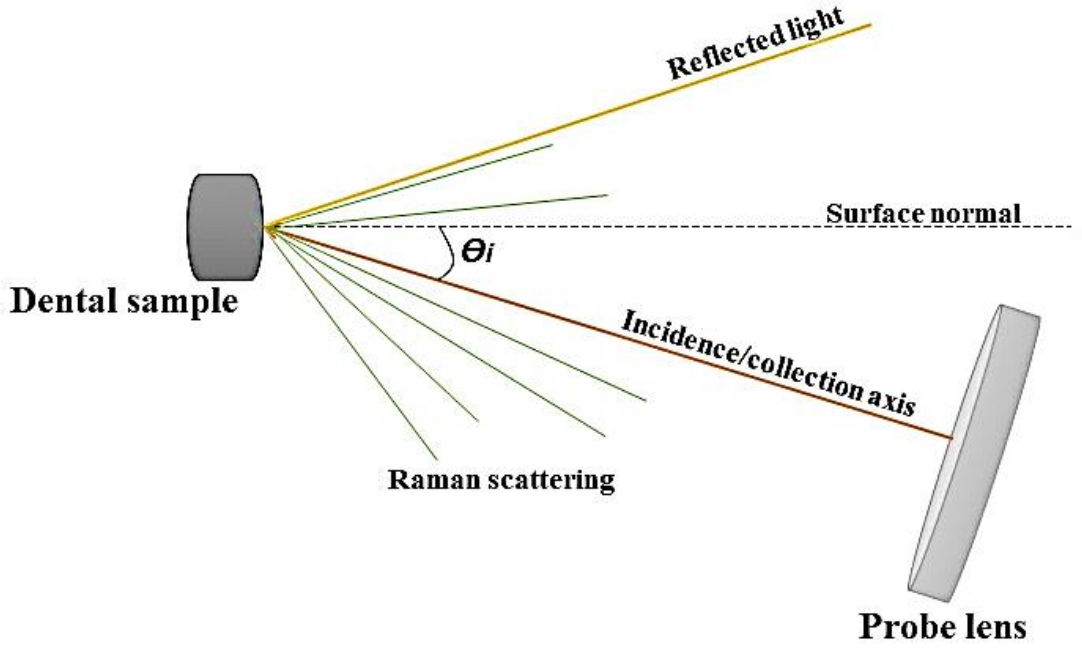

a)

b)

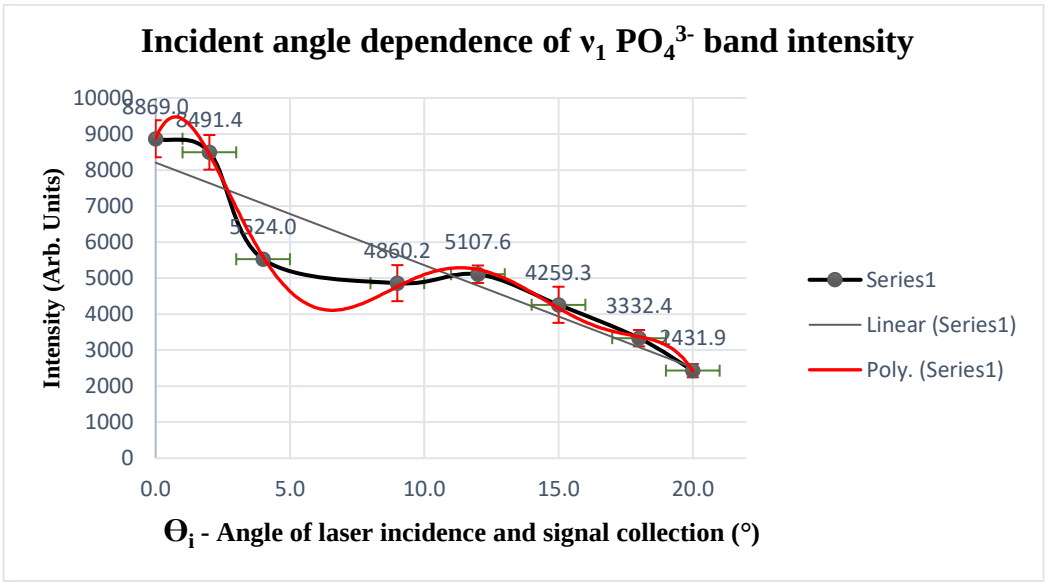

Figure 8.12 – **a)** Schematic representation of the experimental setup for the Raman single-spot measurements on enamel sample by means of remote probe, for the verification of incident angle dependence; **b)** graph showing the incident/collection signal angle dependence of 959 cm^{-1} phosphate band intensity of the superficial HAp layer.

8.9 – Overall uncertainty associated to the distance to sample fluctuations, excitation/collection beam angle incidence variations, and laser wavelength stability

During the experimental Raman spectral acquisitions, with the described remote fiber-coupled probe in the previous section 8.6, it was concluded that this should be held close to the sample, maintaining as much as possible the OWD (between lens and sample surface), with no to minimal angle deviations (ideally, normal to the enamel sample surface), in order to obtain maximal peak intensities for the Raman phosphate bands of interest. The incident excitation laser beam and the collected incoming Raman signal must be both at a 0º angle to the normal direction to the sample surface (90º perpendicular to the superficial analysis spot), since it is used a 180º backscattering configuration (reflection mode). The established error for the angle dependence was calculated for a possible angle variation only up to ± 3° (Table 8.2), for practical reasons and considering the experimental circumstances, resulting in highest percentual error of 8.1 % for the phosphate band intensity, located at 959 cm^{-1}.

The total percentual error of the phosphate band intensity, associated to a slight change of ± 0.1 cm in the optimal working distance between the sample surface and Raman remote probe lens (7.4 %, Table 8.3), to slight angle deviation from the surface normal of ± 3° (8.1 %, Table 8.2), and to small variations of the laser stability during 10 consecutive spectral measurements (6.9 %, Table 8.4), was estimated at ~12.9 %. For benchtop measurements, the total percentual error associated to 12 consecutive spectral acquisitions, is approximately of 5.9 % (Table 8.5).

Table 8.2 – Phosphate band intensity values for different incident angles.

Incident angle (°)	Band intensity (Arb. units)
0° ± 1°	**8290** **8573** **9744**
2° ± 1°	**9146** **7718** **8611**
4° ± 1°	**5489** **5444** **5640**

Table 8.3 – Raman band intensity error associated to ± 0.1 cm variation of the lens **OWD**, for 785 nm laser, 500 µm confocal hole and 200 µm slit, using the Si sample.

Distance to sample (cm)	Band Intensity (Arb. units)
3.18	82065
3.20	84836
3.22	97951
3.23	98466
3.23	96321
3.24	95471
3.25	87480

Table 8.4 – External 785 nm laser stability – same spot, enamel specimen of Group B.
Non-polarized configuration, consecutive probe-based measurements, using:
1200 gr. grating, 200 µm slit, 500 µm c. h., 785 nm laser with 90.0 ± 3.0 mW incident power.

Nr	Band Intensity (Arb. units)	Position (cm^{-1})	Width (cm^{-1})
1	13346	953.0	16.6
2	14863	953.1	16.6
3	12459	953.0	16.7
4	13131	953.2	16.7
5	14252	953.2	16.5
6	14587	953.1	16.8
7	11949	953.1	16.8
8	14141	953.2	16.6
9	13094	953.2	17.2
10	13194	953.2	16.5

Table 8.5 – Internal laser stability – same spot, enamel sample from Group A.
Parallel-polarized configuration, consecutive benchtop measurements, using:
1200 gr. grating, 200 µm slit, 300 µm c. h., 785 nm laser with 9.0 ± 0.4 mW incident power.

Nr	Band Intensity (Arb. units)	Position (cm^{-1})	Width (cm^{-1})
1	20776	962.5	13.2
2	23625	962.5	13.0
3	22611	962.5	13.3
4	21442	962.5	13.2
5	22990	962.6	12.9
6	22774	962.6	13.1
7	23652	962.5	13.4
8	22953	962.6	13.1
9	23875	962.6	13.0
10	24754	962.6	13.3
11	24221	962.6	13.1
12	25760	962.6	13.0

The used formula for the calculation of the percentual total error was:

$$\text{Total error} = \sqrt[2]{(Error\ 1)^2 + (Error\ 2)^2 + (Error\ 3)^2}, \text{ with}$$

- *Error 1* – percentual error associated with distance variation.
- *Error 2* - percentual error associated with angle variation.
- *Error 3* - percentual error associated with laser and optical system stability.

Therefore, for each spectral acquisition achieved with the actual configuration of the fiber-optic remote probe, if measuring with the external NIR laser source (785 nm) at the optimal distance and keeping the probe lens collection axis closest to the surface normal (backscattering geometry), the **maximal percentual error** associated to the measurement of spectral Raman band intensities is approximately **12.9 %** of their displayed values, thus providing a poor repeatability for the spectral measurements. The obtained error is ~ 46 % due to the overall instability of microscope inner components that integrate the signal circuit and detector (5.9 %).

9

ASSESSMENT OF HUMAN DENTAL SOUND AND CARIOUS SAMPLES BY MEANS OF REMOTE PROBE

9.1 - Introduction

In this chapter is described an additional study, performed also *ex-vivo*, on the same human enamel samples described in section 6.2.2, obtaining the Raman spectra by using the described remote probe in Section 8.6, connected to an external laser source [785 nm, with measured power value of 90.0 ± 3.0 mW] and to the Horiba XploRA confocal microscope.

To accomplish this evaluation, it was performed a direct analysis on three main distinct spectral data groups: **A** – spectra obtained from sound and intact teeth (white-white opaque, not affected by caries); **B** – spectra acquired from intact (white opaque or yellow) tissue from a healthier and non-cavitated region of carious teeth; and **C** – spectral measurements of carefully selected single points from the edge of cavitated tissue and cracked regions of the same carious teeth from group B (measured only selected points from the edge of carious lesions and/or cavities).

9.2 - Materials and methods

9.2.1 - Specimen selection and sample preparation

The selected samples for Raman examination were previously described in Section 6.2.2.

9.2.2 - Methodology and experimental groups

The used methodology, including examined sample groups and the Raman equipment were the same as in Section 6.2.2, with the main difference that, in this case, the spectral measurements were performed with the fiber-coupled remote probe connected to an external laser of 785 nm wavelength, and to the microscope objective of 10x magnification. Figure 9.1 shows only a few of the used dental enamel samples, representing the study groups: **A** – sound and intact teeth; **B** – sound regions from carious teeth; **C** – cavity edge of carious and /or cracked teeth.

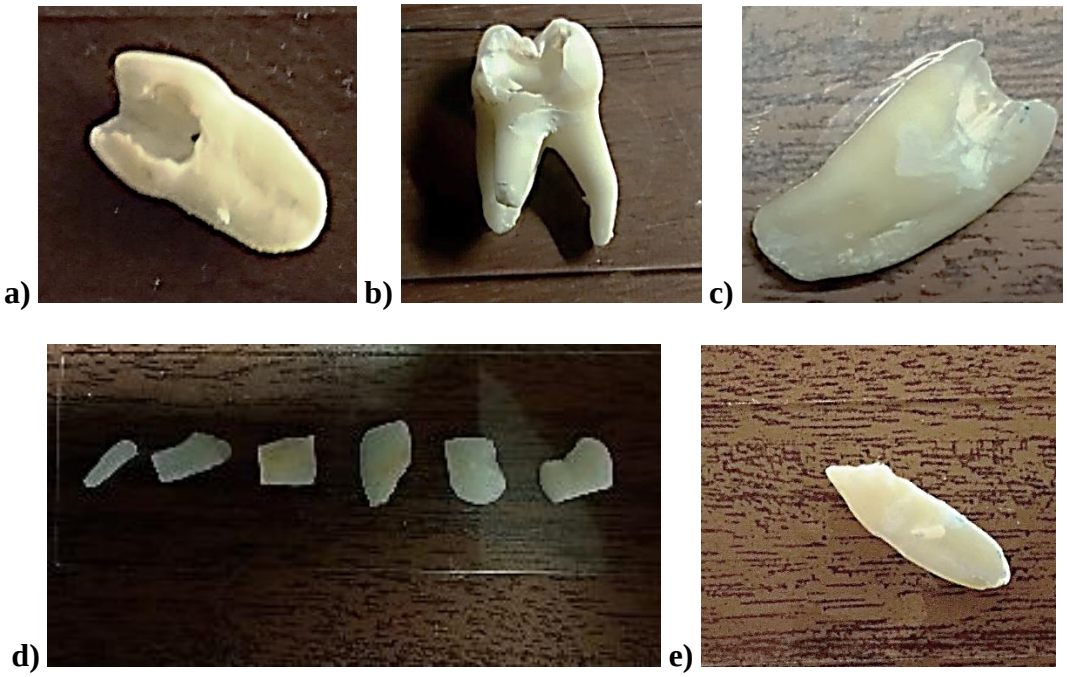

Figure 9.1 - Photographs of three distinct carious samples - **a) b) c)** showing the tooth side containing the cavities. This group of samples derived in two groups, from which were acquired the Raman spectra for groups B (sound and intact region) and C (edge of the cavity/carious lesion margin).; **d)** representative sound enamel specimens from group A; and **e)** an intact sound tooth sample from group A.

9.2.3 - Experimental setup – Raman microscope

All sample groups were analyzed using the Raman technique, by means of the developed remote fiber-coupled Raman probe (Sections 8.6-8.9), connected to an external 785 nm laser source, with varying power, with the instrumental parameters described in the Appendix. The remote probe was connected to the Horiba XploRA Raman confocal microscope (Horiba Jobin Yvon, France), using a collection optical fiber with a core of 200 μm. By setting a 1200 lines/mm grating, the spectral range investigated was from 400 cm^{-1} to 1800 cm^{-1}, resulting in a spectral resolution of < 7 cm^{-1} (value obtained experimentally using the FWHM of the characteristic 520.7 cm^{-1} band from a silicon sample). Using an entrance slit of 200 μm, and a larger confocal hole, set for 500 μm for remote acquisitions, in order to maximize the sample volume and the efficiency of the Raman signal collection, the scattered incoming radiation collected by the objective was dispersed onto the air-cooled CCD array of an Andor iDus detector. The applied 785 nm laser beam (of the external laser source) on the sample' surface had a mean power of approximately 90.0 ± 3.0 mW, measured experimentally at the distal probe lens end. For each examined tooth, were performed 10 measurements, from 10 distinct spots, without using polarization. The time duration for the spectral acquisitions was the same for all samples, with an exposure time of 15 s with 3 accumulations, for each measurement.

Figure 9.2 shows the experimental setup, including the used external laser for remote measurements – 9.2 a), as well as the collection fiber connection configuration to the microscope 10x Olympus objective - 9.2 b) and c), the remote probe during a spectral acquisition from an enamel sample – 9.2 d) and an example of spectral data display – 9.2 e), which can be obtained and visualized during a typical Raman measurement.

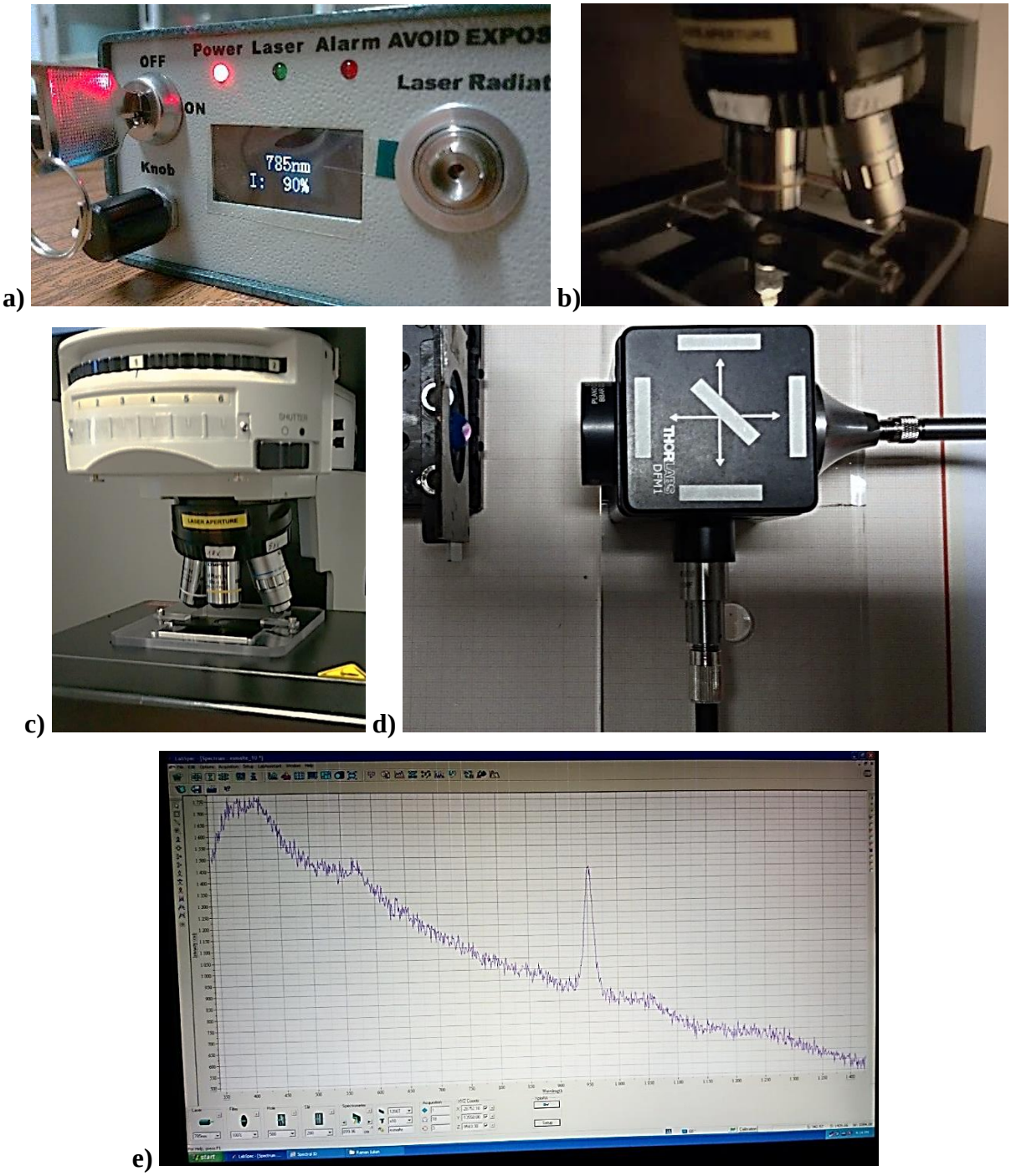

Figure 9.2 – Representations of **a)** the NIR 785 nm external laser, used for remote measurements [CNI Lasers]; **b)** and **c)** the connection of a 200 µm collection fiber to a plaque slit to direct the scattered Raman photons directly into the microscope objective; **d)** depiction of the remote probe during an ongoing spectral acquisition from a fixated sound enamel specimen; and **e)** an example of a displayed Raman raw spectrum (without any type of correction or background removal), acquired from a sound region of a carious sample belonging to group B.

Figure 9.3 shows three types of non-polarized Raman spectra, obtained with the remote probe from distinct sound (group A) and carious enamel samples (groups B and C), the latter from different regions of carious tooth, from which were subtracted and analyzed the following spectral parameters: phosphate υ_1 band position, band width (FWHM) and b-type carbonate ratio.

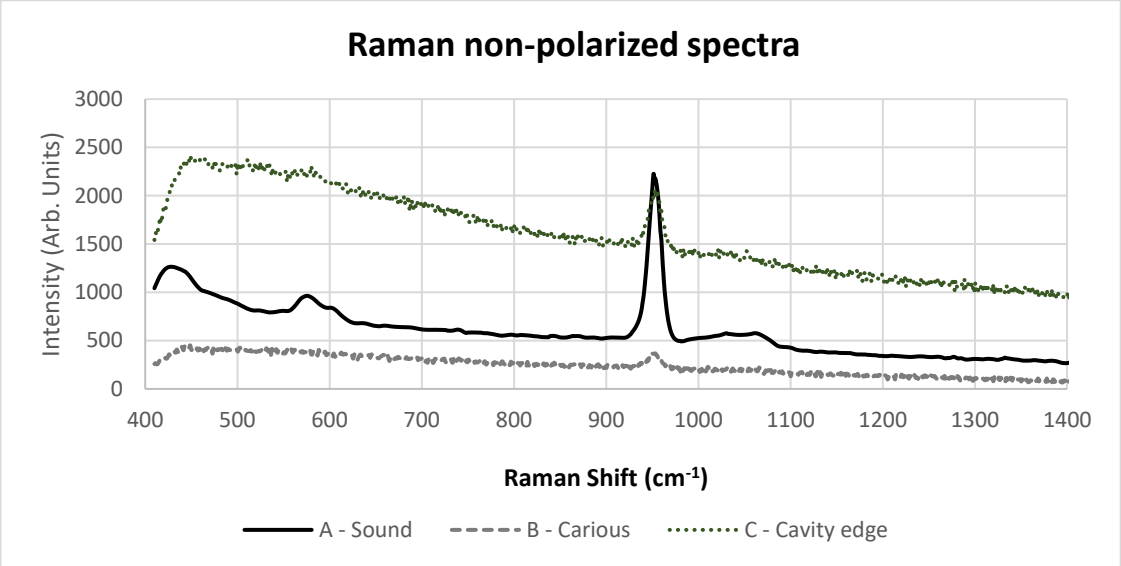

Figure 9.3 – Representation of examples of different Raman raw spectra, without baseline correction, acquired with the remote fiber-optic probe (coupled to the external 785 nm laser), revealing the differences between the spectra obtained from different samples from distinct study groups: Groups A, B and C, respectively.

9.3 - Statistical analysis

All spectral parameters were analyzed using IBM SPSS v27.0 software (IBM Statistics, Inc. Chicago, IL, USA). Parametric tests were used since the study had a sufficiently large sample size (all analyzed variables with N ≈ 300, with N ≈ 100 per group) according to the central limit theorem [62]. ANOVA tests with Tukey post hoc were performed to analyze differences between the groups, for each of the calculated or obtained spectral parameter, since all groups were considered as independent study groups. Even if the groups B and C were originated from the same dental samples, these included spectra obtained from different regions of the teeth, B – sound region and C – cavity edge from carious teeth, and therefore were considered as independent groups. It was considered a statistical significance level of p=0.05.

9.4 – Results

Three study groups – A, B, and C, with ten teeth per group were analyzed by using the developed remote probe. After analysis, all obtained results comprising the mean values and

standard deviations for each of the parameters are graphically represented in Figure 9.4. The results are presented to show the differences between the study groups, for two examining approaches: 1st - Raman benchtop measurements and 2nd - fiber-optic probe-based acquisitions.

In the 1st case - benchtop acquisitions (sub-section 7.2.3), the parameters that have shown significant differences between the groups were the b-type carbonate ratio and band width, which have revealed significant differences only between the Group C and the other groups, with $p<0.01$ Tukey post hoc. No significant differences were observed between groups A and B.

Concerning the 2nd approach - remote fiber-coupled probe measurements, the b-type carbonate ratio parameter revealed significant differences between all the study groups, with $p<0.05$ post hoc between groups A and B, and $p<0.01$ post hoc between the former ones and Group C. The phosphate band width parameter has shown significant differences only between the Group A and the other two groups, with $p<0.01$ Tukey post hoc. No significant differences for this parameter were found between groups B and C. The phosphate band position has not yielded any statistically significant differences between any of the study groups. Pearson correlation tests have revealed low degree statistical associations, with positive low correlation coefficient of +0.20 between the b-type carbonate to phosphate ratio and phosphate band width parameters, and negative low correlation coefficient of -0.15 between the phosphate band position and width parameters.

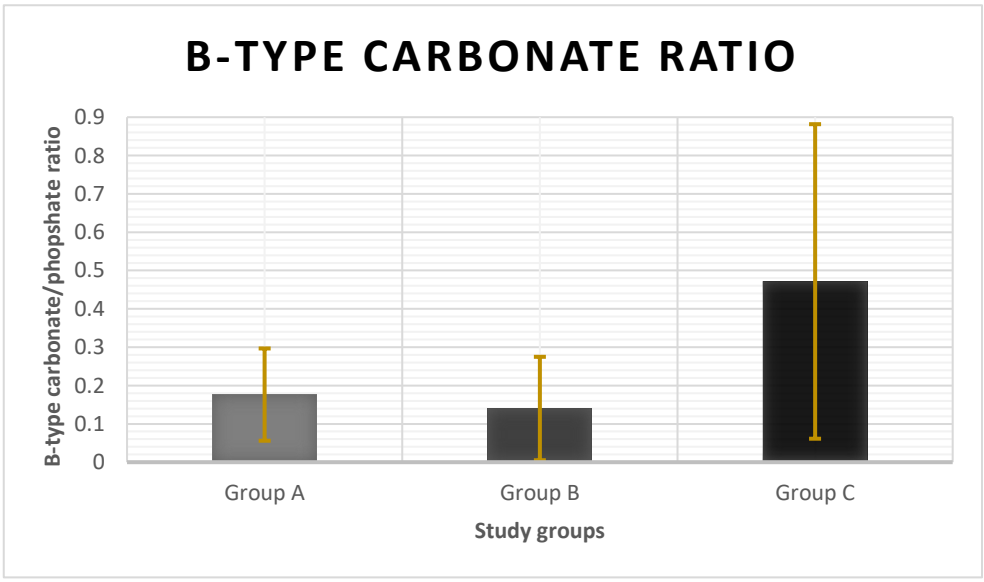

a)

b)

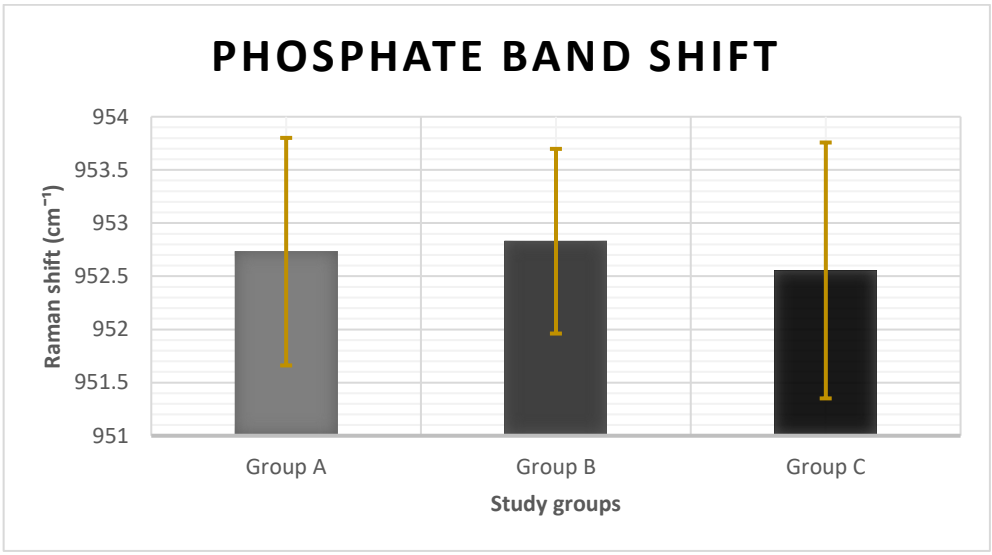

c)

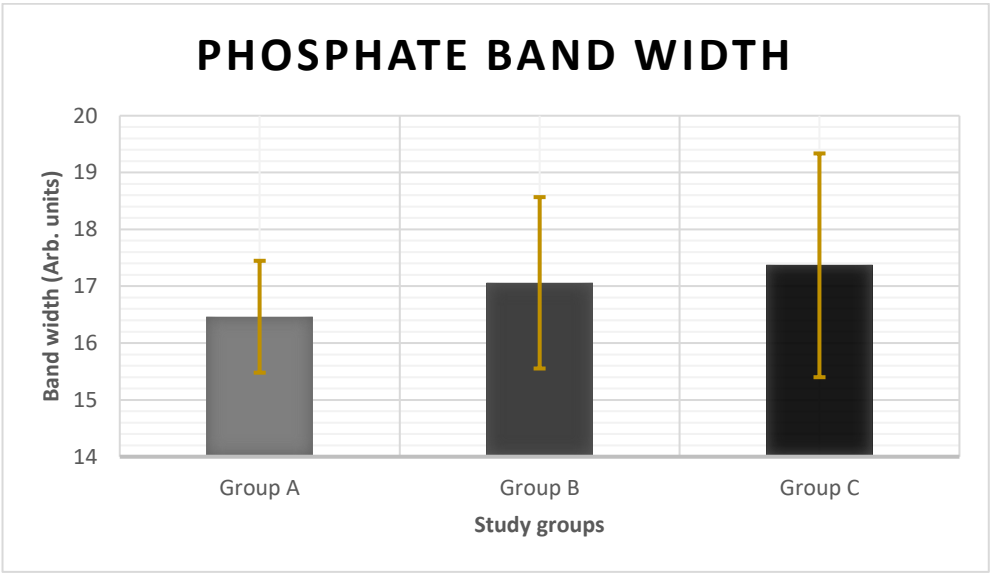

Figure 9.4 - Bar-charts, with the columns representing the mean values and the error bars showing the uncertainty variations, for **a)** b-type carbonate ratio, **b)** phosphate band position and **c)** phosphate band width parameters, for each of the study groups – A, B and C, respectively. Measurements were performed using the remote probe.

a)

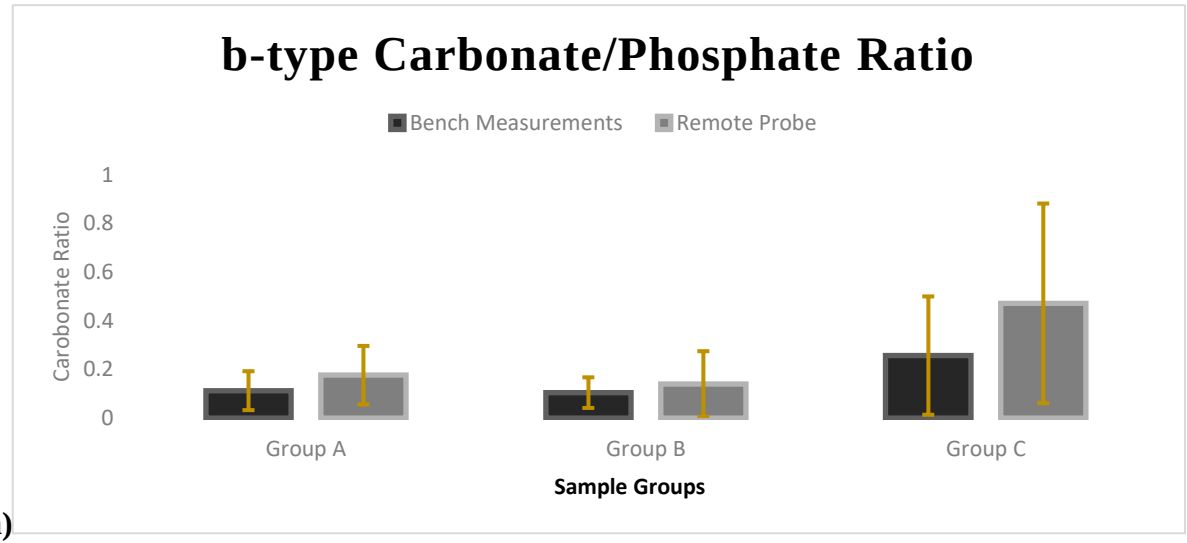

b)

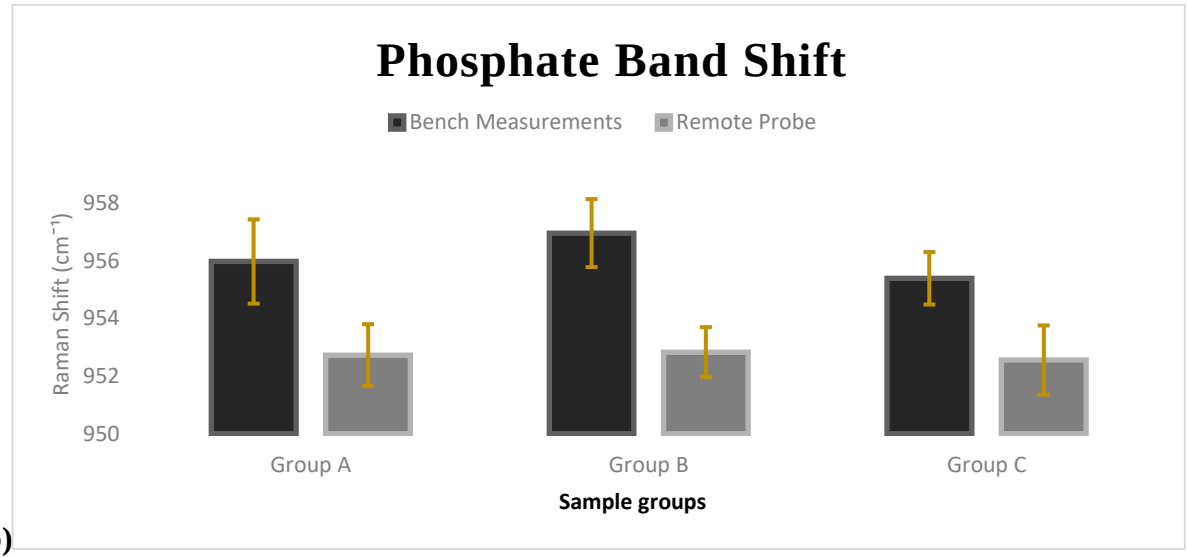

c)

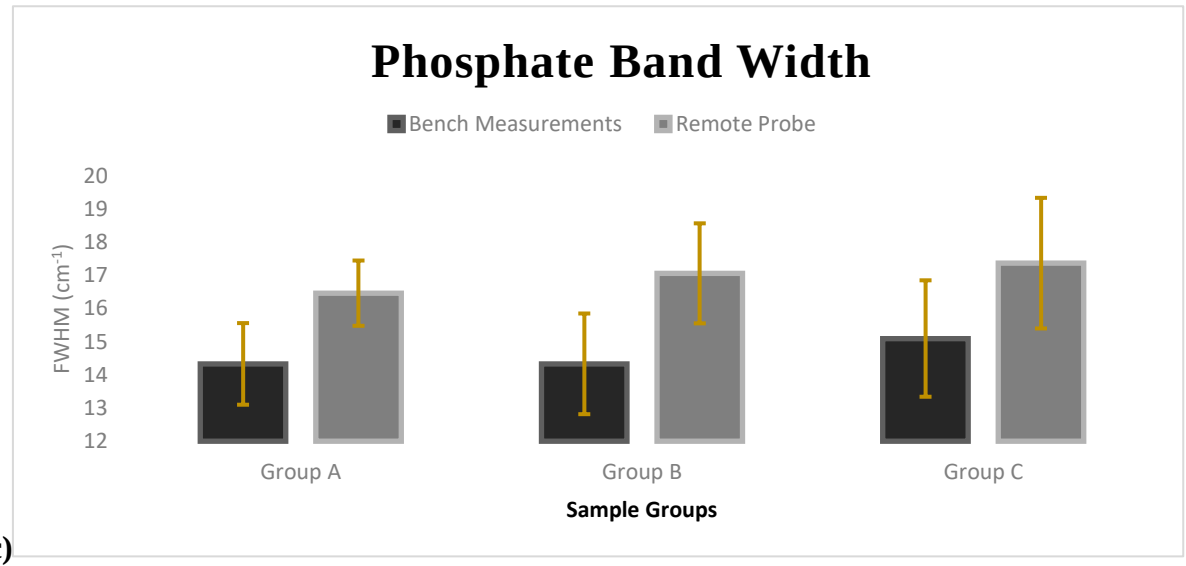

Figure 9.5 – Graphs illustrating clustered bar-charts, with the clustered columns that correspond to different measurement approaches – benchtop and by means of fiber-coupled remote probe, representing the mean values and the error bars showing the uncertainty variations, for **a)** b-type carbonate ratio, **b)** phosphate band position and **c)** phosphate band width parameters, for each of the study groups – A, B and C, respectively.

In Table 9.1 are represented the individual and overall values (in %) for the sensitivity, specificity, and accuracy of different spectral parameters (and derived ratios) subtracted from the phosphate and carbonate bands, for the distinction of each sample group from the other: A from B, B from C and A from C, obtained by applying the logistic regression method. As shown below, the prediction accuracy is slightly higher for the b-type carbonate/phosphate ratio combined with band position and bandwidth parameters.

Table 9.1 – Accuracy of the analyzed spectral parameters in distinguishing the sample groups, acquired by means of remote fiber-coupled probe-based measurements.

Probe acquisitions - b-type carbonate ratio (separately)

COMPARISON	SENSITIVITY (%)	SPECIFICITY (%)	ACCURACY (%)
Groups A-B	58	65	61
Groups B-C	82	78	80
Groups A-C	81	70	75
Overall	**74**	**71**	**72**

Probe acquisitions - b-type carbonate ratio with phosphate band shift and width

COMPARISON	SENSITIVITY (%)	SPECIFICITY (%)	ACCURACY (%)
Groups A-B	64	58	61
Groups B-C	82	75	79
Groups A-C	80	76	78
Overall	**75**	**70**	**73**

9.5 – Discussion

The main objectives of this PhD work consisted in the design, development, testing and implementation of novel instrumentation for the adaptation of a commercial Raman spectrometer (Horiba XploRA) to the *ex-vivo* (and *in-vivo* in a latter stage) remote analysis of human teeth.

In addition, I have performed a more complex and multiple-step study that intended mainly to assess whether the developed Raman fiber-optic probe makes possible the obtention of high-quality Raman spectra that could be used for the assessment of the overall mineralization degree, indication of mineral loss and detection of structural changes of different dental samples, and if the fiber-coupled system can be employed for group and/or sample differentiation.

This way, I have completed a comparison study, performed *ex-vivo*, by means of two different approaches – 1) benchtop measurements and 2) remote fiber-optic probe-based acquisitions, in order to distinguish between three main groups of enamel samples: A – sound (white-white opaque, not affected by caries); B – intact (white opaque or yellow) tissue from a healthier and non-cavitated region of carious teeth; and C – edge of cavities and cracked regions of the same carious teeth from group B (measured only selected points from the edge of carious lesions and/or cavities).

First, it was shown that the remote fiber-optic probe has properly functioned, however not ideally. Although it was possible to transmit, direct, and focus the monochromatic excitation laser to the examined dental sample, as well as to collect and integrate the signal obtained from the small volume of the sample through the probe lens, there were great signal losses due to the beam attenuation and absorption throughout the fibers, due to the fiber coupling, adapter connections and signal attenuation by the probe components, such as dichroic mirror and focusing lenses. There was also a notable increase in the spectral background, due to the fluorescence, mainly caused by the inner fiber spectral background, which has always contaminated especially the incoming Raman signal in the low spectral region (spectral range between 300-800 cm^{-1}). Given the weak nature of Raman scattering (1 in 10^7 photons), it was important to increase the power of the excitation laser, up to 90 ± 3 mW, in order to maximize the signal to noise ratio obtained from the tissue of interest – the outer enamel layers.

Secondly, were obtained Raman spectra, well-defined, with intense signal and high SNR, sharp phosphate bands, relatively high band intensity, and good spectral resolution (< 7 cm^{-1}, for 785 nm laser, 1200 gr./mm grating and 200 µm entrance slit; measured experimentally on enamel and Silicon samples, with non-polarized configuration for probe-based acquisitions and polarized for benchtop measurements, respectively). High spectral resolution is often required for the diagnostic in a clinical setting. However, during the spectral acquisitions by using the probe - 2nd approach, the band shift was the spectral parameter most severely affected, since the phosphate symmetric stretching bands, usually located at ~960 cm^{-1}, were down-shifted to 956-957 cm^{-1} during benchtop measurements, and to 951-953 cm^{-1} for probe-based measurements, mostly due to calibration for internal 785 nm laser, detector related issues and signal interference within/throughout the cores of the used optical fibers. Therefore, this parameter could not be considered as precise as phosphate peak width, phosphate and carbonate peaks intensities, and the resulting b-carbonate/phosphate ratio.

Third, the obtained data, in both approaches, have demonstrated strong evidence of an overall significant loss in mineral content of the carious samples, particularly in the regions near the non-cavitated lesion margins or cavity edges. Therefore, this reduction in mineral content is the most prominent in Group C, resulting in significantly higher depolarization ratios (ρ_{959}), dramatically decreased anisotropy values (A_{959}) and increased b-type carbonate ratios, which in 2nd approach, has shown significant differences between the three groups of study. This indicates that the remote probe is viable for a precise assessment of the teeth, with reliable results, and the parameters derived from band intensity ratios, as well as the band width, can

be certainly used for the overall mineralization assessment (de/remineralization studies), detection of enamel lesions, identification of hypo-mineralized samples or sample regions belonging to the same sample, and most important, distinction between samples with different degrees of mineralization, structural arrangement variations and lesion severity.

Fourth, this work concerns a remote Raman probe build only with single-fiber configurations, operating in a backscattering geometry (reflection mode, with 180° between the excitation laser and Raman signal collection directions), while the angle between the incident laser beam to the sample surface must be ideally of exactly 90°. Slight changes of the beam incidence angle reduce the collection of the Raman photons, which can lead to significant decrease in phosphate peak intensity, while minor movements or small position changes of the probe relative to the examined sample surface (outer layer) can result in defocusing, and consequently result in decreased collection efficiency, also lowering the intensity of Raman peaks.

Fifth, the major technical difficulties that were mentioned at the beginning of my PhD thesis, that were, overwhelmed, if not totally, at least partially, are the following:

(1) tissue fluorescence – by means of the 785 nm NIR laser and use of appropriate filters, incorporated internally in the probe and the benchtop equipment; (2) the extremely weak Raman signal from tissue – through 10-fold higher excitation power and increased collection times to obtain spectra with acceptable signal-to-noise ratios; (3) contamination signal from the delivery and collection fiber optics – noise and spectral background caused by the Raman scattering and fluorescence signals that are originated within the silica core of the excitation and collection fibers – through the use of low-OH optical fibers, with relatively small core diameter and appropriate NA; and (4) probe lens focus difficulty – the employed remote probe had to be maintained constantly at approximately the same distance during all the measurements, according to the ≈ 32 mm optimal working distance (which was established experimentally during repeated benchtop measurements with varying distance between the sample enamel and the plano-convex 35 mm lens). This way, it was maximized the delivery efficiency of the 785 nm laser excitation monochromatic beam to the dental sample, maximizing the collection efficiency of the Raman scattered signal as well, in direction to the spectrometer. On the other hand, by using a lens instead of a high magnification objective, the diameter of the incident laser spot in the 2nd approach was significantly larger, comparing to the 1st approach, yielding information from an increased and wider probed area, turning the spectral measurements less precise and with a reduced level of accuracy. Instead, it provides an average Raman spectrum of more Raman spectra from a greater area that corresponds to a multitude of smaller

individual points, included in this larger incidence spot, turning, this way, the remote probe measurements vaster and more general.

Sixth, since all the spectral acquisitions relied on single-point measurements – the acquisition of the Raman spectra is very relative, the spectral characteristics can vary considerably even within small regions (less than 1 mm^2) of the same sample (intra-tooth variability). Also, the spectral band intensity can vary substantially even during different consecutive measurements on the same spot. Therefore, it is extremely necessary and strongly recommended to analyze numerous and representative single points of the same sample, in order to obtain more precise and reliable data.

Seventh, during the measurements with the remote probe, Raman mapping, and real-time visualization of the amplified region of interest (ROI) of the sample was not possible, since the use of the remote handheld probe does not imply the real-time 2D visualization on the monitor, as occurs during the benchtop measurements. This represents a major limitation, since is not possible to focus properly on selected individual specific points, nor to visualize the overall condition of the amplified ROIs of the sample surface.

Eighth, the probe does not have an adjustable or self-focusing lens, so it is very sensitive to small movements or slight position changes, since these can defocus or alter the collection angles, or even deviate from the measuring point, diminishing the collection efficiency or even obstruct the entire measurement procedure. Thus, it cannot be handheld during measurements. Instead, it requires to be well-fixed, continuously during the measurement duration, in a specific selected and stable position, placed in normal direction to the sample surface, at the OWD. Otherwise, the overall quality, SNR and band intensities of the spectra can be very affected.

Lastly, however very important, before applying the probe *in-vivo*, it must be considered the sample local heating, which can result in both hard (enamel and dentine) and soft (pulp, cement, nerves, and gingiva) tissue irreversible damage. To minimize the risk of temperature temporary increase that might induce a critical and/or irreversible condition of the surrounding and inner tissues of a vital tooth, it must be established a limit for the time duration of spectral acquisition, depending on the combination of excitation laser monochromatic beam wavelength and power incident on the sample. This must be in accordance with the specific heat values for enamel and dentine [33, 34]. An *ex-vivo* examination requires less caution, compared to an *in-vivo* measurement of a vital tooth, which is more critical. However, the same rules apply for both methods, in order to avoid burn or denaturation by over-heating.

Overall, the aforementioned objectives were partially accomplished, confirming however, the utility and the functioning principle of the Raman remote probe concept, which could be implemented *in-vivo* to assess the demineralization, appearance of white spot lesion and caries progression.

9.6 – Conclusion

The presented study is in agreement with the revised literature and has confirmed, once again, that Raman spectroscopy can be successfully applied, ***ex-vivo***, to assess and monitor the mineral content alteration in mineralization/demineralization processes, and to distinguish and compare the results from distinct groups of tooth samples, with different conditions – varying from sound and highly mineralized to carious, with cavities and/or hypo-mineralized specimens. Raman spectroscopy can be considered extremely useful and valuable, representing a precise, minimally invasive, non-destructive, and accurate analytical technique in the biomedical field, providing fast and real-time results, yielding specific parameters that characterize the overall condition of the tooth which can bring improved solutions and new imminent bright perspectives for diagnostic spectroscopy, imaging, and image guided treatment in dentistry in the close future.

9.7 – Future Work

In the upcoming future, in case that further studies based on remote sample measurements are going to be achieved, the described in-house built Raman remote fiber-optic probe requires for additional improvements and supplementary components, to be added to the actual configuration, as follows:

1) **Long-pass (edge) filter or Notch filter.**

In Figures 8.3 and 8.4 were shown two designs, one with a larger signal circuit – 8.3, and another with a simplified configuration – 8.4, revealing the functioning principle of the developed remote Raman probe. The monochromatic NIR 785 nm excitation laser light beam is delivered by fiber and collimated to pass through a band-pass filter for the removal of undesired silica Raman background originated from the excitation fiber. Then the 785 nm excitation beam is reflected by a dichroic mirror and focused on the sample through a 35mm plano-convex lens. The generated Raman signal is collected backwards by the same lens (in backscattering

configuration or reflection mode), and afterwards it should be passed through a long-pass filter to suppress the Rayleigh line. Finally, the Raman scattered light is directed by the coupler into a collection fiber, which is attached to a spectrometer. The spectrometer disperses the Raman signal into spectral components and images the received signal on a charged coupled device (CCD). The presented probe structure lacks a band-pass or a Notch filter, that can suppress the elastically scattered - Rayleigh photons.

2) Linear polarizer.

Another additional component to the probe configuration would be a film linear polarizer, extremely relevant for obtaining polarized Raman spectra, with different parallel and cross-polarizations. This component should be mounted in the excitation laser path, before it reaches the sample, requiring also for polarization-maintaining optical fibers, or with a smaller core diameter, preferentially of 50 µm or up to 100 µm.

3) Bundle of collection optical fibers.

A major, however, optional improvement for a higher collection efficiency of the Raman input would be the replacement of just one collection fiber with the use of a fiber bundle, composed by numerous N multi-channel collection setup, from 7 up to 18 collection fibers, with core diameters of 200 µm, 100 µm or 50 µm, depending of the number of employed fibers, with an overall NA parameter that should not exceed the required 0.22 NA at the fiber entrance of the bench equipment, in order to avoid substantial signal losses at the fiber coupling.

4) Lens with an adjustable focus.

Instead of fixed focus probe, that requires a fixed, stable (steady) and constant position over time, a probe with an auto-focusing lens can achieve a fast focus adjustment in order to stabilize the signal, improving significantly the collection efficiency, without the risk of defocusing or deviate from the selected single-point of measurement. The implementation of this novel alternative self-adjustable lens does not require major modifications regarding the used probe design, being sufficient only the replacement of the former lens. However, this requires the inclusion of new electronic circuits, since this type of auto-focusing lens with fast and stable adjustments is usually controlled by a voltage circuit (voltage-driven liquid adapting lens) and an ultrasonic distance sensor [85].

5) Probe design improvement and volume reduction.

Since the developed probe was built from separate ordered components, it has another limitation - is quite large and rigid, with a volume that may not be appropriate for *in-vivo* examination of vital teeth situated in the intra-oral environment. It needs an optimized optical design, a custom-modified structure, with a more compact arrangement which requires for smaller internal components, resulting in a more compact housing of a reduced size, so that the overall volume would be suitable for measurement conditions within small working-space, more appropriate for short distance to sample and easier to handle.

The overall probe setup configuration must remain simple as it is, with improvement in the geometrical arrangement of smaller optical components, continuing the use of low-OH and low-loss optical fibers, increase the quality of the main focusing lens, as well as the collimating lenses from the adapters.

BIBLIOGRAPHY

References

1) M. Monteiro, F. Chasqueira and S. Pessanha. "Raman spectroscopy in the characterization of carious dental tissues". Spectroscopy Europe, 30:3, 2018.

2) T. Vo-Dinh. Biomedical Photonics Handbook. (CRC Press, Boca Raton, 2003).

3) R. Ramakrishnaiah, G. Rehman, S. Basavarajappa, A. A. Al Khuraif, B. H. Durgesh, A. S. Khan and I. ur Rehman. "Applications of Raman Spectroscopy in Dentistry: Analysis of Tooth Structure". Applied Spectroscopy Reviews, 50:4, 332-350, 2015. DOI: 10.1080/05704928.2014.986734.

4) T. Buchwald, Z. Okulus and M. Szybowicz. "Raman spectroscopy as a tool of early dental caries detection–new insights". Journal of Raman Spectroscopy, 2017. DOI 10.1002/jrs.5175.

5) A. Akkus, O. Akkus, R. Roperto and L. Lang. "Investigation of Intra-and Inter-individual, Variations of Mineralisation in Healthy Permanent Human Enamel by Raman Spectroscopy". 2016. DOI: 10.3290/j.ohpd.a36098.

6) https://en.wikipedia.org/wiki/Human_tooth - 10.10.2022.

7) R.M. Loureiro, D.V. Sumi, H.L.V.C. Tames, S.P.P. Riibeiro, C.R. Sores, R.L.E. Gomes, M. M. Daniel, "Cross-Sectional Imaging of Third Molar–Related Abnormalities", American Journal of Neuroradiology Sep 2020, **DOI:** 10.3174/ajnr. A6747.

8) E. A. Pankrushina, D. V. Kiseleva, Yu. V. Mandra and N. V. Ozhgikhina. AIP conference proceedings [AIP publishing the 2nd international conference on physical instrumentation and advanced materials 2019 - Surabaya, Indonesia (22 October 2019)] The 2nd International Conference on Physical Instrumentation and Advanced Materials 2019 - Raman Hyper mapping of Human Teeth: Analysis and Statistical Approaches. 2314, 050044. Doi:10.1063/5.0032410.

9) J. Hicks, F. Garcia-Godoy, and C. Flaitz. "Biological factors in dental caries: role of saliva and dental plaque in the dynamic process of demineralization and remineralization (part1)". Journal of Clinical Pediatric Dentistry, 28:47-52, 2003.

10) C. Robinson, R.C. Shore, S.J. Brookes, S. Strafford, S.R. Wood, and J. Kirkham. The chemistry of enamel caries. Crit Rev Oral Biol Med, 11:481–495, 2000.

11) E. Marin, N. Hiraishi, T. Honma, F. Boschetto, M. Zanocco, W. Zhu, T. Adachi, N. Kanamura, T. Yamamoto and G. Pezzotti. "Raman spectroscopy for early detection and monitoring of dentin demineralization". Dental Materials, 2020. S0109564120302803–. doi:10.1016/j.dental.2020.10.005.

12) R. Al-Obaidi, H. Salehi, P. Collart-Dutilleul, B. Jacquot, H. Tassery, F. Cuisinier, C. Gergely, and T. Cloitre, Thierry." Relationship between Changes in Chemical Composition of Enamel Subsurface Lesions and the Emitted Nonlinear Optical Signals: An in vitro Study". Caries Research, 1–10, 2020. doi:10.1159/000505904.

13) V. Bulatov, L. Feller, Y. Yasman, and I. Schechter. "Dental enamel caries (early) diagnosis and mapping by laser Raman spectral imaging". Instrum. Sci. Technol., 36: 235–244, 2008.

14) Soma Datta., et al. "A Complete Review on Dental Carious Lesion Detection Methods and its Challenges". Acta Scientific Dental Sciences 3.9, 74-81, 2019.

15) M. Melo, J. L. Sanz, L. Forner, F.J. Rodríguez-Lozano and J. Guerrero-Gironés, J. "Current Status and Trends in Research on Caries Diagnosis: A Bibliometric Analysis". Int. J. Environ. Res. Public Health 2022, 19, 5011. https://doi.org/10.3390/ ijerph1909501.

16) E. Zain, H. P. Chew. "Update on Clinical Detection Methods for Non-cavitated Fissure Caries". World J Dent, 11(1):81–88, 2020.

17) A. C.-T. Ko, M. Hewko, M. G. Sowa, C. C.S. Dong, B. Cleghorn and L. P. Choo-Smith. "Early dental caries detection using a fibre-optic coupled polarization-resolved Raman spectroscopic system". Optics Express, 16: 9, pp. 6274-6284, 2008. https://doi.org/10.1364/OE.16.006274.

18) J. Bader. "Diagnosis and management of dental caries". Number 36. AHRQ Publication No.01-E055, Rockville, MD: Agency for Healthcare Research and Quality, 2001.

19) A. I. Ismail. "Visual and Visuo-tactile detection of dental caries," J. Dent Res. 83, C56-C66 2004.

20) Mohanraj, et al. "Diagnostic Methods for Early Detection of Dental Caries" – A Review.

21) P. Vandenabeele. "Practical Raman Spectroscopy – An Introduction". John Wiley & Sons, Ltd., Raman spectroscopy–Study and teaching, 2013. QD96.R34V36 2013.

22) T. Vargas-Koudriavtsev, R. Durán-Sedó, P. Sáenz-Bonilla, V. Bonilla-Mora, M. Guevara-Bertsch, R. Jiménez-Corrales and O. A. Herrera-Sancho. "Effect of tooth-bleaching agents on phosphate concentration in dental enamel by means of Raman spectroscopy". Revista Odontológica Mexicana, 19(4), e228–e235, 2015. doi:10.1016/j.rodmex.2015.10.013.

23) J. Toporski, T. Dieing, and C. Heim. Raman Microscopy (Confocal), 2011. https://doi.org/10.1007/978-1-4020-9212-1_173.

24) H. Tsuda. "Micro-raman spectroscopy in dental research". PhD thesis, 1996.

25) https://www.horiba.com/int/ - 22.10.2022.

26) https://www.renishaw.com/en/raman-spectroscopy--6150 - 06.02.2022.

27) J. R. Ferraro, K. Nakamoto and C. W. Brown. "Introductory Raman Spectroscopy", 2003. Elsevier, Second Edition, ISBN: 978-0-12-254105-6.

28) H. Tsuda and J. Arends. "Raman Spectroscopy in Dental Research: A Short Review of Recent Studies". ADR 1997, 11: 539, 1997. DOI: 10.1177/08959374970110042301, http://adr.sagepub.com/content/11/4/539.

29) P. Matousek, M. Morris. "Emerging Raman Applications and Techniques in Biomedical and Pharmaceutical Fields", 2010. ISBN:978-3-642-02648-5.

30) Y. Zhang, L. Ren, Q. Wang, Z. Wen, C. Liu, and Y. Ding. "Raman Spectroscopy: A Potential Diagnostic Tool for Oral Diseases". Front. Cell. Infect. Microbiol. 12:775236, 2022. doi: 10.3389/fcimb.2022.775236.

31) A. Orlando, F. Franceschini, C. Muscas, S. Pidkova, M. Bartoli, M. Rovere, and A. Tagliaferro. "A Comprehensive Review on Raman Spectroscopy Applications". Chemosensors. 9(9):262, 2021. https://doi.org/10.3390/chemosensors9090262.

32) https://www.sas.upenn.edu/~lineje/ramanspectroscopy.html - 06.02.2022.

33) E. Eberhardt, C. Stiebing, C. Matthäus, M. Schmitt, and J. Popp. "Advantages and limitations of Raman spectroscopy for molecular diagnostics: an update", Expert Rev. Mol. Diagn. 15:6, 773–787, 2015.

34) M. F. Magalhães, R. A. N. Ferreira, and R. M. Andrade. "Medição do calor específico do esmalte dentário humano por meio de calorimetria diferencial exploratória (2010)", VI National Congress of Mechanical Engineering – CONEM 2010.

35) M. Tatarkovič, A. Synytsya, L. Šťovíčková, B. Bunganič, M. Miškovičová, L. Petruželka, and V. Setnička. "The minimizing of fluorescence background in Raman optical activity and Raman spectra of human blood plasma." Analytical and Bioanalytical Chemistry, 407:5, 1335–1342, 2015. doi:10.1007/s00216-014-8358-7.

36) T. Buchwald, Z. Buchwald and A. Daktera-Micker. "The fluorescence background in Raman spectra of sound enamel", Vibrational Spectroscopy 115, 103275, 2021. https://doi.org/10.1016/j.vibspec.2021.103275.

37) H. Kinoshita, N. Miyoshi, Y. Fukunaga, T. Ogawa, T. Ogasawara, and K. Sano. "Functional mapping of carious enamel in human teeth with Raman micro-spectroscopy." J. Raman Spectrosc, **39**: 655–660, 2007. (www.interscience.wiley.com) DOI: 10.1002/jrs.1908.

38) A. C. Ko, L. P. Choo-Smith, M. Hewko, L. Leonardi, M. G. Sowa, C. C. S. Dong, and P.Williams, B. Cleghorn. "Ex-vivo detection and characterization of early dental caries by optical coherence tomography and Raman spectroscopy" J. Biomed. Opt., 10(3), 031118, 2005. Doi: 10.1117/1.1915488.

39) A. C. Ko, L. P. Choo-Smith, M. Hewko, and M. G. Sowa. "Detection of early dental caries using polarized Raman spectroscopy". Optics Express, 14:1, 203, 2006. doi: 10.1117/1.1915488.

40) Choo-Smith et al.: Towards early dental caries detection with OCT and polarized Raman spectroscopy. Head & Neck Oncology, 2:1, O43, 2010.

41) https://www3.nd.edu/~kamatlab/facilities_spectroscopy.html - 29.12.2022

42) https://www.witec.de/resources-and-education/knowledge-base/ - 10.10.2022.

43) https://hubner-photonics.com/applications/lasers-for-raman-spectroscopy/ - 10.09.2021.

44) A. D. Elliott. Confocal microscopy: Principles and modern practices. *Current Protocols in Cytometry*, 92, e68, 2020. doi: 10.1002/cpcy.68.

45) M. Nehir, C. Frank, S. Aßmann, and E.P. Achterberg. "Improving Optical Measurements: Non-Linearity Compensation of Compact Charge-Coupled Device (CCD) Spectrometers". Sensors, 19, 2833, 2019. https://doi.org/10.3390/s19122833.

46) I. Pence and A. Mahadevan-Jansen. "Clinical instrumentation, and applications of Raman spectroscopy". Chem Soc Rev, 29, 45:7, 1958–1979, 2016. doi:10.1039/c5cs00581g.

47) I. Ionita. "Early diagnosis of tooth decay using fluorescence and polarized Raman spectroscopy". Optoelectronics and advanced materials – rapid communications, 3:10, 1122-1126, 2009.

48) E. V. Timchenko, P. E. Timchenko, L. T. Volova, A. Yu Rosenbaum, A. Yu Kulabukhova. "Analysis of tooth tissues using Raman spectroscopy". Journal of Physics: Conference Series, 769, 012047, 2016. doi:10.1088/1742-6596/769/1/012047.

49) E. Timchenko, P. Timchenko, L. Volova, O. Frolov, M. Zibin, and I. Bazhutova. "Raman Spectroscopy of Changes in the Tissues of Teeth with Periodontitis". Diagnostics, 10:11, 876, 2020. doi:10.3390/diagnostics10110876.

50) T. Buchwald and Z. Okulus. "Determination of storage solutions influence on human enamel by Raman spectroscopy". Vibrational Spectroscopy, 96: 118-124, 2018. https://doi.org/10.1016/j.vibspec.2018.04.003.

51) T. Buchwald and Z. Buchwald. "Assessment of the Raman spectroscopy effectiveness in determining the early changes in human enamel caused by artificial caries". The Analyst, 2019, 10.1039. C8AN01494A–. doi:10.1039/c8an01494a.

52) D. V. Prikule, V. I. Kukushkin, A. V. Mitronin, and V. F. Prikuls. "Studying the Degree of Tooth Enamel Mineralization through Raman Spectroscopy in Various Spectral Ranges." Biophysica, 1, 269–278, 2021. https://doi.org/10.3390/ biophysica1030020.

53) I. Otel, K. Dias, R. Pereira, M. Fonseca, A. P. Jesus, A. Mata, V. Vassilenko, J. M. Silveira, and S. Pessanha. "Investigation of the protective suitability of a dental fluorinated varnish by means of X Ray fluorescence and Raman spectroscopy". Journal of Trace Elements in Medicine and Biology, Volume 71, 2022, 126938, ISSN 0946-672X, https://doi.org/10.1016/j.jtemb.2022.126938.

54) J. M. Silveira, S. Longelin, A. Mata, and M. Luísa. "Identification of oxygen in dental enamel following tooth bleaching using confocal micro-Raman spectroscopy". J Raman Spectroscopy, 43, 1089-1093, 2012. https://doi.org/10.1002/jrs.3153.

55) G. Luís, H. Silva, J.M. Silveira, V. Manteigas, A. Mata, D. Marques, A. Jesus, M. Fonseca, and S. Pessanha. "Evaluation of enamel demineralization and fluorine uptake caused by gustatory stimulants of salivary secretion (GSSS) using Raman spectroscopy and proton induced gamma-ray emission (PIGE)". Journal of Raman Spectroscopy, 50, 380-386, jrs.5532, 2018. https://doi.org/10.1002/jrs.5532.

56) J. M. Silveira, S. Coutinho, D. Marques, J. Castro, A. Mata, M. L. Carvalho, and S. Pessanha. "Raman spectroscopy analysis of dental enamel treated with whitening product – Influence of saliva in the remineralization". Spectrochimica Acta - Part A: Molecular and Biomolecular Spectroscopy. 198, 145–149, 2018. https://doi.org/10.1016/j.saa.2018.03.007.

57) P. Kanzow, F.J. Wegehaupt, T. Attin, and A. Wiegand. "Etiology and pathogenesis of dental erosion", Quintessence International, 47, 275–278, 2016. https://doi.org/10.3290/j.qi.a35625.

58) V. F. Passos, M. A. S. Melo, S. J. Park, and H. E. Strassler. "Current Concepts and Best Evidence on Strategies to Prevent Dental Erosion". Compend Contin Educ Dent. 40, 80–86, 2019.

59) J.A. Cury and L.M. Tenuta. "How to maintain a cariostatic fluoride concentration in the oral environment". Advances in Dental Research. 20, 13–16, 2008.

https://doi.org/10.1177/154407370802000104.

60) E. Medjedovic, S. Medjedovic, D. Deljo, and A. Sukalo. "Impact of fluoride on dental health". Mater Sociomed. 27, 395–398, 2015. https://doi.org/10.5455/msm.2015.27.395-398.

61) A. de Arruda, P. dos Santos, R. Sundfeld, S. Berger, and A. Briso. "Effect of Hydrogen Peroxide at 35% on the Morphology of Enamel and Interference in the De-remineralization Process: An In Situ Study". Operative Dentistry. 37, 518–525, 2012. https://doi.org/10.2341/11-112-L.

62) R. V. Hogg and E.A. Tanis, D.L. Zimmerman, Probability, and statistical inference, 2015.

63) S. Bollineni, R.K. Janga, L. Venugopal, I.R. Reddy, P.R. Babu, and S.S. Kumar. "Role of fluoridated carbamide peroxide whitening gel in the remineralization of demineralized enamel: An in vitro study". Journal of International Society of Preventive & Community Dentistry, 4, 117–21, 2014. https://doi.org/10.4103/2231-0762.137638.

64) S. Pessanha, S. Silva, J. M. Silveira, I. Otel, H. Luis, V. Manteigas, A. P. Jesus, A. Mata, and M. Fonseca. "Evaluation of the effect of fluorinated tooth bleaching products using polarized Raman microscopy and particle induced gamma-ray emission". Spectrochim. Acta Part A: Biomol. Spectrosc. 236, 118378, 2020. https://doi.org/10.1016/j.saa.2020.118378.

65) J. Janiszewska-Olszowska, A. Drozdzik, K. Tandecka, and K. Grocholewicz. "Effect of air-polishing on surface roughness of composite dental restorative material-comparison of three different air-polishing powders". BMC Oral Health, 20:1, 1–7, 2020. https://doi.org/10.1186/s12903-020-1007-y.

66) M. Amato, R. Weiger, and C. Walter. "A systematic review on the effects of air polishing devices on oral tissues". International Journal of Dental Hygiene, 1–14, 2015. https://doi.org/10.1111/idh.12120.

67) J. Bühler, M. Amato, R. Weiger, and C. Walter. "A systematic review on the patient perception of periodontal treatment using air polishing devices". International Journal of Dental Hygiene, 14:1, 4–14, 2016.. https://doi.org/10.1111/idh.12119.

68) J. Bühler, F. Schmidli, R. Weiger, and C. Walter. "Analysis of the effects of air polishing powders containing sodium bicarbonate and glycine on human teeth". Clinical Oral Investigations, 19(4), 877–885, 2014. https://doi.org/10.1007/s00784-014-1317-z.

69) J. T. Newton and K. Asimakopoulou. "Minimally invasive dentistry : Enhancing oral health related behaviour through behaviour change techniques". British Dental Journal, 223:3, 147–150, 2017. https://doi.org/10.1038/sj.bdj.2017.659.

70) S. Tamilselvi, R. R. Nagate, M. Al-Ahmari, G. Kokila, S. Tikare, and S. Chaturvedi. "Comparison of the effect of sodium bicarbonate and glycine air polishing systems on tooth surface roughness: An atomic force microscopic analysis". Technology and Health Care 29:3, 489–498, 2021. https://doi.org/10.3233/THC-202210.

71) G. Petersilka, C. M. Faggion, U. Stratmann, J. Gerss, B. Ehmke, I. Haeberlein, and T. Flemmig. "Effect of glycine powder air-polishing on the gingiva". Journal of Clinical Periodontology, 35:4, 324–332, 2008. https://doi.org/10.1111/j.1600-051X.2007.01195.x

72) S. J. Fraser, A. K. Natarajan, A. S. Clark, B. K. Drummond, and K. C. Gordon. "A Raman spectroscopic study of teeth affected with molar-incisor hypomineralisation". Journal of Raman Spectroscopy, 46:2, 202–210, 2015. doi:10.1002/jrs.4635.

73) I. Otel, J. M. Silveira, V. Vassilenko, A. Mata, and S. Pessanha. "Application of Machine Learning Methods to Raman Spectroscopy Technique in Dentistry". DoCEIS 2021, IFIP AICT 626, pp. 339–348, 2021. https://doi.org/10.1007/978-3-030-78288-7_33.

74) I. Otel, J. M. Silveira, V. Vassilenko, A. Mata, M.L. Carvalho, J.P. Santos, and S. Pessanha. "Application of Unsupervised Multivariate Analysis Methods to Raman Spectroscopic Assessment of Human Dental Enamel". Computers, 11, 5, 2022. https://doi.org/10.3390/computers11010005.

75) J. L. Gonzalez-Solis, E. Martinez-Cano, and Y. Magana-Lopez. "Early detection of dental fluorosis using Raman spectroscopy and principal component analysis". 2014. DOI 10.1007/s10103-014-1638-9.

76) C. C. Barrera-Ortega, A. R. Vazquez-Olmos, R. Y. Sato-Berru, and M. A. Araiza-Tellez. "Study of demineralized dental enamel treated with different fluorinated compounds by Raman spectroscopy". J Biomed Phys Eng 10:5, 635-644, 2020. DOI 10.31661/JBPE.V0I0.2003-1089.

77) J. Mihály, V. Gombás, A. Afishah, and J. Mink. "FT-Raman investigation of human dental enamel surfaces". J. Raman Spectrosc. 40, 898–902, 2009.

78) T. Izawa, M. Wakaki, P. Rechmann, and D. Fried. SPIE Proceedings [SPIE Biomedical Optics 2005 - San Jose, CA (Saturday 22 January 2005)] Lasers in Dentistry XI - <title>Application of laser Raman spectroscopy to dental diagnosis, 5687, 1–8, 2005. doi:10.1117/12.590211.

79) C. Krafft, S. Dochow, I. Latka, B. Dietzek, and J. Popp. "Diagnosis and screening of cancer tissues by fiber-optic probe Raman spectroscopy". J Biomed Spectrosc and Imaging, 1:1, 39-55, 2012. DOI**:** 10.3233/BSI-2012-0004.

80) Y. Sa, X. Feng, C. Lei, Y. Yu, T. Jiang, Y. Wang. "Evaluation of the effectiveness of micro-Raman spectroscopy in monitoring the mineral contents change of human enamel in vitro". Lasers in Medical Science, 32:5, 985–991, 2017. doi:10.1007/s10103-017-2197-7.

81) https://www.thorlabs.com – seen on 23.10.2022.

82) W. He, B. Li, and S. Yang. "High-Frequency Raman Analysis in Biological Tissues Using Dual Wavelength Excitation Raman Spectroscopy". Applied Spectroscopy, 000370281988176, 2019. doi:10.1177/0003702819881762.

83) https://bwtek.com/spectrometer-part-8-fiber-optic-probes/ - seen 10.10.2022.

84) O. Stevens, I. E. Iping Petterson, J. C. C. Daya and N. Stone. "Developing fiber-optic Raman probes for applications in clinical spectroscopy". Chem. Soc. Rev., 45, 1919-1934, 2016. DOI: 10.1039/c5cs00850f.

85) W. Yang, F. Knorr, J. Popp, and I. W. Schie. "Development and evaluation of a hand-held fiber-optic Raman probe with an integrated autofocus unit". Optics Express, 28:21, pp. 30760-30770, 2020. DOI: 10.1364/OE.401207.

APPENDIX A

In this Appendix are included the instrumental and technical details of the external NIR laser source of 785 nm wavelength, used for the remote fiber-coupled probe measurements.

Model:FC-D-785nm-450mW-DE51613(PO#223)

Inspection reports

Items of specs	Testing	Attachments
Output Power after Fiber	512mW	Graph 1
Power Stability over 4 hours	0.381%	Graph 1
Operating Mode	CW	/
Fiber connector	IN:FC/PC OUT:SMA905	/
Fiber	100um@1m	/
Wavelength	784.552nm	Graph 2
Spectrum Line Width	< 0.06nm	Graph 2
P-I after Fiber	/	Graph 3
Wavelength Stability after Fiber @2 hours	< 10pm	Graph 4
Warm-up Time	< 5min	/
Dimensions of Laser Head	141.4×97×49mm^3	/
Weight	1.0kg	/
Power Supply	85-264VAC	/
TTL modulation at 100K	239mW	/

Graph1. Output power and Stability testing after fiber

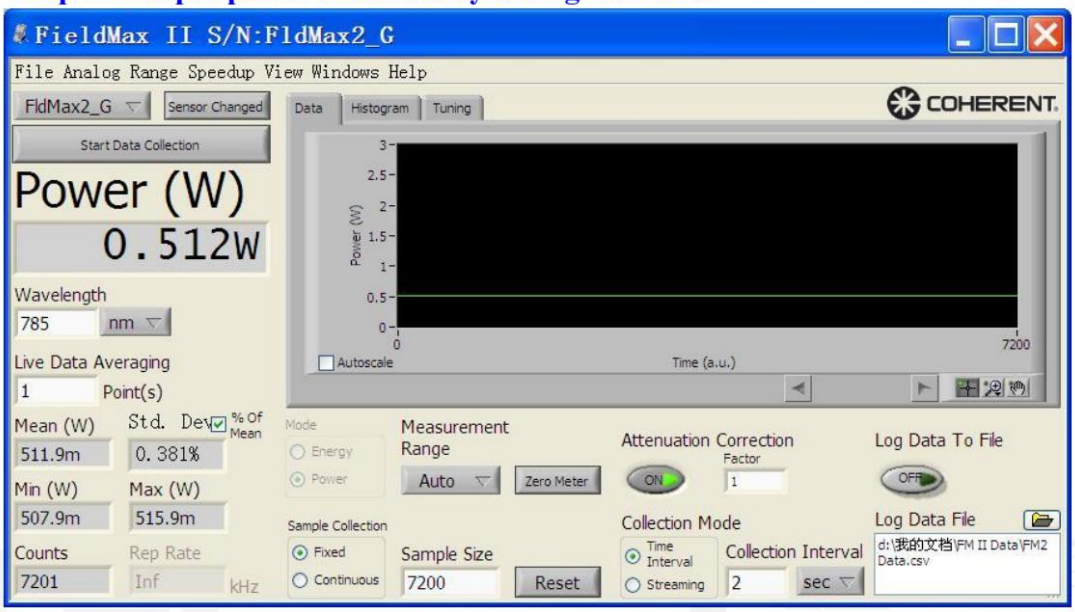

Graph2. Spectrum

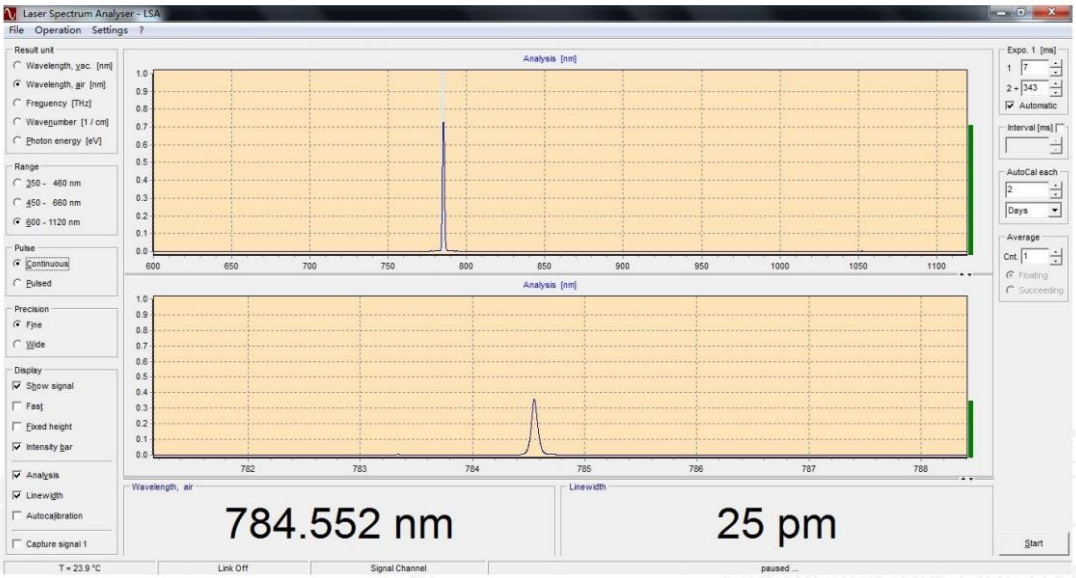

Graph3. P-I after fiber

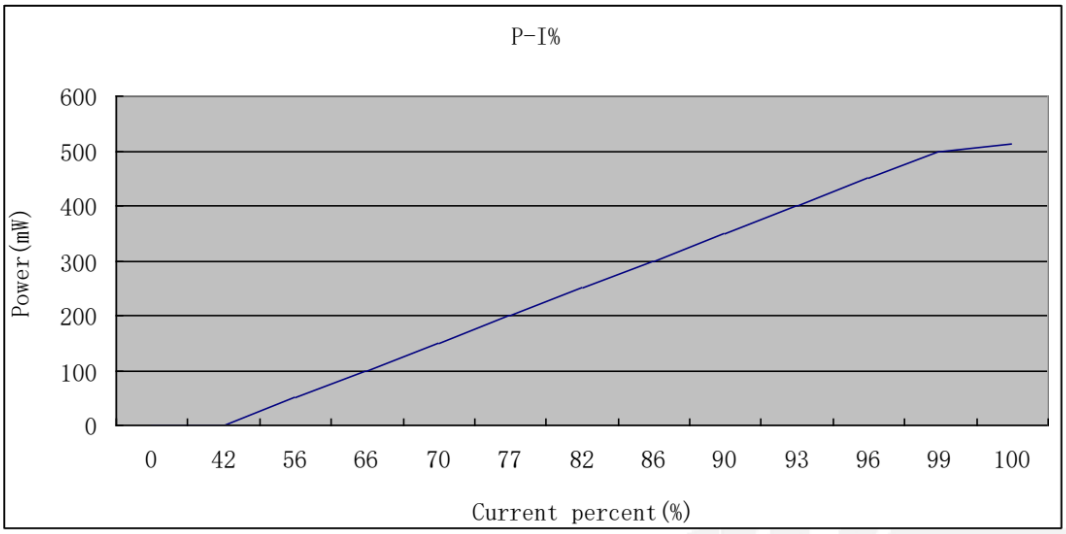

Current percent(%)	0	42	56	66	70	77	82
Power (mW)	0	1	50	100	150	200	250
Current percent(%)	86	90	93	96	99	100	
Power (mW)	300	350	400	450	500	512	

Graph4. Wavelength Stability after Fiber @2 hours

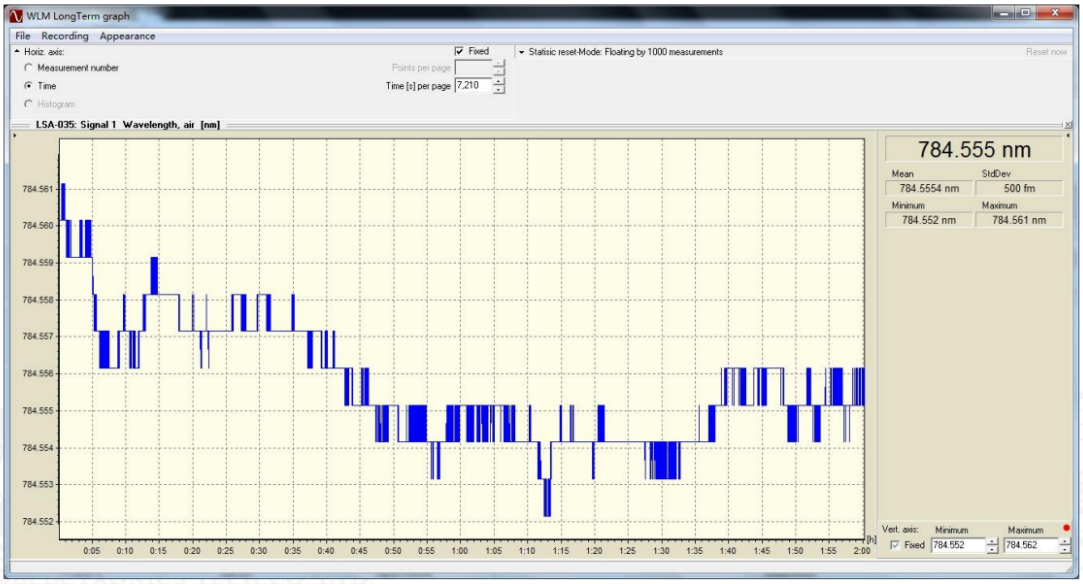

APPENDIX B

In this Appendix are shown the technical details of the external probe casing – DFM1 filter cube, dichroic mirror, CVH-100COL and F200-FC adapters, and the optic-fibers, used for the remote probe measurements.

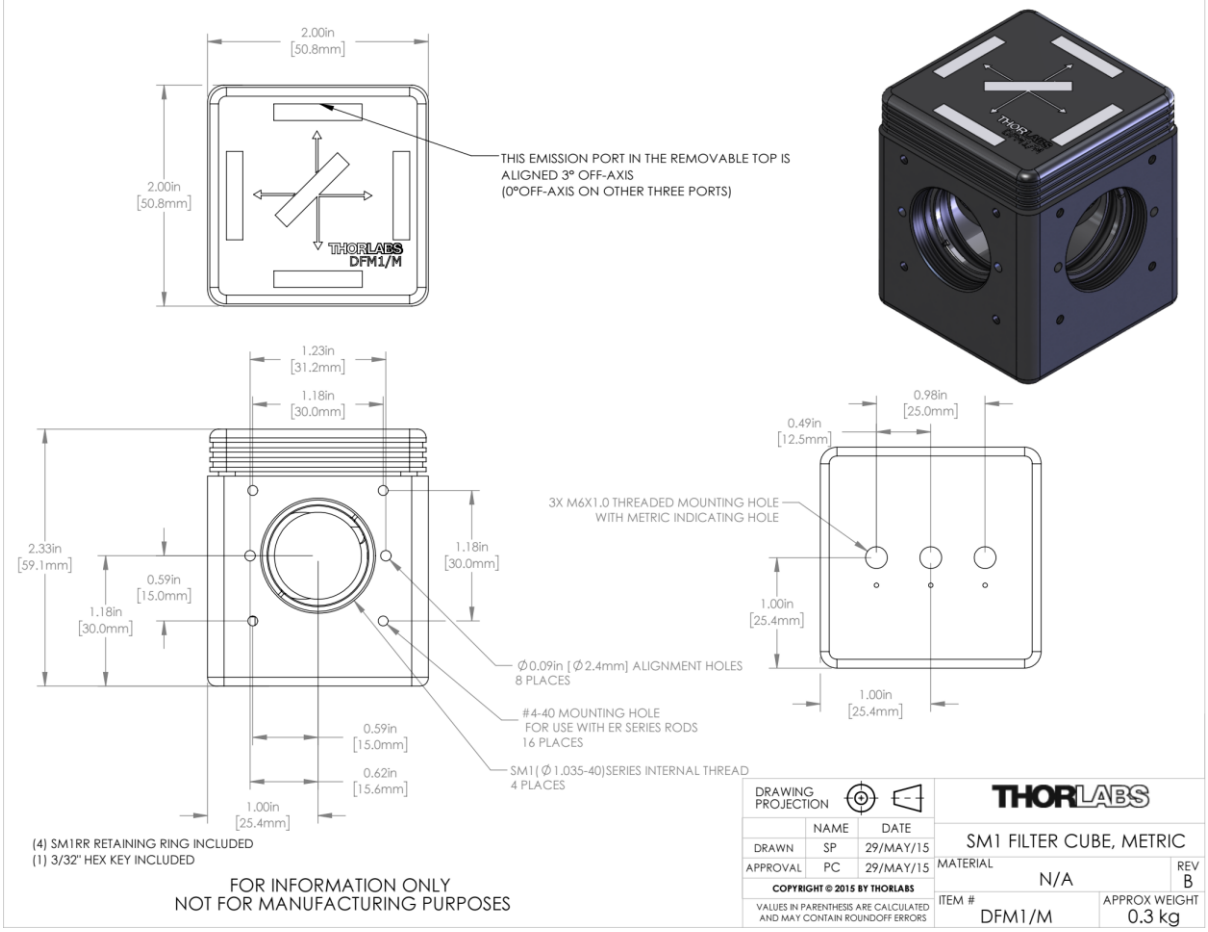

Figure B1 – Representation of the external casing of the remote probe – DFM1 filter cube.

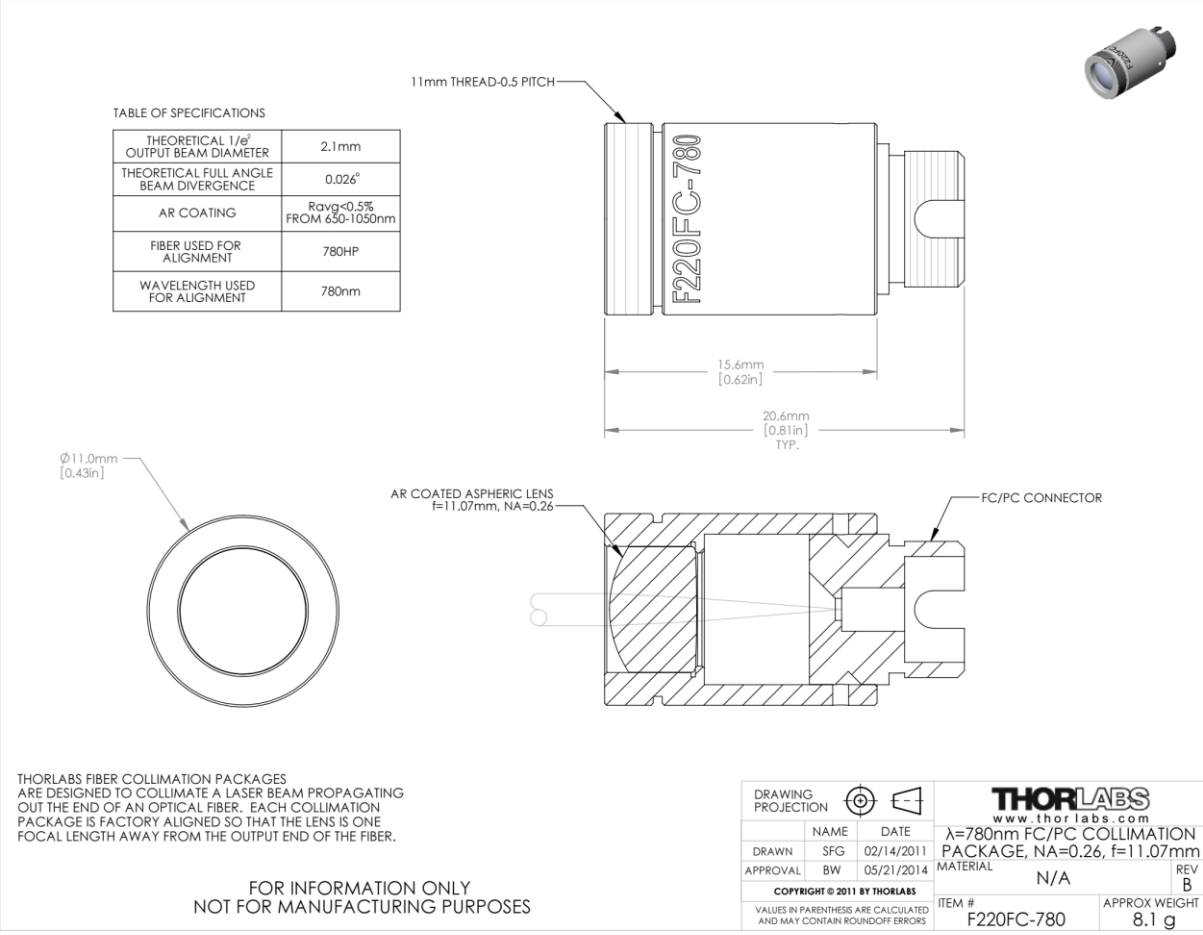

Figure B2 – Representation of the F220-FC-780 adapter, used for connecting the Raman probe to the excitation optic-fiber.

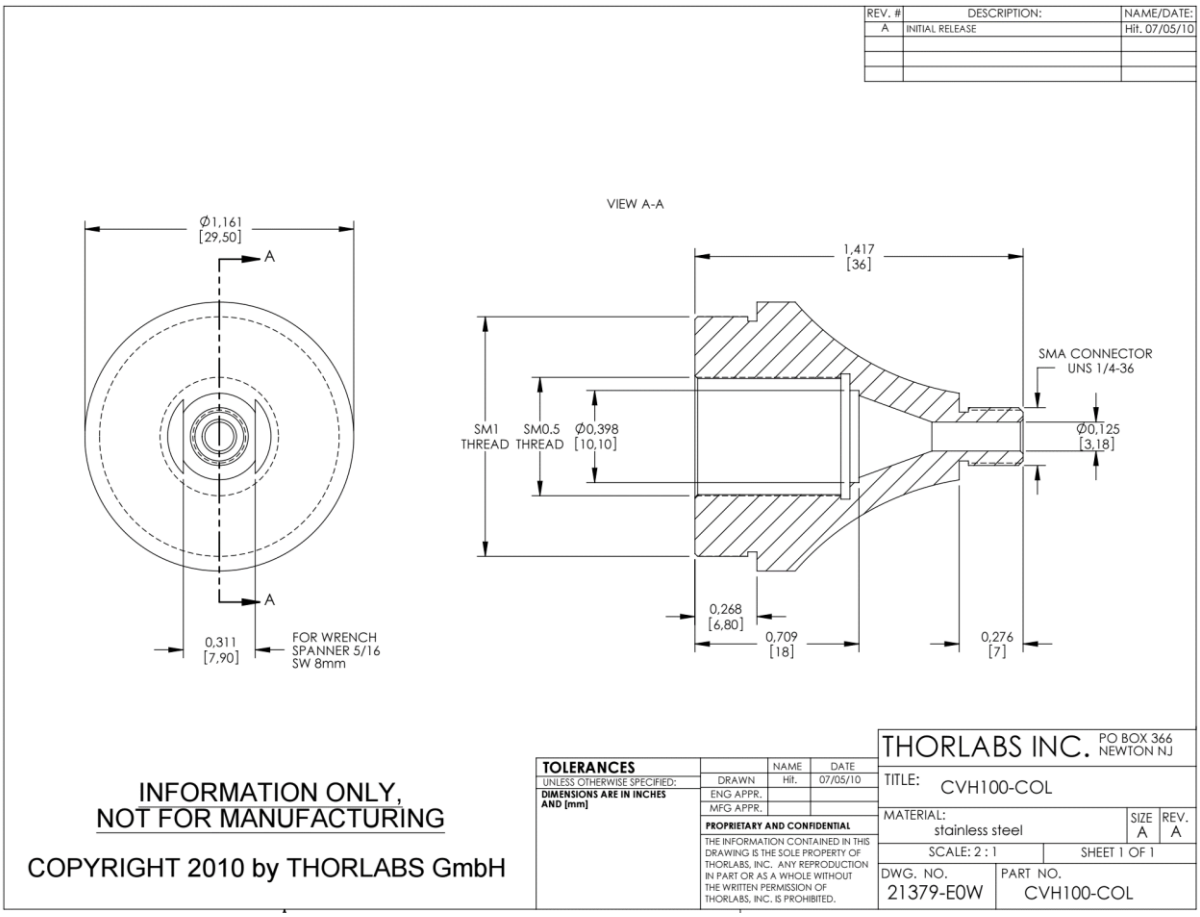

Figure B3 – Representation of the CVH-100COL adapter, used for connecting the Raman probe to the collection optic-fiber.

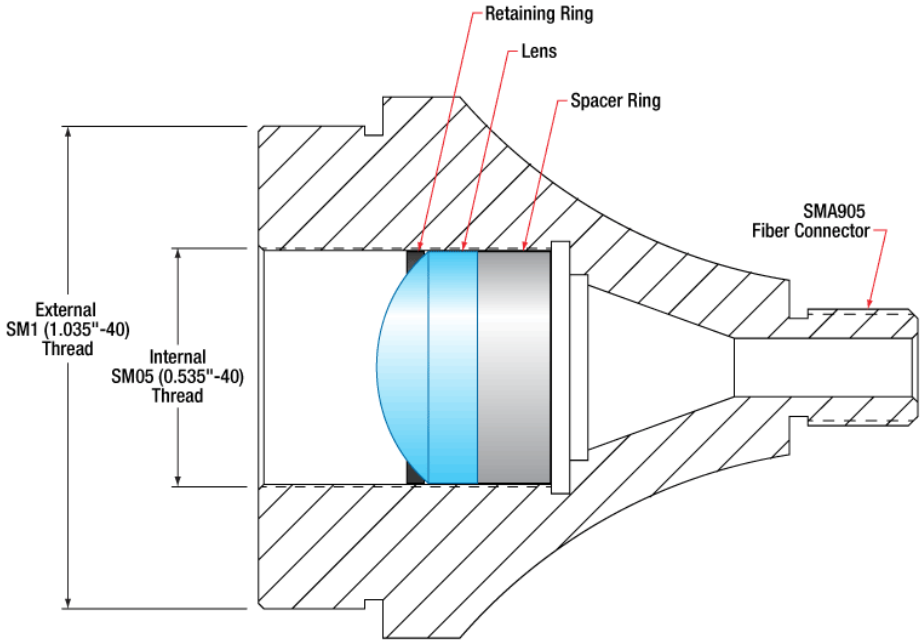

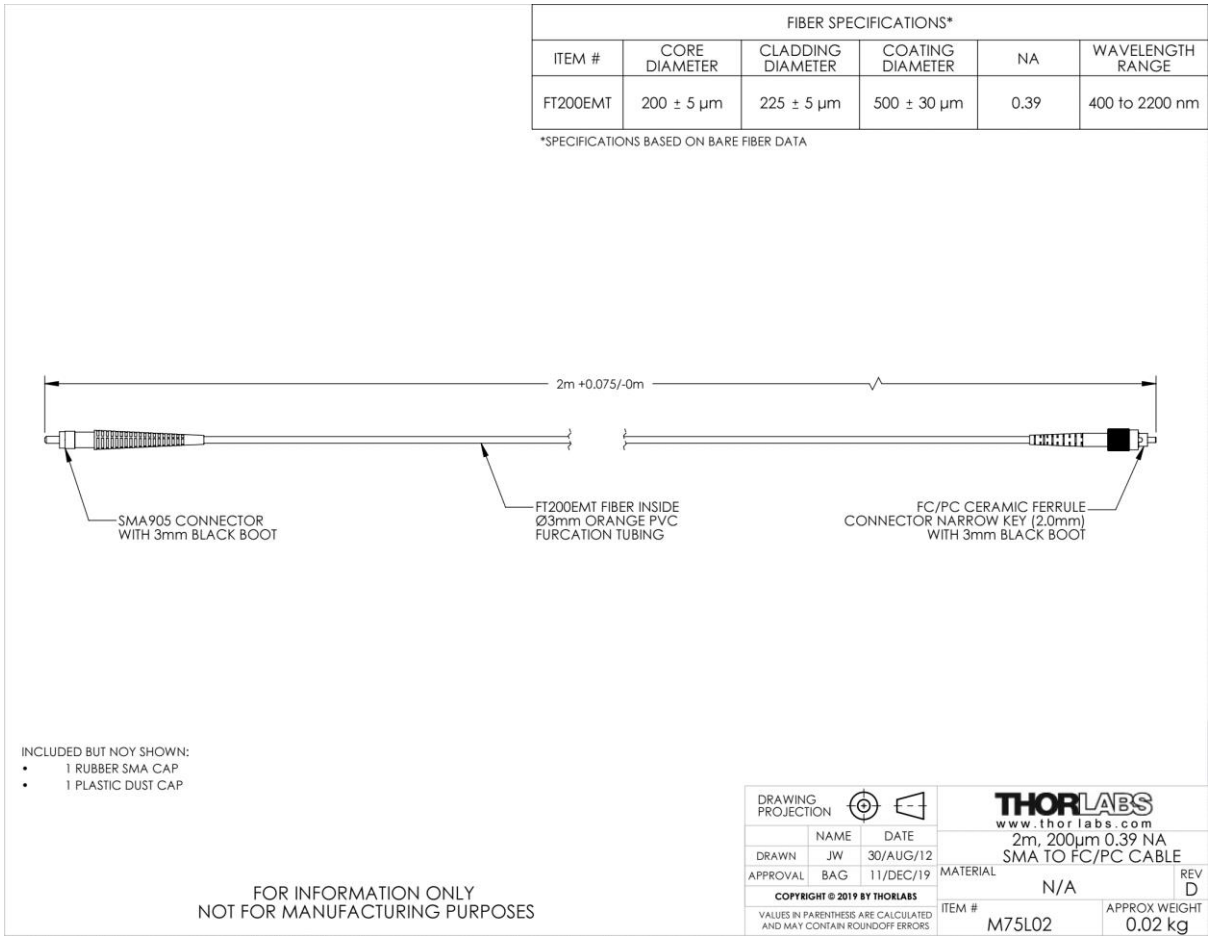

Figure B5 – Schematic representation of the collection optic-fiber – 200 µm core and 0.39 NA.

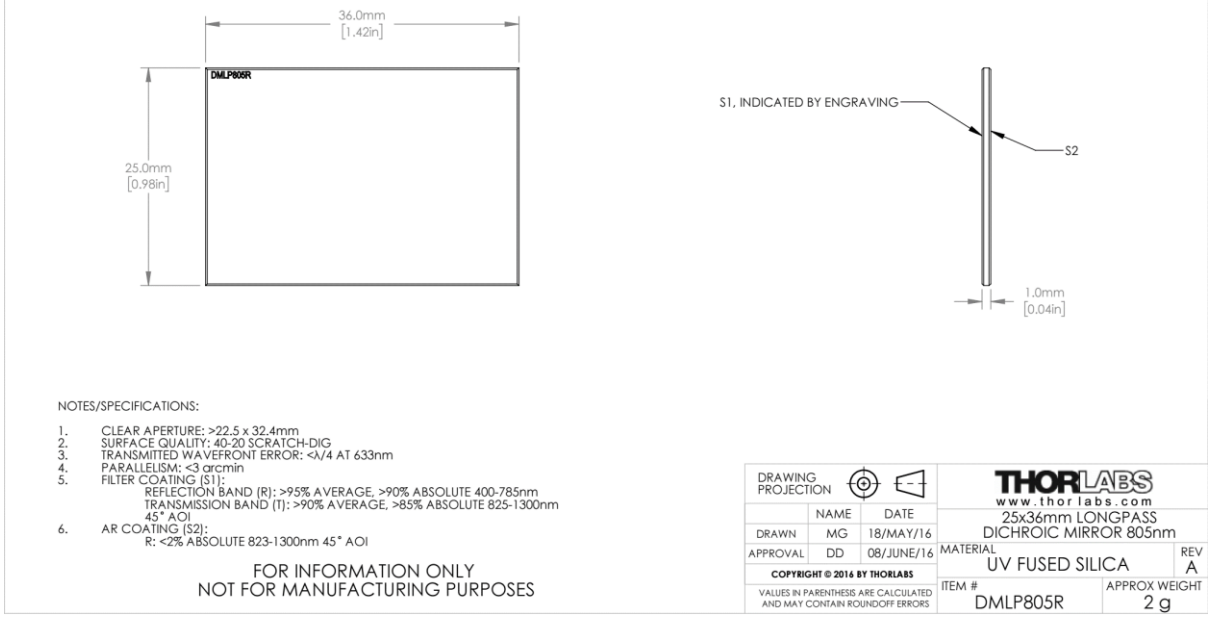

Figure B6 – Schematic representation of the used dichroic mirror – DMLP805R, long-pass, with cut-off from 805 nm.

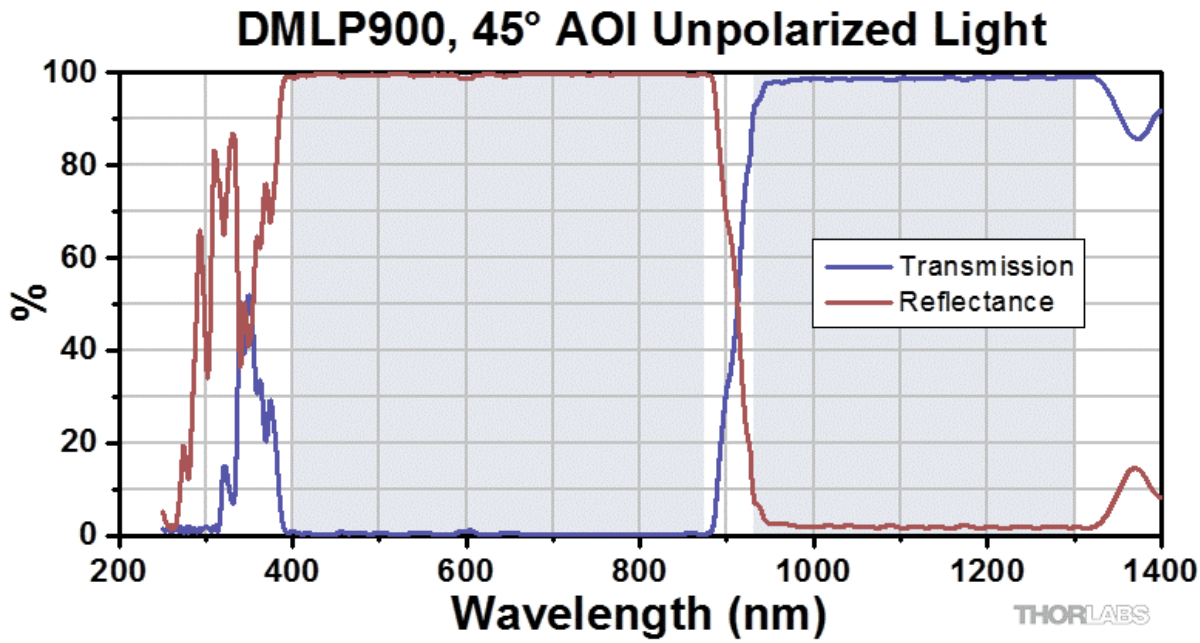

Figure B7 – Transmission graph of the employed dichroic mirror – DMLP805R.

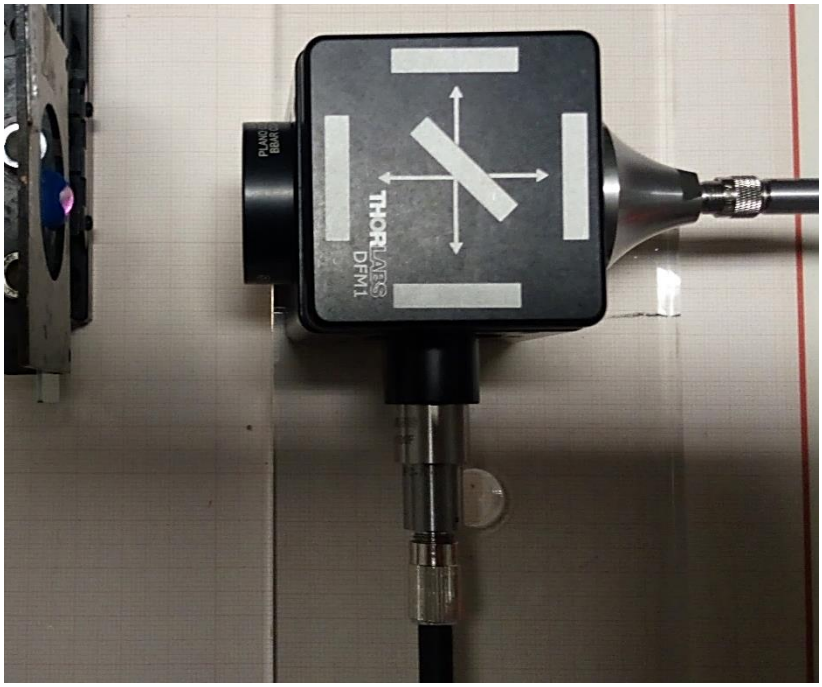

Figure B8 – Representation of the assembled fiber-coupled remote probe, connected to the external laser (input laser radiation beam) and microscope objective (output Raman signal), coupled to delivery and collection fibers, with 200 µm core diameter, during a spectrum acquisition from a sound enamel sample.

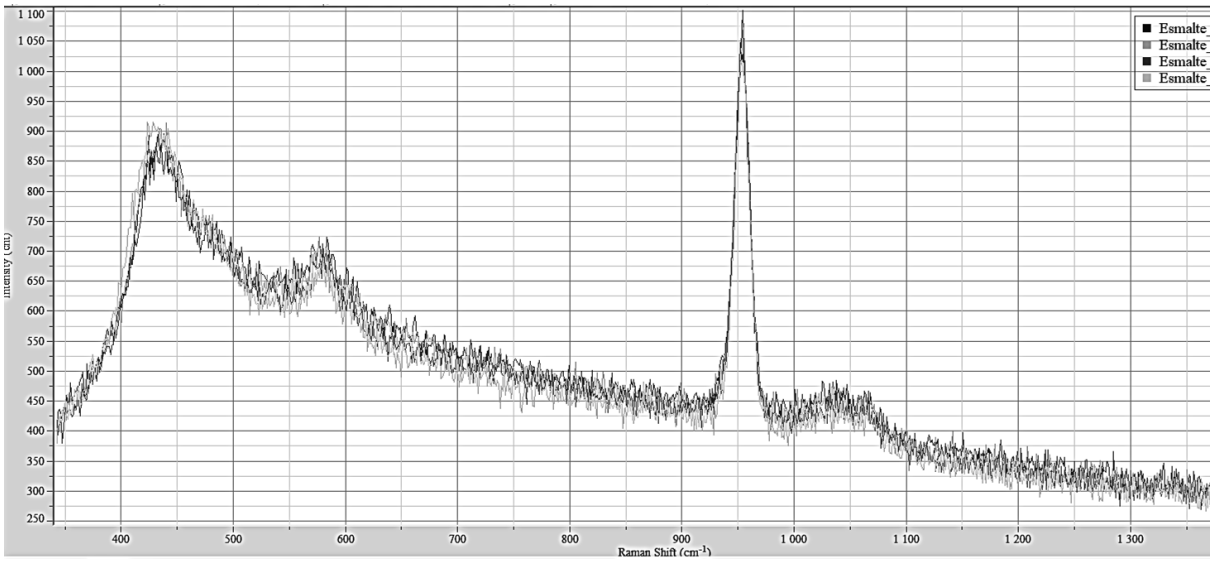

Figure B9 – Representation of raw Raman spectra, without baseline correction, acquired from a sound enamel specimen, using the remote probe, connected to the external laser using the F200-FC adapter and a collection fiber with core diameter of 200 µm.

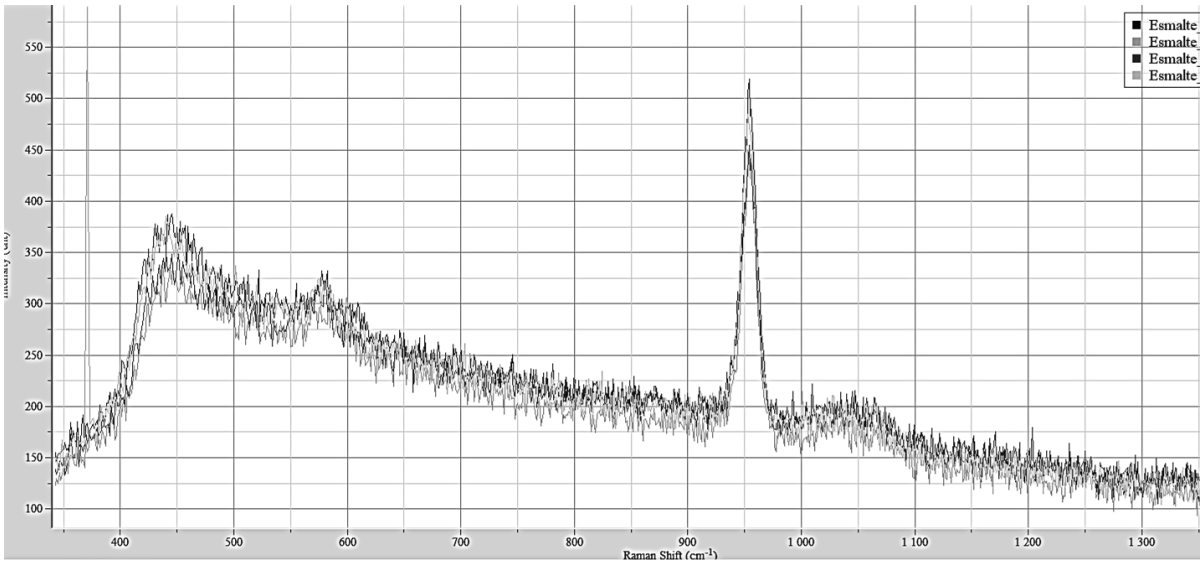

Figure B10 – Representation of raw Raman spectra, without baseline correction, acquired from a sound enamel specimen, using the remote probe, connected to the external laser using the CVH-COL100 and a collection fiber with core diameter of 105 µm.

DEVELOPMENT OF RAMAN SPECTROSCOPY INSTRUMENTATION FOR DENTAL RESEARCH

IULIAN OTEL

March, 2023